NASA/CR–2011-217303

Blended Wing Body Concept Development with Open Rotor Engine Integration

David M. Pitera, Mark DeHaan, Derrell Brown, Ronald T. Kawai, Steve Hollowell, Peter Camacho, David Bruns, and Blaine K. Rawden
The Boeing Company, Huntington Beach, California

November 2011

NASA STI Program . . . in Profile

Since its founding, NASA has been dedicated to the advancement of aeronautics and space science. The NASA scientific and technical information (STI) program plays a key part in helping NASA maintain this important role.

The NASA STI program operates under the auspices of the Agency Chief Information Officer. It collects, organizes, provides for archiving, and disseminates NASA's STI. The NASA STI program provides access to the NASA Aeronautics and Space Database and its public interface, the NASA Technical Report Server, thus providing one of the largest collections of aeronautical and space science STI in the world. Results are published in both non-NASA channels and by NASA in the NASA STI Report Series, which includes the following report types:

- TECHNICAL PUBLICATION. Reports of completed research or a major significant phase of research that present the results of NASA programs and include extensive data or theoretical analysis. Includes compilations of significant scientific and technical data and information deemed to be of continuing reference value. NASA counterpart of peer-reviewed formal professional papers, but having less stringent limitations on manuscript length and extent of graphic presentations.

- TECHNICAL MEMORANDUM. Scientific and technical findings that are preliminary or of specialized interest, e.g., quick release reports, working papers, and bibliographies that contain minimal annotation. Does not contain extensive analysis.

- CONTRACTOR REPORT. Scientific and technical findings by NASA-sponsored contractors and grantees.

- CONFERENCE PUBLICATION. Collected papers from scientific and technical conferences, symposia, seminars, or other meetings sponsored or co-sponsored by NASA.

- SPECIAL PUBLICATION. Scientific, technical, or historical information from NASA programs, projects, and missions, often concerned with subjects having substantial public interest.

- TECHNICAL TRANSLATION. English-language translations of foreign scientific and technical material pertinent to NASA's mission.

Specialized services also include creating custom thesauri, building customized databases, and organizing and publishing research results.

For more information about the NASA STI program, see the following:

- Access the NASA STI program home page at *http://www.sti.nasa.gov*

- E-mail your question via the Internet to help@sti.nasa.gov

- Fax your question to the NASA STI Help Desk at 443-757-5803

- Phone the NASA STI Help Desk at 443-757-5802

- Write to:
  NASA STI Help Desk
  NASA Center for AeroSpace Information
  7115 Standard Drive
  Hanover, MD 21076-1320

NASA/CR–2011-217303

Blended Wing Body Concept Development with Open Rotor Engine Intergration

David M. Pitera, Mark DeHaan, Derrell Brown, Ronald T. Kawai, Steve Hollowell, Peter Camacho, David Bruns, and Blaine K. Rawden
The Boeing Company, Huntington Beach, California

National Aeronautics and
Space Administration

Langley Research Center
Hampton, Virginia 23681-2199

Prepared for Langley Research Center
under Contract NNL10AA05B

November 2011

Available from:

NASA Center for AeroSpace Information
7115 Standard Drive
Hanover, MD 21076-1320
443-757-5802

1.1 *Table of Contents*

1.2 Table of Figures

1.3 Table of Tables

2 Introduction

The BWB concept has been studied extensively due to the potential it has to significantly reduce fuel burn, emissions and noise levels compared to current and future conventional tube-with-wing subsonic transport configurations. The BWB concept has been studied with a variety of propulsion options, including podded nacelles, embedded engines, geared fans and open rotors. Open rotor technology has the potential to provide the greatest fuel burn reduction relative to all other potential propulsion options for the BWB. In addition, the BWB offers the potential for noise shielding, thus ameliorating one of the main drawbacks of the open rotor. However, open rotor integration with the BWB has not been studied as extensively as the podded or embedded engine options. The main purpose of this study is to perform a systems analysis of a BWB open rotor concept at the conceptual design level. This concept will be utilized by NASA to estimate overall noise and fuel burn performance, utilizing recent test data. The configuration is intended for entry into service (EIS) in 2025. The study was performed from the fall of 2010 to summer of 2011 by the Boeing Research and Technology organization in Huntington Beach, CA.

This study will also investigate the problem of Propulsion Airframe Integration (PAI) due to the installation of an open rotor configuration on a BWB. Open rotor engines have unique problems relative to turbo fans. The rotors are open, exposed to flow conditions outside of the engine. The flow field that the rotors are immersed in may be higher than the free stream flow and it may not be uniform, both of these characteristics could increase noise and decrease performance. The rotors sometimes cause changes in the flow conditions imposed on aircraft surfaces. At high power conditions such as takeoff and climb out, the stream tube of air that goes through the rotors contracts rapidly causing the boundary layer on the body upper surface to go through an adverse pressure gradient which could result with separated airflow. The BWB / Open Rotor configuration must be designed to mitigate these problems in order to reach fuel burn and noise goals.

The title of the project was long and cumbersome; an acronym was developed within Boeing to quickly refer to the project. The project was commonly referred to as OREIO, which stands for Open Rotor Engine Integration On a BWB.

3 Requirements - Contract Task (3.1)

The purpose of the requirements is to support a design effort of a realistic airplane that supports further study by NASA. The requirements are based primarily on the requirements in development for the NASA/Boeing Environmentally Responsible Aviation (ERA) study of Blended Wing Body (BWB) and conventional airliners and freighters - specifically for the Preferred System Concept portion of the study. The hope is that common requirements will yield similar airplanes in both studies and

that the in-depth analysis performed in this study will be valuable to the ERA study and its successors. It is recognized that the ERA requirements will evolve over time.

The following is intended to clarify how we arrived at the requirements. Only a few key requirements are spelled out for the ERA study. Other requirements are generally chosen to be representative of similar, existing airplanes to enhance the realism of the study.

Detailed requirements are shown in Table 4 at the end of this section.

Payload

A cargo payload is chosen instead of a passenger payload. In most ways, a cargo payload is simpler than a passenger payload and permits the design of a realistic airplane with less concentration on the payload. This permits increased effort on propulsion-airframe integration – the object of this study.

We have chosen the point-of-departure (POD) airplane for the related ERA study effort as the starting point for this study as well. This airplane originated as an airliner, so despite the freighter-only payload, the airplane is configured to be a good airliner as well. It features a main passenger deck and a lower, central cargo hold.

The preliminary design of the POD airplane, presently called the ERA-224, includes the selection of cargo unit load devices (ULD). These are similar to existing ULD designs, but are not the same in that their dimensions (particularly height) are tailored for the BWB passenger cabin and lower hold dimensions.

The cargo arrangement is shown in Figure 1. There are 40 total positions of which 22 are on the main deck. 18 primary ULDs 96” x 125” x 84” high are oriented widthwise in the three cargo bays. These are shown in yellow. Two additional ULDs 88” x 125” with a tapered height from 82” to 62” fit into the forward end of the two outboard bays, as shown in cyan.

In the lower hold, 18 rectangular ULDs 60.4” long x 61.5” wide by 46” high fit in two columns into the center bay. An alternative arrangement for the lower hold is 9 widthwise pallets 60.4” long by 125” wide by 46” high.

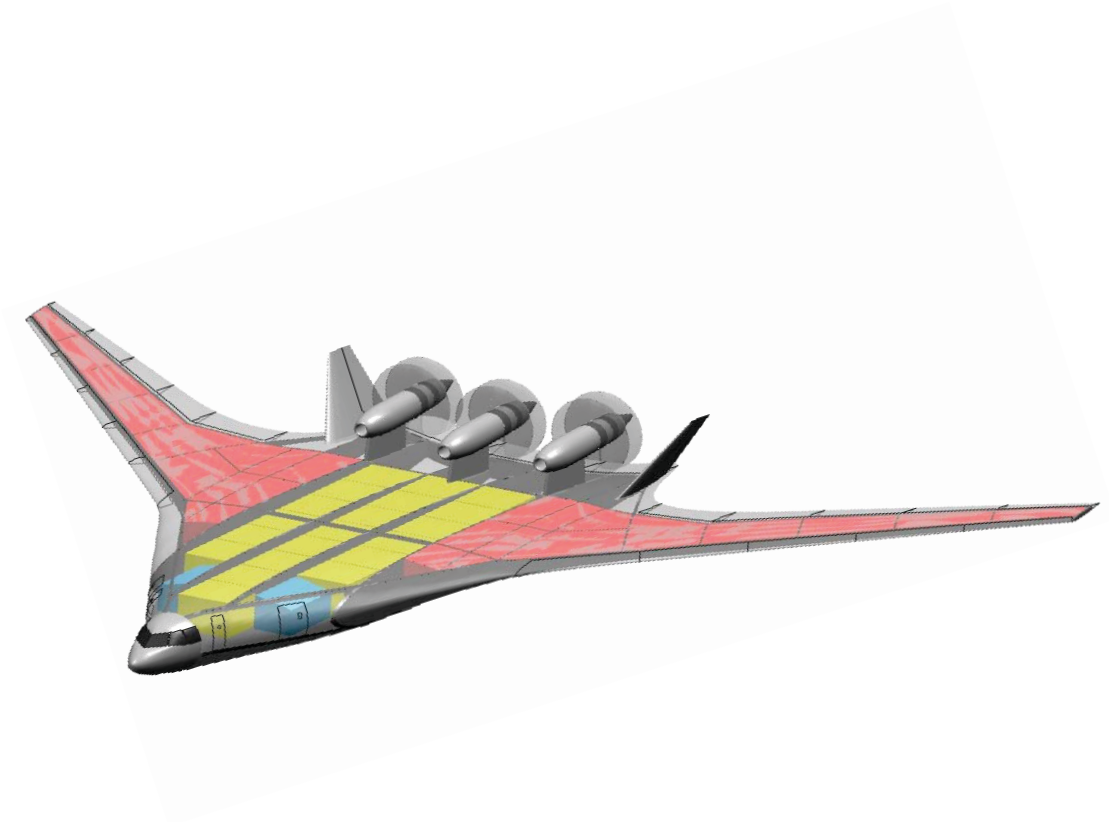

Figure 1. BWB ERA-224 Upper Deck Cargo Arrangement.

Tare weights for unit load devices are estimated from data presented in Reference 1. Tares are estimated for two types of ULDs – all-containers and all-pallets with netting. The tare weights are substantial, especially for the containers.

Internal volumes of each of the container types is estimated based on the ratio of internal volume reported in Reference 1 compared to the volume of the ULD envelope (length x width x height). This ratio is approximately 92%.

Estimated tare weights of the ULDs in container-only form are shown in Table 1. Total container tare weight is estimated to be 18,119 lb. Estimated tare weights of the ULDs in pallet-only form are shown in Table 2. Total tare weight is 60% lighter at 7228 lb.

In practice, a mix of ULD types is used. Container loads are less expensive to build and more secure but more expensive to fly. Pallets are labor-intensive to build but are considerably lighter in tare weight. For the purpose of selecting a tare weight, a 50-50 mix of containers and pallets is assumed. Results from this mix are shown in Table 3 with a total tare weight of 12,673 lb. Total cargo volume of the 50-50 mix, including an assumed 400 ft^3 of bulk cargo is 13,689 ft^3 as shown in Table 3.

Table 1. Container-Only Tare Weight and Internal Volume.

Containers Only	
Tare Weight	
M1 Container reduced to 125" x 96" x 84"	15051.4
LD9 Container mod to 82/62" tapered height	1019.4
Lower Deck Containers	2048.4
Total tare weight (lb)	18,119
Container Internal Volume	
M1 Container reduced to 125" x 96" x 84"	10868
LD9 Container mod to 82/62" tapered height	833
Lower Deck Containers	1638
Bulk Cargo (assumed) (ft^3)	400
Total internal volume (ft^3)	13,738
Assumed net cargo weight (lb)	100,000
Net cargo density (lb/ft^3)	7.279

Table 2. Pallet-Only Tare Weight and Internal Volume.

Pallets w/ Nets Only	
Tare Weight	
Main deck primary pallets w/ nets	5183.0
Main deck secondary pallets w/ nets	469.1
Lower deck pallets w/ nets	1575.6
Total tare weight (lb)	7,228
Container Internal Volume	
Main deck primary pallets w/ nets	10733
Main deck secondary pallets w/ nets	843
Lower deck pallets w/ nets	1664
Bulk Cargo (assumed) (ft^3)	400
Total internal volume (ft^3)	13,641
Assumed net cargo weight (lb)	100,000
Net cargo density (lb/ft^3)	7.331

Table 3. Half-and-Half Mix of Containers and Pallets Tare Weight and Internal Volume.

50-50 Containers and Pallets	
Tare Weight	
Main deck primary	10117
Main deck secondary	744
Lower deck pallets	1812
Total tare weight (lb)	12,673
Container Internal Volume	
Main deck primary	10800
Main deck secondary	838
Lower deck pallets	1651
Bulk Cargo (assumed) (ft^3)	400
Total internal volume (ft^3)	13,689
Assumed net cargo weight (lb)	100,000
Net cargo density (lb/ft^3)	7.305

NASA has specified a 100,000 lb cargo payload both for the ERA study and for the BWB Open Rotor Integration study. Initially it was not clear if this weight was to include or exclude the ULD tare weight. This choice influences the total payload of the airplane and the density of the cargo. NASA has now clarified the payload specification; the tare weight is included in the 100,000 lbs.

A more detailed study of NASA requirements shows that a BWB freighter of the ERA-224 configuration works well with at total (net + tare) payload of 100,000 lb. Although this payload yields a net cargo density of only 6.4 lb/ft3, the range at this payload is unusually long. When fuel is traded for payload, practical combinations of range and payload are achieved. A cargo density of 10.0 lb/ft3 yields an estimated range of about 3000 nm. This density is at the high end of commercial freighter densities while the range is at the low end, so this airplane nicely covers the typical range and density spectrum of commercial freighters. For comparison, the cargo density of the 767-300F is 7.2 lb/ft^3 with a range of 3256 nm and the 777F is 9.9 lb/ft^3 at 4885 nm. The approximate relationship between the BWB, 767F and 777F payload densities and ranges is shown in Figure 2.

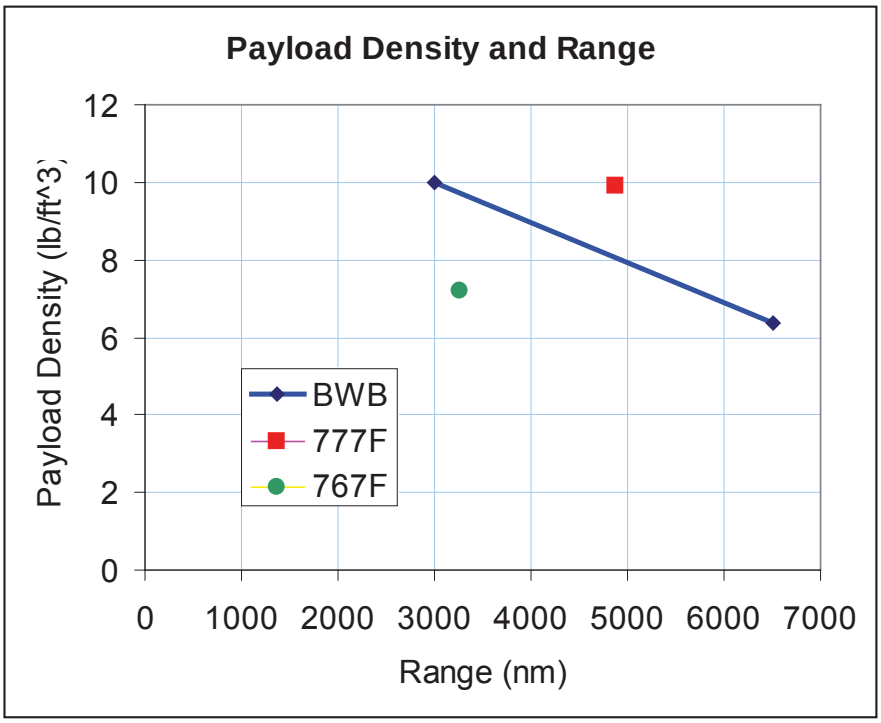

Figure 2. Payload Density versus Range.

Performance

Performance requirements are again based on the NASA ERA requirements. The primary exception is that the cruise speed is reduced from Mach 0.85 to Mach 0.80. This reduction is to accommodate open rotor propulsion. Mach 0.80 is selected based on the consensus of the NASA-Boeing team.

Performance of the airplane will be estimated using Boeing's standard advanced design assumptions as used in the recent NASA studies. These include:

- Performance is governed by Federal Aviation Regulations (FARs) for commercial transports.
- Boeing's mission rules are used. These rules are significantly more efficient than current practice but are not as aggressive as those proposed for next generation airspace. These rules pertain to climb and descent profiles, hold times, taxi times, etc.
- A cruise-climb is assumed. This is representative of future airspace rules.
- A thrust reserve in cruise sufficient to provide at least 100 ft/min climb rate is required.

Airport Compatibility
Airport compatibility is addressed in three requirements. The load classification number (LCN) describes the load imparted by the landing gear on the airport surfaces and in turn defines the construction of these airport surfaces. A greater

number indicates that a stronger surface is needed. The LCN is specified as being less than or equal to 90. 90 is a typical value for larger long range airliners. In advanced design, LCN is addressed by selecting the diameter and spacing of the main gear tires according to their loading.

Wingspan is constrained to 65 meters (213.25 ft). This is the limit for ICAO Code E airports, a reasonable limit for this capacity BWB that, unconstrained, optimizes near this span. Wing folding is not permitted in the interest of study simplicity although it may be entertained in future studies if the 65 meter limit proves to be a significant constraint.

Detailed Requirements

Detailed requirements are listed in Table 4 below.

Measure of Merit

The initial configuration of the airplane will address noise with configuration features that may include canted inboard verticals for engine noise shielding, a forward engine location and extended and broadened aft fuselage for additional engine noise shielding and perhaps an outer wing free of leading edge devices to reduce slat noise. Once these features are selected and implemented, their refinement will be based primarily on drag considerations. Refinement of noise characteristics is beyond the scope of this study but may be addressed in the future.

Evolution and sizing of the airplane will consider fuel consumption as the measure of merit. This measure has proven effective in recent NASA sponsored studies of BWBs.

Conclusion

The requirements described are intended to result in a practical, certifiable design. They are also intended to result in an airplane similar to that which results from the related ERA study.

Table 4. Final Requirement.

		BWB-224	Comments
Payload:			
Pallet Positions		40	
Tare Weight	lb	12,673	1/2 Containers and 1/2 Pallets with Nets
Total Cargo Volume	ft^3	13,689	
Design Payload Density	lb/ft^3	6.379	Computed w/o tare weight
Design Payload w/o Tare	lb	87,327	
Design Payload w/ Tare	lb	100,000	
Max Payload Density		10.000	
Max Payload w/o Tare		136,892	
Max Payload w/ Tare		149,565	
Limit Load Factor	g's	2.5	
Sizing Unit Load Device (ULD) Type		96 x 125 x 84	1/2 Containers and 1/2 Pallets with Nets
Sizing ULD Chamfering		FALSE	
Primary ULD Type and Number		(20) 96 x 125 x 84	
Primary ULD Volume	ft^3	10,800	
Reduced Primary ULD		(2) 88 x 125 x 82>62	1/2 Containers and 1/2 Pallets with Nets
Reduced Primary ULD Volume	ft^3	838	
Lower Deck Payload Type and Number		(18) 60.4L x 61.5W x 46H	1/2 Containers and 1/2 Pallets with Nets
Lower Deck Payload Volume	ft^3	1651	
Bulk Payload	ft^3	400	Assumed
Crew		2	
Performance:			
Range with design payload	nm	6500	
Range with maximum payload		Fallout	
Ferry range	nm	Fallout	
Critical Field Length (SL Std Day @ MTOGW)	ft	10,500	
Standard for field length		FAR	
Max Landing Weight	%	TBD	Landing Weight (MLW) shall be the maximum zero fuel weight (MZFW) plus the reserve fuel required for a design range mission with
Approach Speed	KCAS	155	
Landing Field Length (SL Std @ MLW)		5200 (dry)	
Initial Cruise Altitude	ft	35,000	
Minimum Cruise Mach Number		0.80	
Maximum Sinkrate @ Landing	fps	8	Advanced Landing System
Airport Compatibility:			
Runway Load Classification Number		LCN <= 90	90 typ for LR airliners; 777-300ER = 100
Wingspan Constraint	meters	65 meters	(213.25 feet)
Folding Wings		FALSE	
Noise		Emphasize a low noise design - but no specific requirement in terms of dB.	Include noise-shielding configuration features such as canted inboard verticals, forward-mounted engines and a widened and lengthed aft centerbody.
Measure of Merit		Gross payload ton-nm per lb fuel burned	At design range. Aircraft acoustic features uncompromised.

4 Configuration

4.1 Wing-Body Development– Contract task (3.2)

The wing and body lines were developed from the ERA-224 configuration shown in Figure 3. The ERA-224 configuration is a close match for the requirements from the previous section with the exception of the cruise Mach number. The 0.85 cruise Mach number for the ERA was recognized as being too high for open rotors. The cruise Mach number specified for this study is 0.80. The wing body lines of the ERA-224 configuration had to be changed primarily by reducing the wing sweep to match the cruise Mach number.

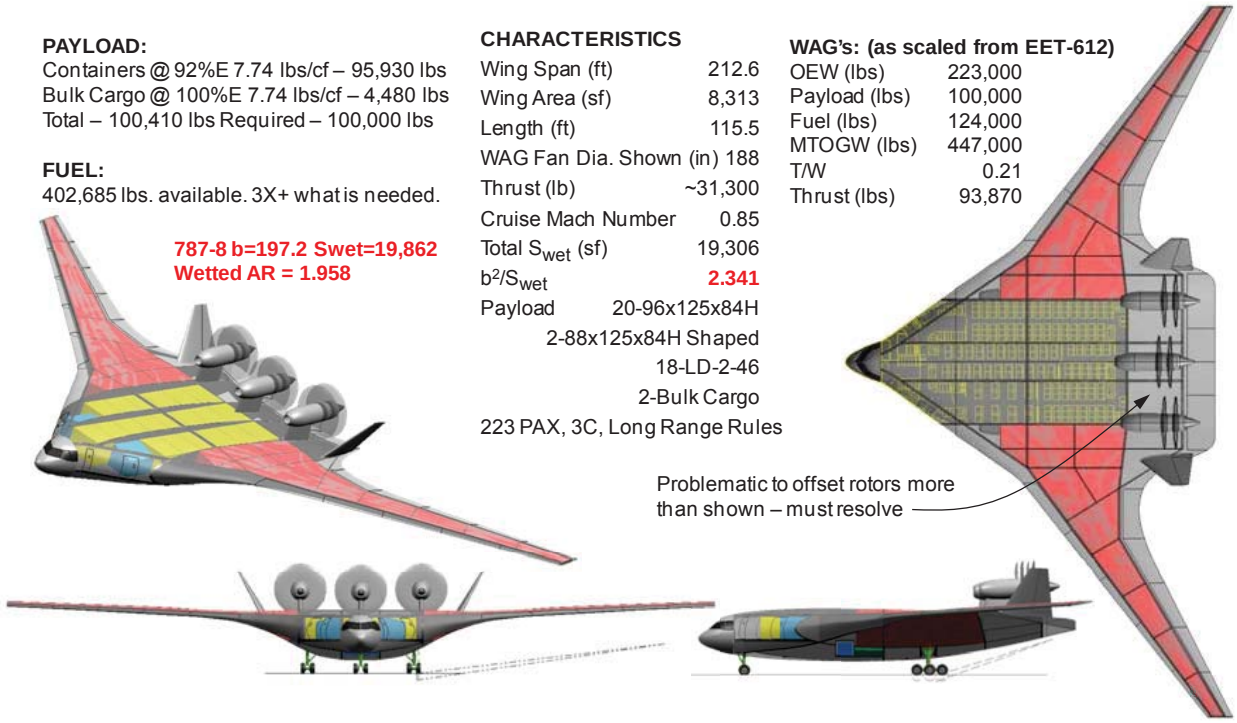

Figure 3. ERA-224 Point of Departure Configuration

The wing sweep was modified in 3 steps. First, a new sweep angle was determined based on sweep-thickness requirements for a conventional wing. Second, the body centerline chord was increased to allow more room for the propulsion system and to increase the body area aft of the engines for better noise shielding. Third, the aerodynamic characteristics were improved by using the MDOPT code to optimize the configuration. The three configurations are labeled ERA-080, ERA-080REV2, and ERA-080R2DLR3 and are shown in Figure 4.

The centerline chord was increased mainly because it was felt that the upper surface of the body may have to be carved out or "area-ruled" to reduce the interference between the engines and the body. The volume removed for area-ruling was estimated to begin forward of the rear spar and there was not enough room at the rear spar to reduce the height of the body. The increased centerline chord length relieved this problem. Also, by increasing the chord while maintaining the same

thickness reduced the thickness to chord ratio which reduced the aerodynamic penalty for adding the extra wetted area.

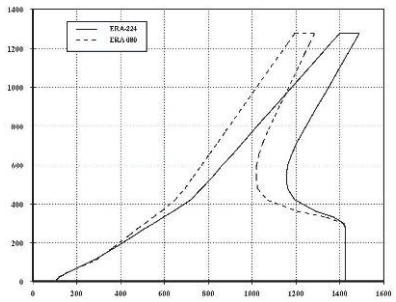

ERA-224 to ERA-080

- Reduced sweep for reduced Mach
- M = 0.85 - 0.80

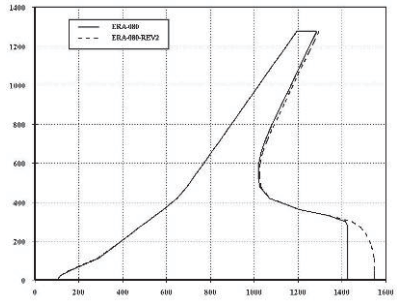

ERA-080 to ERA-080REV2

- Increased centerline chord
- Improved propulsion installation options and noise shielding
- Maintain T_{max} not $(T/C)_{max}$

GROSS PLANFORM AREAS	
ERA-224	7967 FT^2
ERA-080	7967 FT^2
ERA-080REV2	8499 FT^2
ERA-080R2DLR3	8377 FT^2

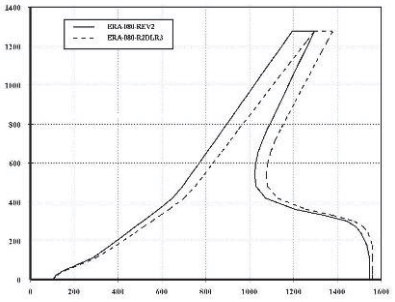

ERA-080REV2 to ERA-080R2DLR3

- MDOPT optimization with trim constraint
- CDISC design to smooth pressures for a smooth loft
- Manual geometry smoothing

Figure 4. Wing-Body Planform Changes

However, the increased centerline chord ultimately proved to be a problem and was removed for the final configuration. CFD analysis during the propulsion airframe integration task indicated that in order to position the nacelle and pylon in slower velocity air flow field they should be located as close to the trailing edge as possible. The increase in the centerline chord moved the trailing edge aft; the nacelle and pylon moved aft along with the trailing edge. The increased planform area and the aft movement of the engines increased the increased overall weight and resulted with a center of gravity too far aft for proper balance of the configuration.

The optimization was done using MDOPT an aero and multidisciplinary constrained optimization that is based on a design of experiments. The CFD code that was coupled to the optimizer for this work was TLNS (Thin Layer Navier-Stokes). Only the wing and body were modeled for ease of gridding and speed of computation. A table of constraints used in MDOPT is contained in Table 5. The optimization also constrained the center of pressure between 39% and 40% of the MAC. Thrust effects were accounted for by assuming that thrust equals drag and that the moment arm for the thrust vector was 180” above the center of gravity. The optimization was done at a lift coefficient of 0.25 and an altitude of 35,000 ft.

After the MDOPT optimization was complete the pressure distribution was smoothed using CDISC, a CFD based inverse design tool coupled with a flow solver called CFL3D. The final geometry was then smoothed manually.

Table 5. List of Constraints for the MDOPT Optimization of the Wing Body Geometry

- Optimization done on clean wing (no N/P or verticals)
- Maximize L/D subject to the center of pressure constraint 39%MAC < C.P. < 40%MAC at CL=0.25/35KFT
- C.P. includes effect of thrust
- Thrust = Drag
- Moment arm assumed at 180" above wing surface at rotor location
- Thrust axis alignment considered secondary effect and ignored

Design Variable Table

Index	Type	Lower Bounds	Upper Bounds	Station Location	Final Value
1	Sweep	-5	5	0	2.52
2	Taper Ratio	-0.05	0.05	0	-0.013
3	Span	-0.05	0.05	0	0.002
4	Twist	-0.01	0.01	0.157	0.01
5	Twist	-2	2	1	1.21
6	Max T/C Location	-0.01	0.01	0.157	-0.006
7	Max T/C Location	-0.1	0.1	0.6	-0.070
8	Max T/C Location	-0.1	0.1	1	0.047
9	TE Deflection	-3	3	0	-0.93
10	TE Deflection	-3	3	0.157	-0.69
11	TE Deflection	-0.1	0.1	0.235	0.06
12	Camber Splines	-0.0001	0.0001	0.157	-0.00009
13	Camber Splines	-0.0001	0.0001	0.157	-0.00001
14	Camber Splines	-0.0001	0.0001	0.157	0.00003
15	Camber Splines	-0.01	0.01	0.6	0.00422
16	Camber Splines	-0.01	0.01	0.6	0.00773
17	Camber Splines	-0.01	0.01	0.6	0.00930
18	Camber Splines	-0.01	0.01	1	-0.00676
19	Camber Splines	-0.01	0.01	1	0.00398
20	Camber Splines	-0.01	0.01	1	0.00086

NOTES: TE hinge line at X/C=0.65
Camber spline knots at X/C=0.2, 0.5, 0.8

The optimized wing-body geometry has more sweep and more outboard loading than the original wing-body. These changes not only improved the lift-to-drag ratio for the configuration but also helped to balance the airplane at 39% of the MAC with thrust effects from the engine mounted 180" above the upper surface of the body. The increased sweep is shown in Figure 4. The increased outboard loading is evident in the pressure distribution shown in Figure 5 and the spanload distribution shown in Figure 6. A 3-view was completed base on the final geometry after optimization and smoothing. The 3-view drawing is shown in Figure 7.

The maximum lift-to-drag ratio for the final wing-body configuration is in line with other wing-body designs from CFL3D as shown in Figure 8. Note that the efficiency of the wing-body alone configurations will shift over to the left slightly when the extra wetted area of the nacelles, pylons and vertical tails are added.

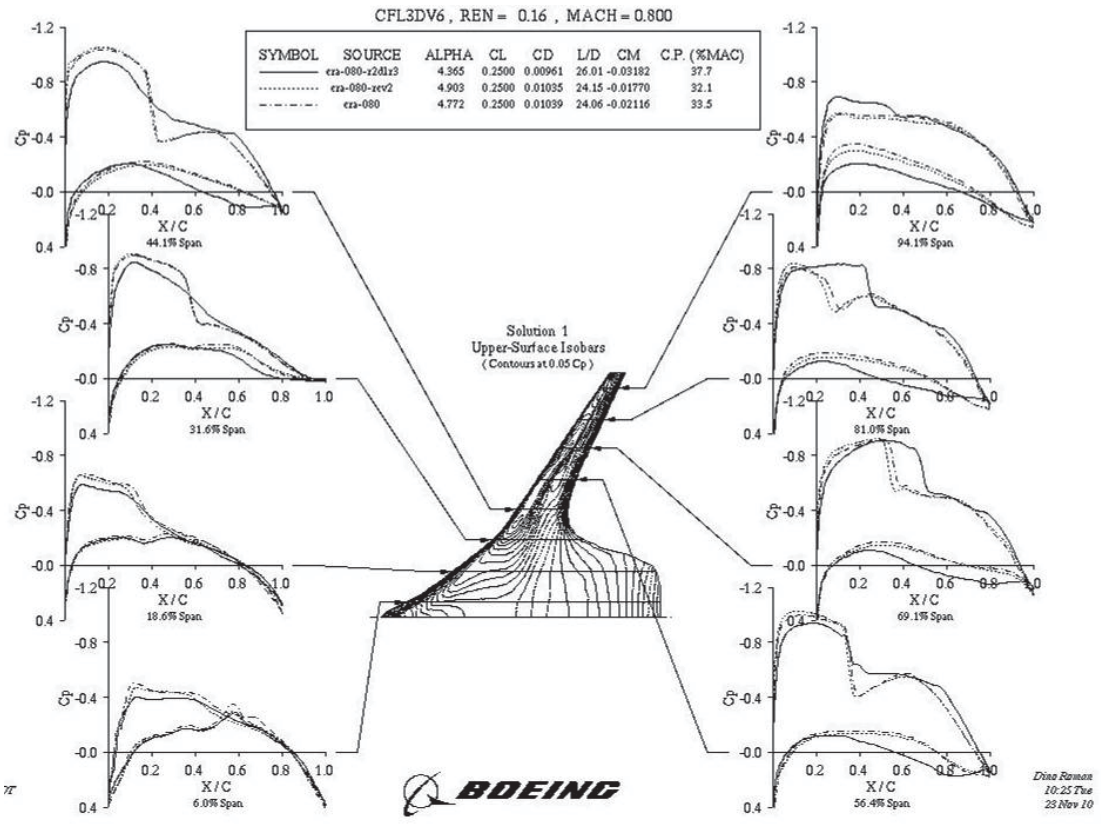

Figure 5. Pressure Distributions for Different Wing Body Configurations

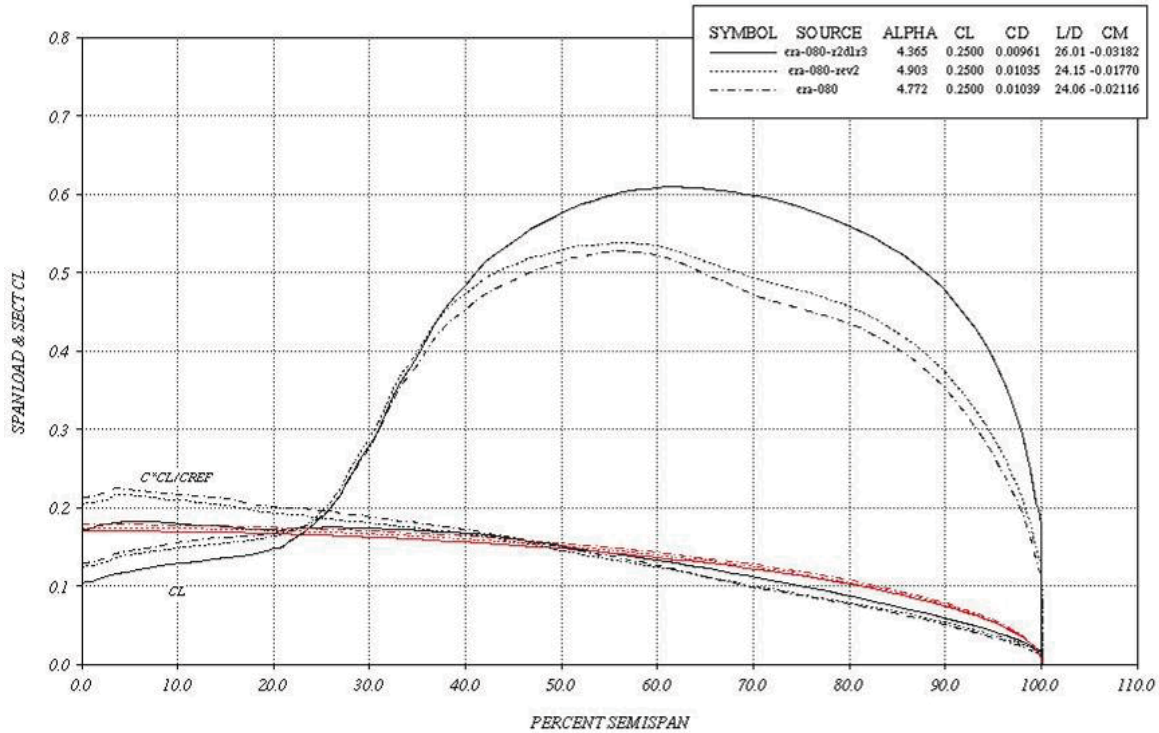

Figure 6. Spanload for different Wing Body Configurations

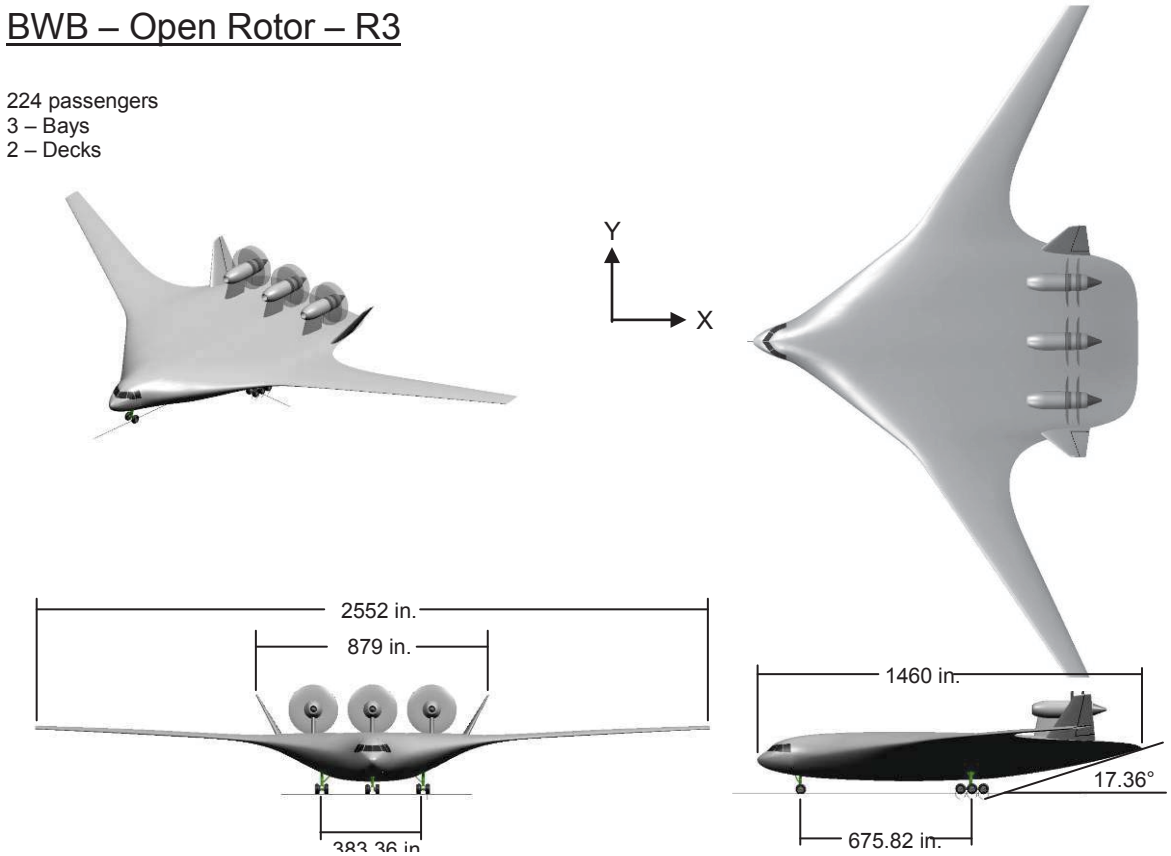

Figure 7. 3-View Drawing Based on Final Optimized Geometry

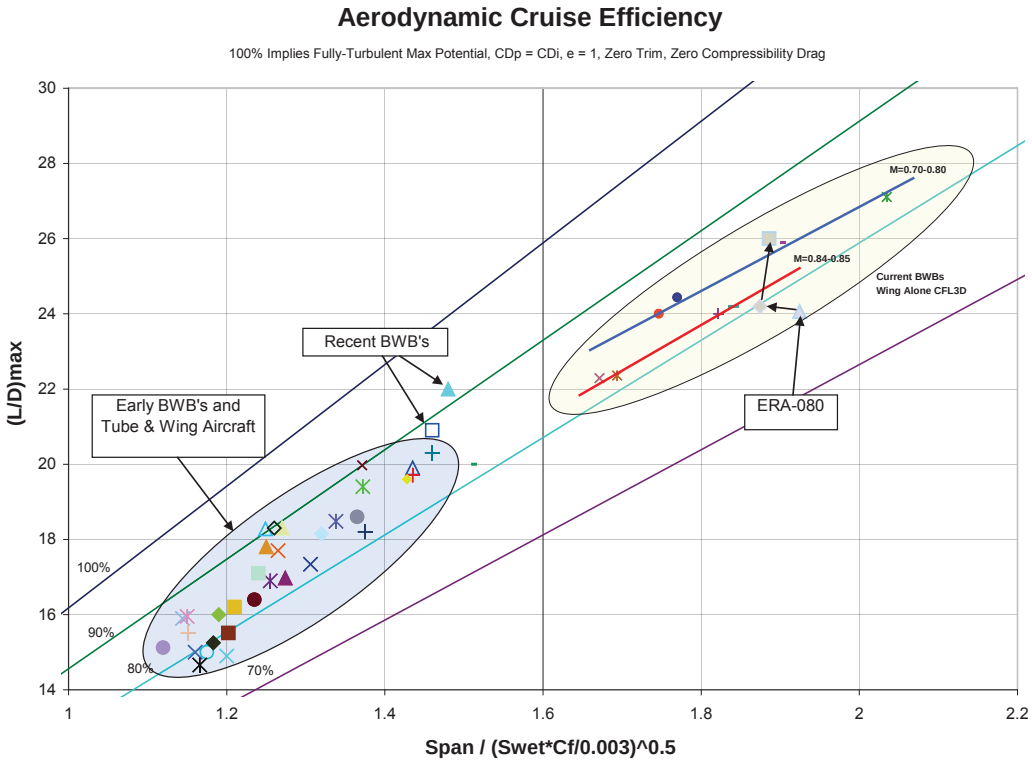

Figure 8. Aerodynamic Efficiency

4.2 Vertical Tail

A revised vertical tail was developed for the CFD analysis. The new tail was necessary because the sweep on the vertical tail used for the original OREIO configuration is too low for an aircraft with a cruise Mach number of 0.80. The new tail is based on the area and taper ratio of the tail from the original OREIO configuration. The quarter chord sweep of the new tail was set at 35 deg which is appropriate for a cruise Mach number of 0.80 based on conventional sweep and thickness charts. The Mach capability of the tail must be greater than the wing to maintain control for all conditions. Standard symmetrical airfoils were used; they were twisted to get zero lift at cruise based on the flow field of the wing-body.

The revised vertical tail was also checked relative to rules of thumb from NASA based on results from the acoustic testing in the LSAF tunnel. Based on results from acoustic testing in the LSAF tunnel, NASA suggested sizing rules for the root chord and tip chord relative to the forward rotor diameter. The root chord should be about 1.25 times the front rotor diameter and the tip chord should be about 0.60 times the front rotor diameter. The root chord and tip chord for the revised vertical tail are 1.13 and 0.48 times the front rotor diameter. The revised vertical tail is close to the recommended size for acoustics but slightly undersized.

The size of the vertical tail was also checked relative to requirements for stability and control. The OREIO configuration and the X-48C are very similar, and the X-48C was evaluated in great detail. The X-48C tail volume should be a very good preliminary sizing requirement for OREIO. The tail volumes are shown in Table 6. Two OREIO configurations are shown: the original OREIO configuration (Figure 7), and the final OREIO configuration (Figure 63) which will be discussed in Section 10.1. The OREIO configurations have approximately the same tail volume as the X48-C, which implies that the OREIO tails are the correct size for stability and control. Therefore the vertical tail size was not increased.

Table 6. Vertical Tail Sizing

Vertical Tail Sizing for Stability and Control
Match the Tail Volume of the X-48C

	X-48C	Original OREIO Configuration	Final OREIO Configuration
Tail Arm	68.652	572.21	492.20
Tail Area	1.7	169.6	169.6
Wing MAC	90.797	887.9	824.3
Wing Area	100.48	8379.8	8002.5
Tail Volume	0.01279	0.01304	0.01265

The final geometry resulted with the height of the top of the front rotor approximately equal to the height of the top of the vertical tail. This is shown in Figure 29. The front rotor-to-body spacing shown in Figure 28 is 3 ft based on requirements for minimum air flow separation on the upper surface of the body at takeoff conditions explained in Section 8.2.

4.3 Nacelle Geometry

The external nacelle geometry is based on the nacelle geometry received from NASA shown in Figure 9. The design is based on the GE UDF open rotor work from the 1980's. The external cowl and inlet were not sufficiently defined so standard design methods were used. The external nacelle cowl was defined based on a DAC 3 shape. A two to one ellipse was used for the inlet lip. The geometry of the inlet cowl is shown in Figure 10.

The technology level of the rotors used by NASA is also based on 1980's work. The latest technology open rotors generally have a higher blade count, increased clipping of the rear rotor diameter relative to the front rotor, and a lower thrust loading. The lower thrust loading (thrust per square foot of rotor area) for the latest technology rotors results in a larger diameter. The original 3-view drawing for the OREIO project was set up assuming the latest technology rotors with an 18" rotor tip to body spacing. The NASA rotors have a smaller diameter so when the NASA rotors were placed in the same engine location as the 3-view the rotor tip to body spacing was increased to 30".

An alternate nacelle was developed and used for some of the CFD solutions. The alternate nacelle was developed because CFD solution with the baseline nacelle indicated high levels of interference between nacelles, with the body, and with the pylons when they were included. The alternate nacelle is shown in Figure 11. The baseline nacelle has a large diameter because it was designed for a Mach number of 0.72. The alternate nacelle has a smaller maximum diameter and therefore lower external velocities and less interference with other parts of the configuration. The diameter of the alternate nacelle is sufficient to enclose the engine, and provide the proper external flow characteristics around the inlet and cowl including low spillage drag. However, the alternate nacelle does not have the same shape or diameter near the rotor hubs and will therefore have different airflow characteristics in the rotor planes. The alternate nacelle has a constant diameter in front of the rotor planes. The baseline nacelle has a continuously varying diameter reaching a maximum at the end of the cowl and then reducing forward of the rotor planes. The alternate nacelle would have a different flow field at the rotors because it lacks the conditioning provided by the shape of the baseline nacelle. The baseline nacelle was not changed because of concern about changes to the rotor flow field. However, some CFD solutions were produced with the alternate nacelle for comparison to the baseline configuration.

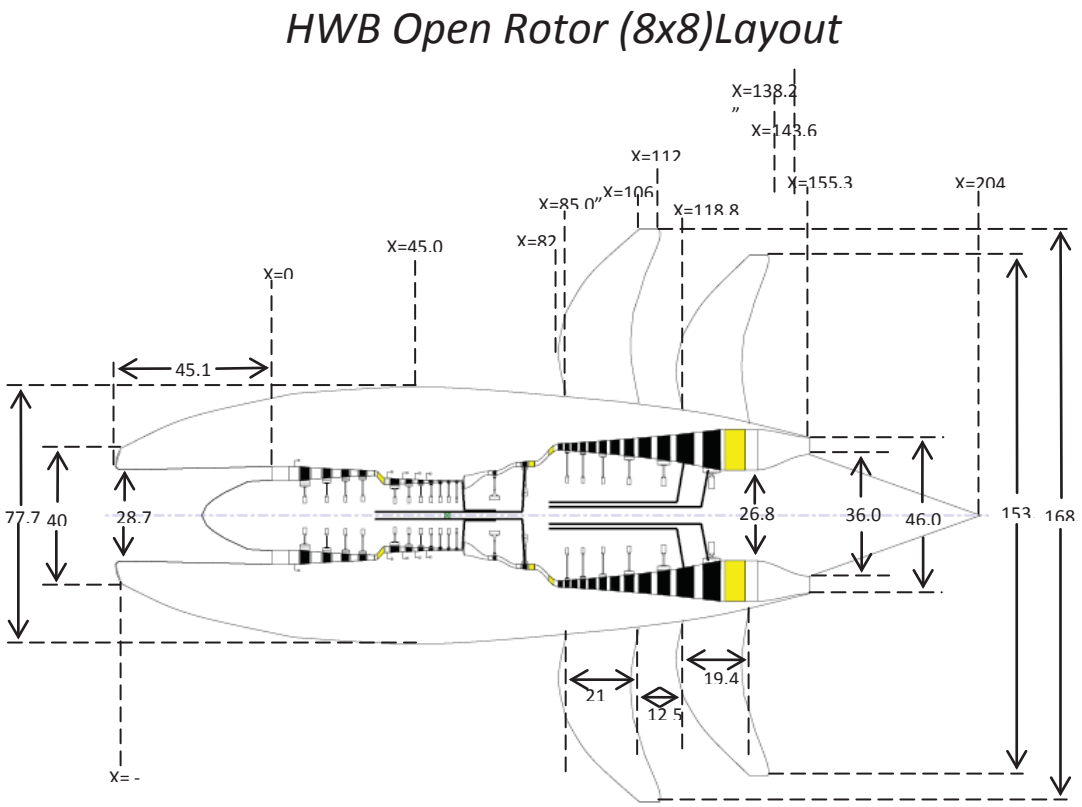

Figure 9. Nacelle Geometry received from NASA GRC

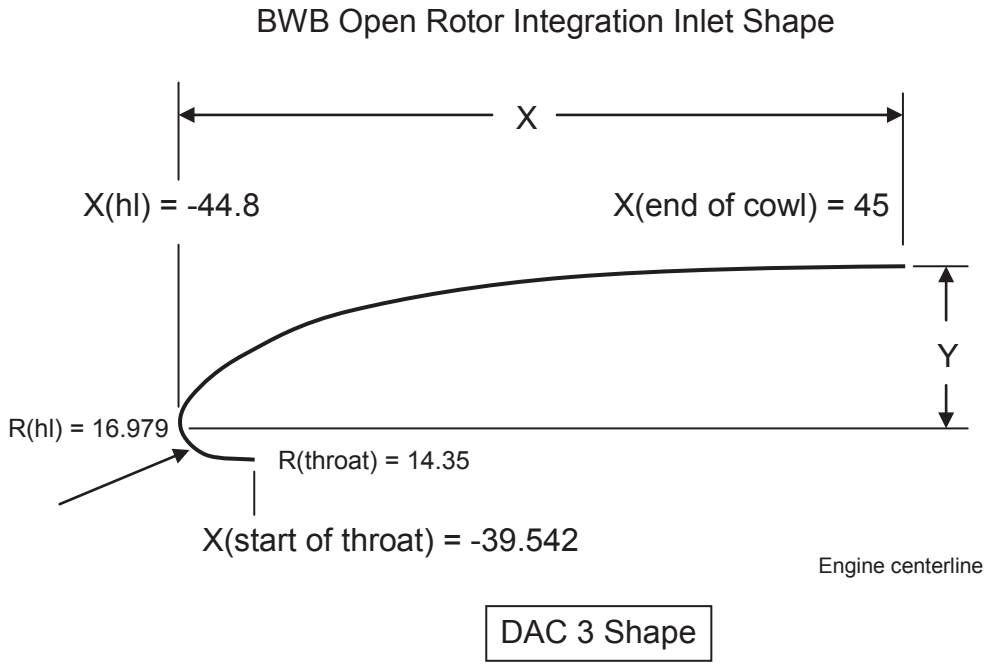

Figure 10 . Definition of Inlet Cowl and Internal Lip

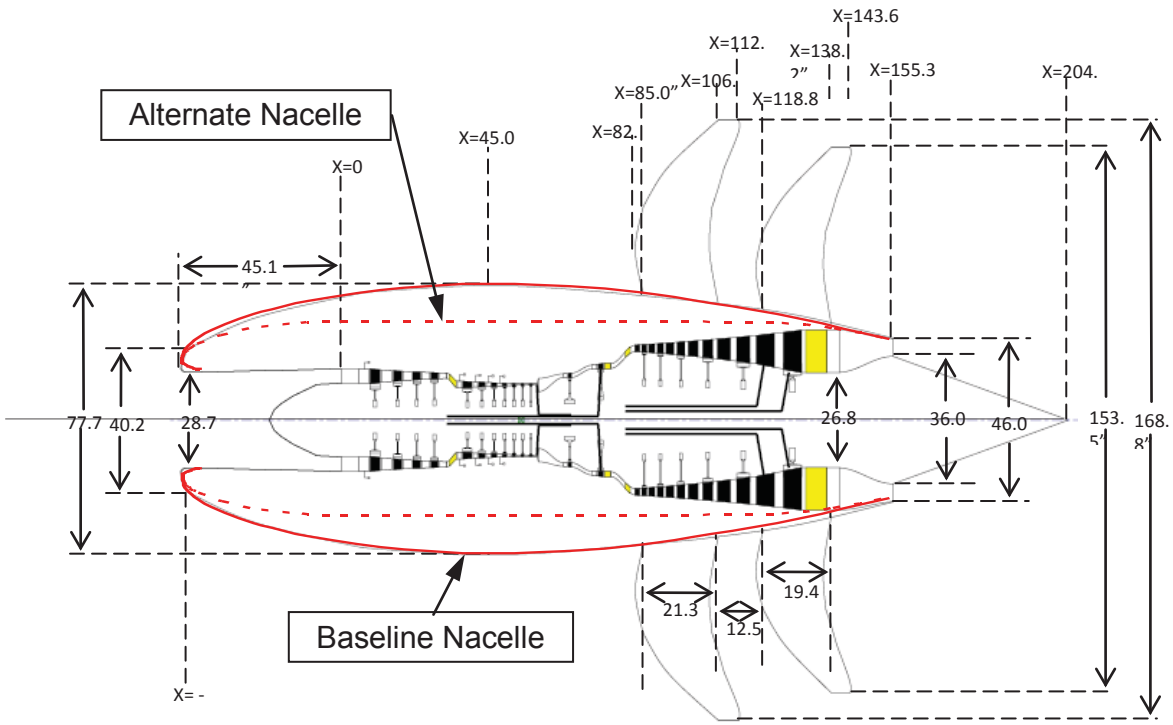

Figure 11. Baseline and Alternate Nacelle

5 Propulsion Airframe Integration at Cruise, Unpowered

5.1 Overflow CFD Code

The Overflow RANS (Reynolds Averaged Navier-Stokes) code was used for most of the CFD analysis. The Overflow code was selected because it has proven accuracy and Boeing in Huntington Beach has a large amount of experience with it. The accuracy of Overflow is well documented in a series of papers from the AIAA's Drag Prediction Workshop. The Overflow code was also selected because it has a rotor model which has been used for helicopter and open rotor work on other projects. Overflow is a structured code that uses overset grids. The structural grid can take more time to prepare than an unstructured code, but Boeing has so much experience with it that many short cuts have been developed. Also the geometry for this project is rather simple. Many of the configuration changes involved moving the nacelles for configurations without a pylon. The grid preparation for these cases was a quick and easy process even when using a structured code.

5.2 Isolated Nacelle

Isolated Overflow solutions for the baseline and alternate nacelles were produced at 0.80 and 0.84 Mach number. A mass flow plug was developed to set the mass flow ratio to 0.60 which is appropriate for this type of engine. The mass flow plug was taken from another application and scaled to get the correct mass flow ratio. The plug is shaped differently than what is shown in Figure 9 but the specific shape of the plug aft of the exit plane will have little impact on the solutions. The solution for Mach number 0.80 for the baseline nacelle is shown in Figure 12 and for the alternate nacelle in Figure 13. The pressure coefficient is shown in the lower right corner of each figure. The internal pressure coefficients are positive and are nearly identical for both the baseline and alternate nacelles. The external pressure coefficients are more negative for the baseline configuration indicating that the external velocities are higher. The biggest difference in the pressure coefficients occurs in the area where the alternate nacelle has a constant section. The alternate nacelle has less negative pressure coefficients in this area which indicates lower velocities. The lower velocities outside the alternate nacelle indicate that it should produce less interference drag than the baseline nacelle.

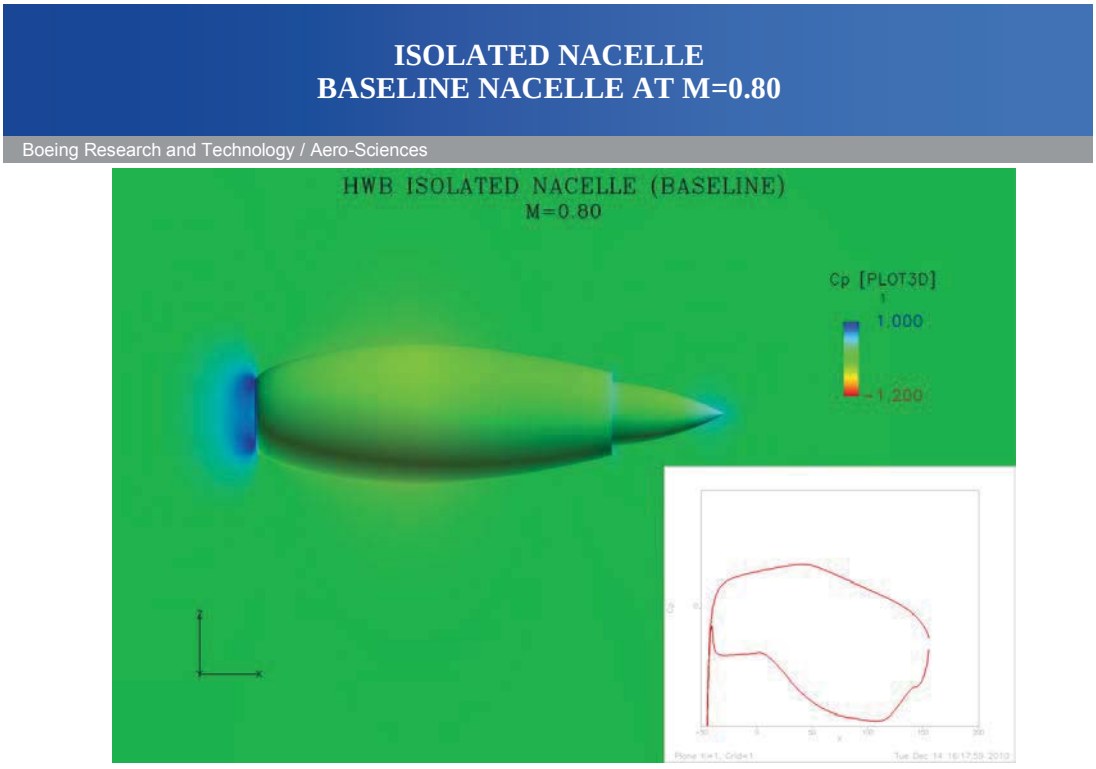

Figure 12. Isolated Baseline Nacelle Mach 0.80

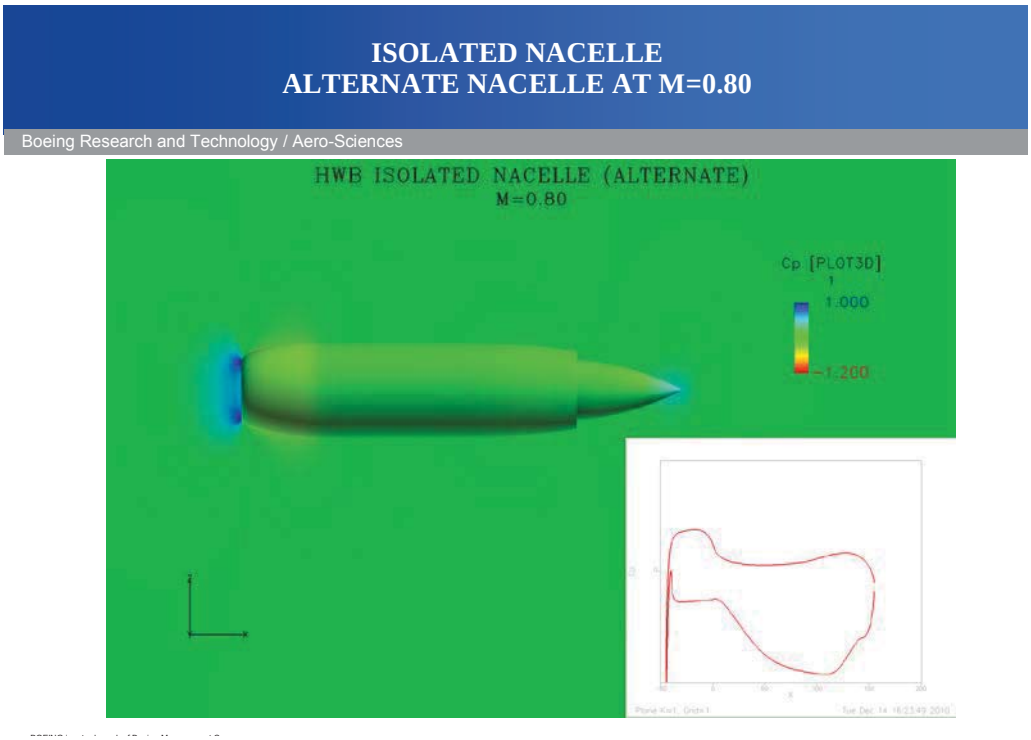

Figure 13. Isolated Alternate Nacelle at Mach 0.80

5.3 Wing-Body

An Overflow solution for the baseline wing-body is shown in Figure 14. The wing body solution is very similar to the results produce by CFL3D during the wing-body development.

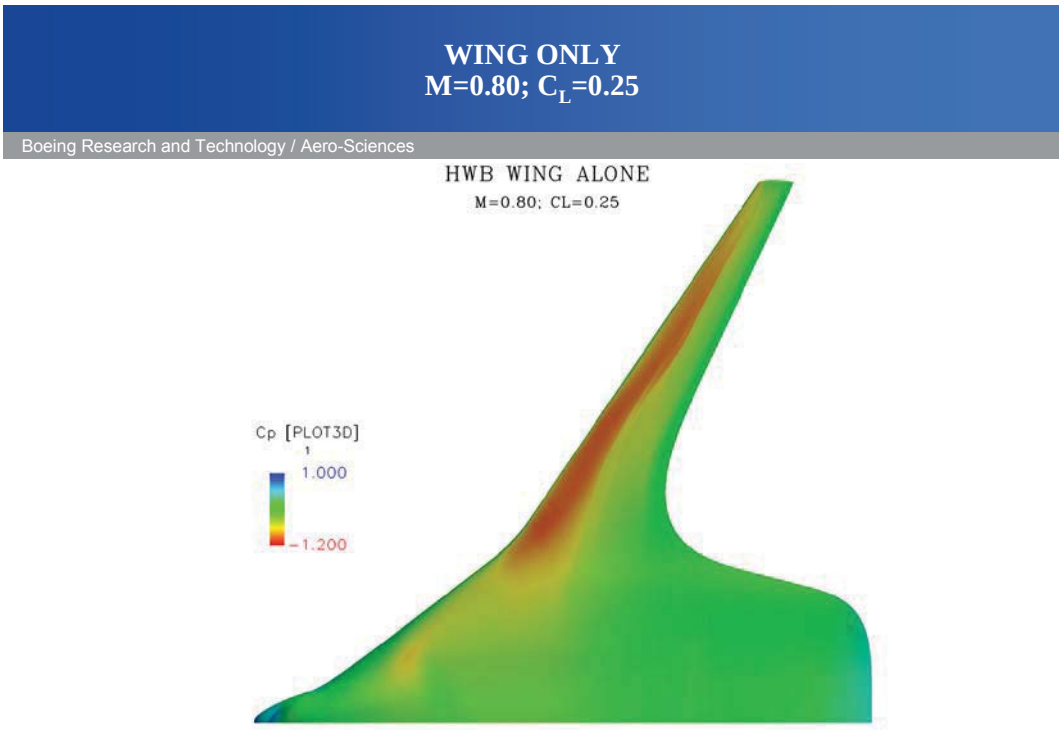

Figure 14. Baseline Wing-Body Overflow Solution at M=0.80

5.4 Wing-Body-Nacelle

The engine integration work was started by evaluating the interference drag of the wing-body-nacelle configuration. Pylons were not included because of the complexity of gridding the geometry and the difficulty in developing an acceptable configuration. The interference caused by a pylon would be so large that it would be difficult to determine the effects of nacelle positioning. Vertical tails were not included for the same reason, although it was assumed that the interference due to the vertical tails would be less than the interference from the pylon. It was also recognized that vertical tails are critical for the noise shielding aspects of the configuration and would have to be evaluated before long.

The wing, body, nacelle work started by evaluating the nacelles in the position shown on the 3-view drawing. The 3-view drawing shown in Figure 7 placed the nacelles side-by-side next and quite far forward of the trailing edge. The distance between the nacelles and the trailing edge was increased due to the trailing edge extension that was discussed in Section 5.1. The interference drag was high for this configuration. The Overflow solution for this configuration is shown in Figure 15; the interference drag is 8.1 counts. Note that the interference drag is calculated by subtracting the drag for the wing-body and three isolated nacelle solutions from the wing-body-nacelle solution. The total drag of the configuration is about 110 counts, so 8.1 counts is approximately 7% of the total drag.

An indication of interference drag is evident in the pressure distribution. The pressure distribution for the isolated nacelle is shown in Figure 12. The pressure distribution for the installed nacelles is shown in Figure 15. The same scaling was used for the pressure coefficients in both figures. The pressure distributions for the installed case have regions of high velocity that are not found in the isolated pressure distributions. Higher velocities are indicated by the increased amount of red on the nacelle surface for the installed case. Note that there are two legends shown in Figure 15. The legend on the lower left shows the pressure coefficients on the surface of the nacelles and aft body. The legend on the upper right shows the local Mach number in off body planes above and below each nacelle. A peak local Mach number near 1.2 is shown in the off-body planes indicating a moderate recompression shock between the nacelles and the body. The recompression shock is also evident on the body and on the sides of the nacelles.

A second rotor tip to body spacing was also evaluated. The rotor tip to body spacing for the configuration in Figure 15 is 30 inches. This spacing resulted because the rotor provided by NASA has a smaller diameter than the rotor that was used for the original 3-view. This was discussed in Section 5.3. The desired rotor tip to body spacing is 18 inches. This spacing will lower the engines and reduce the nose down pitching moment due to the thrust axis. The Overflow solution with a spacing of 18 inches is shown in Figure 16. The interference drag increased from 8.1 to 10.4 counts when the rotor tip to body spacing was reduced from 30" to 18". The increased shock strength on the body is evident under the nacelles.

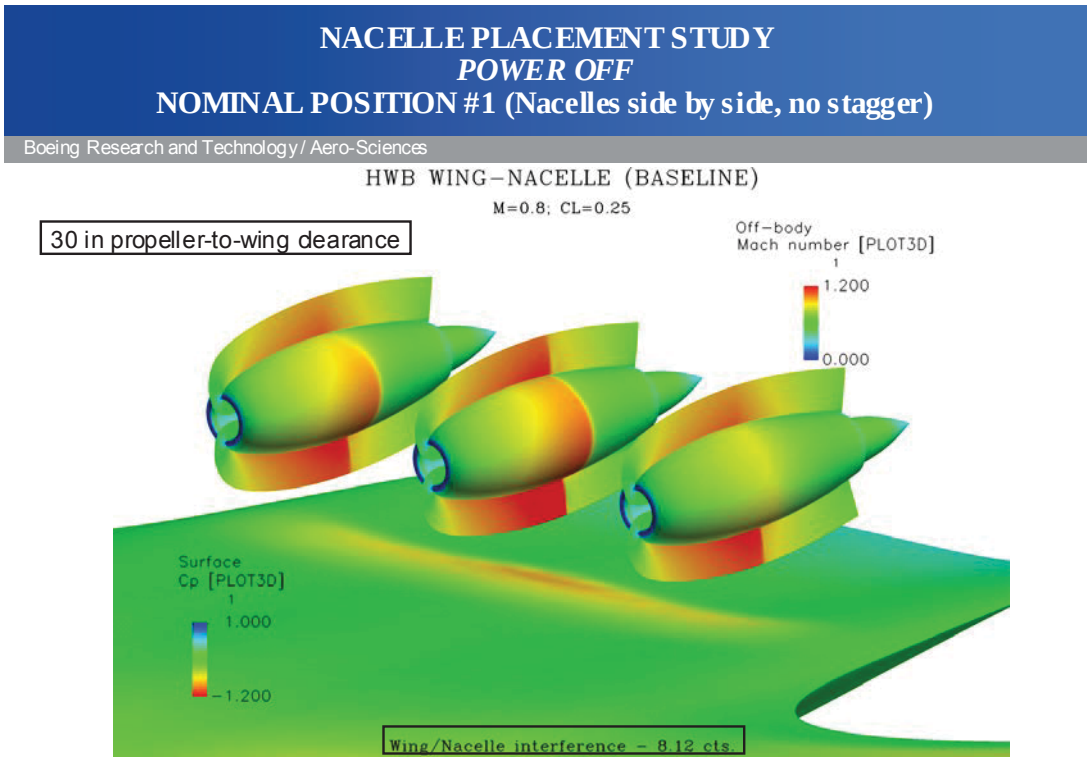

Figure 15. Initial Wing-Body-Nacelle Solution

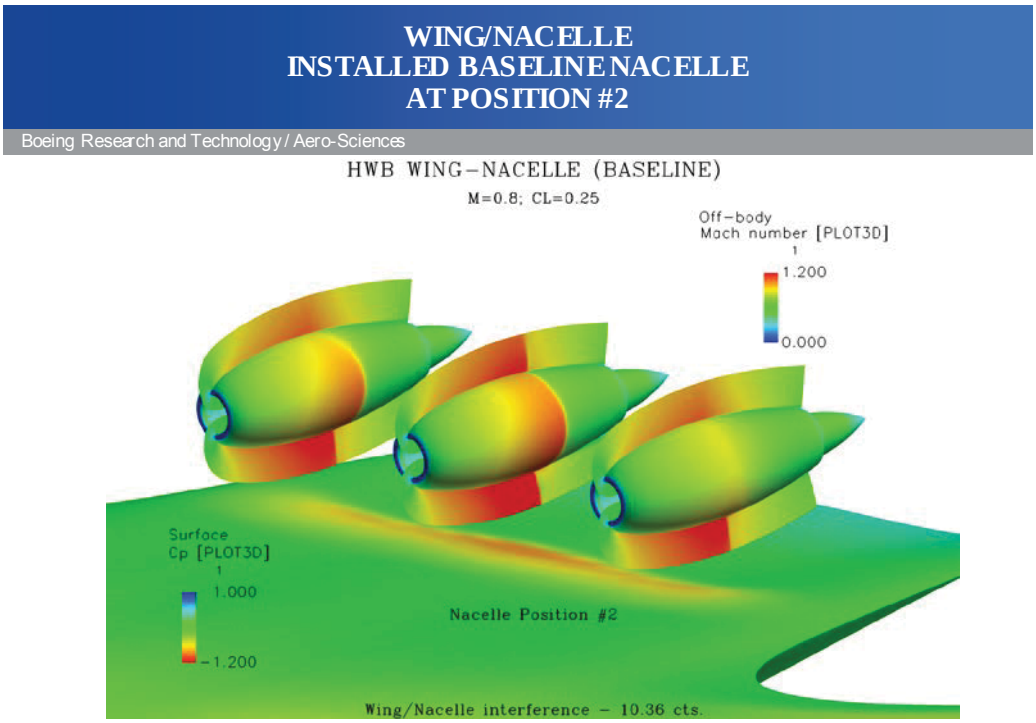

Figure 16. CFD solution with a rotor tip to body spacing of 18 inches

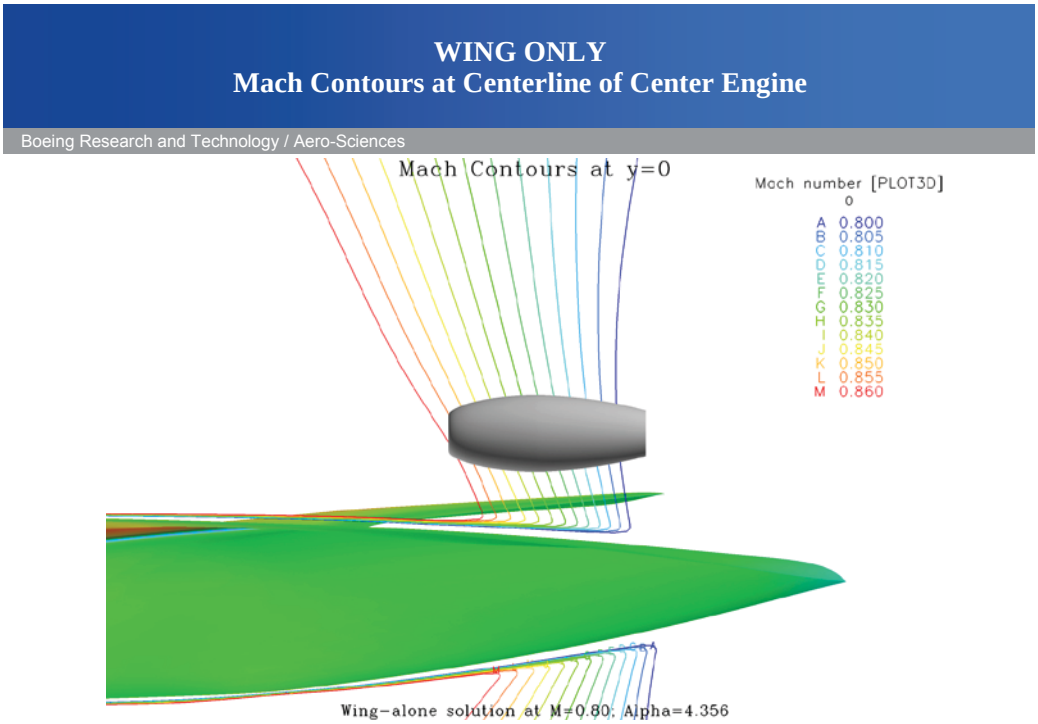

Figure 17. Wing-Body Flow Field at the Centerline Nacelle Location

The interference drag was attacked in two ways. First, the flow field in which the nacelle was immersed was evaluated from the wing-body grid solution. This flow

field, shown in Figure 17, indicated that the nacelle should be moved aft. There are strong velocity gradients over the body caused by its shape and the lift that it generates. From the front to the back of the imaginary nacelle the velocity decreases from Mach 0.85 to Mach 0.80. The nacelle was not actually in the solution; it is just shown for reference. The second method of reducing the interference drag was to stagger the nacelles. The original positioning of the nacelles side-by-side created a local maxima of cross sectional area that caused a spike in velocity. This maximum cross sectional area could be reduced by staggering the nacelles.

The interference drag was reduced by about two thirds by moving the nacelles aft and staggering them. The interference drag for several wing-body-nacelle combinations is shown in Figure 18. The first group of nacelle position changes was to move the center nacelle aft in 20" increments; the interference drag dropped quickly as the stagger increased. The stagger was stopped at 60" assuming that positioning the engines and blades at a significantly different fuselage station would not be good for acoustics or for integrating the engines to the back of the wing-body.

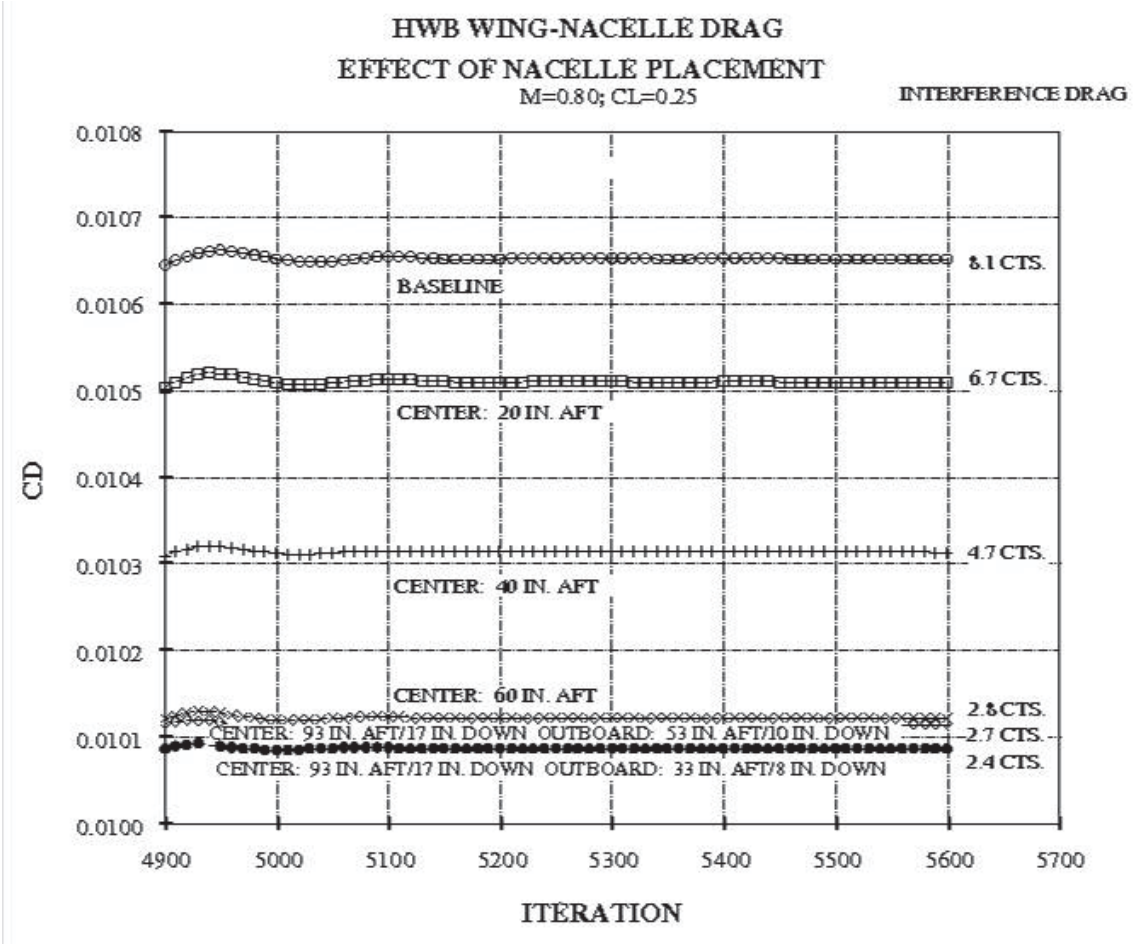

Figure 18. Effect of Nacelle Placement at Cruise

A second group of nacelle position changes consisted of just two configurations where all three nacelles were moved aft closer to the trailing edge. The interference

drag was lower for the second group of configurations. One configuration had a 40" stagger and 2.7 counts of interference drag. The other had a 60" stagger and 2.4 counts of interference (Figure 18). The Overflow solution for the 60" stagger is shown in Figure 19.

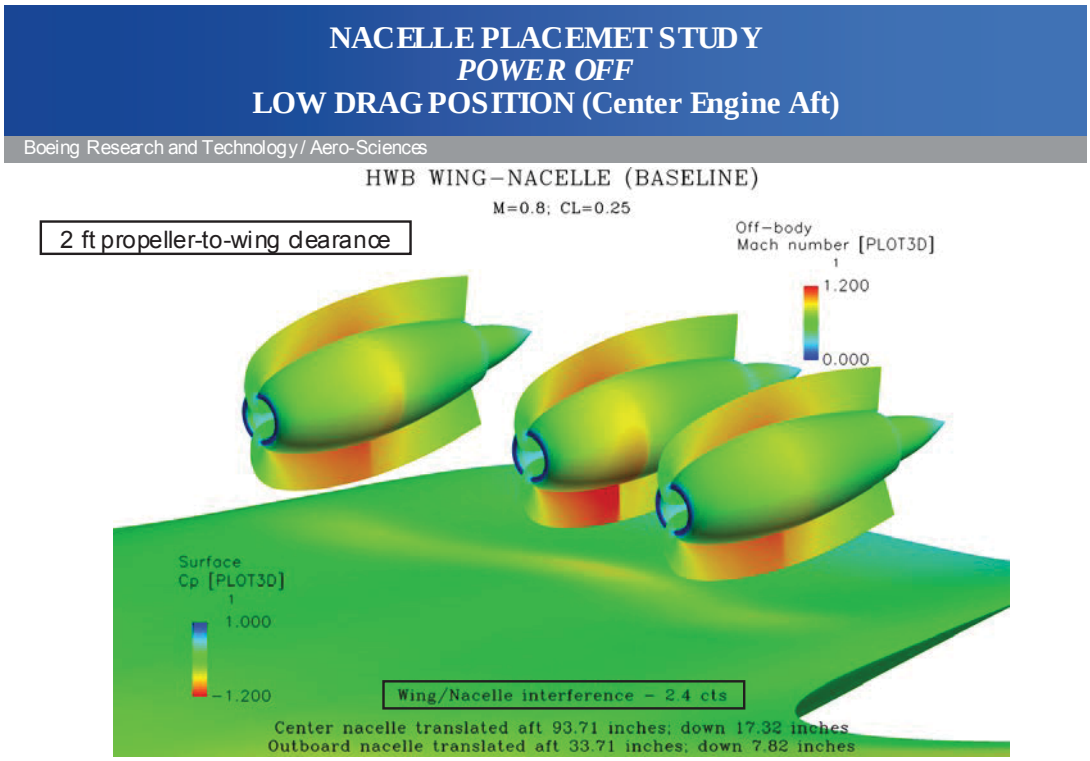

Figure 19. Low Drag Position of the Nacelles

The spacing between the rotor tip and the body was less for the second group of configurations. The nacelles in the first group were moved aft but not down. The nacelles in the second group were adjusted down when they were moved aft. The decreased spacing penalized the interference drag of the second group, but the interference drag of this group was still lower than the first group because all three nacelles were moved aft to slower air near the trailing edge.

The movement of the nacelles aft closer to the trailing edge of the body was limited by a criterion supplied by NASA; to ensure adequate noise shielding the middle of the forward and aft rotors should be at least one forward rotor diameter from the trailing edge.

The movement of the nacelles close to the trailing edge ruined the reasoning for adding the 80" trailing edge extension on the body. The extension moved the trailing edge of the body further aft than the original configuration but then the nacelles were moved aft to the lower velocities near the trailing edge. The additional structure associated with the 80" longer body and aft location of the nacelles created a weight and balance problem that was solved by reducing the extension by 80" for the Concept Design Data Summary (Section 10.1).

The stagger of the nacelles was changed based on inputs from NASA for low noise. The center engine was staggered 60” forward of the outboard engines instead of 60” aft. This way the center engine would be further from the trailing edge and have more noise shielding and the outboard nacelles would be shielded by the vertical tails. Results from the Overflow solution for this inverted stagger configuration are shown in Figure 20. The interference drag increased slightly from 2.4 counts to 2.5 counts.

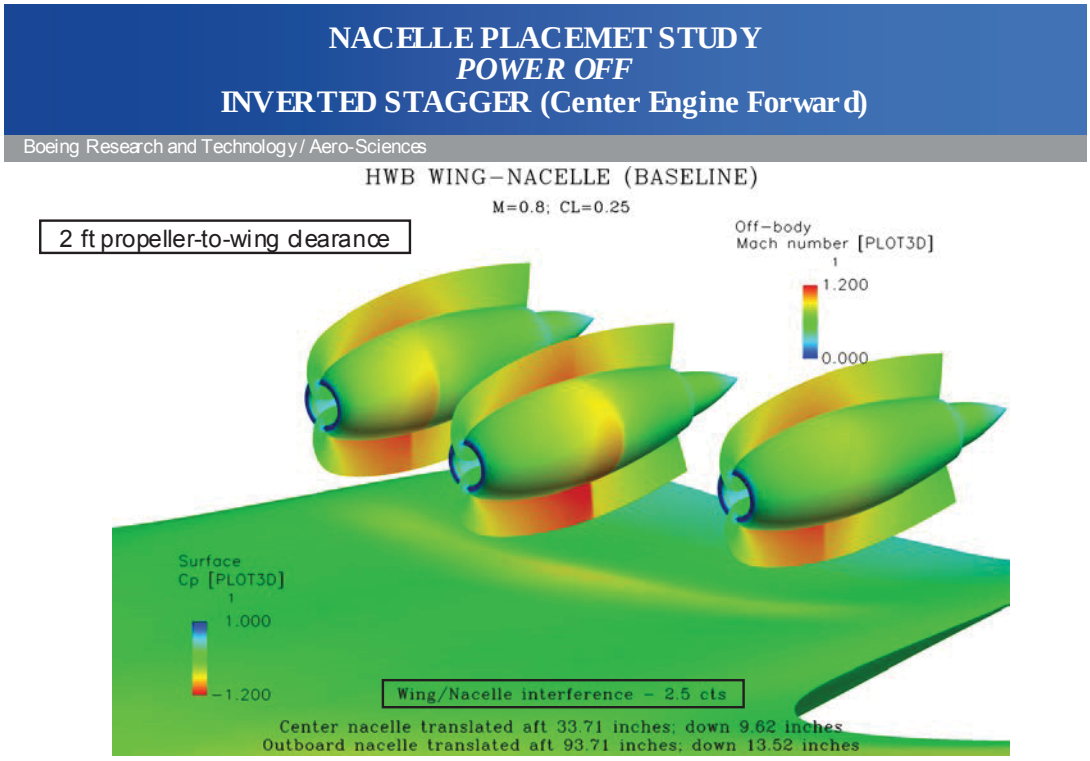

Figure 20. Preferred Stagger Arrangement for Low Noise

The low speed evaluation in Section 8 also had an influence on the nacelle and pylon configuration. The Overflow solution at stall speed with high power resulted with a significant amount of separation on the upper surface of the body with a 24” separation between the rotor tip and the body. In order to reduce the amount of separation on the upper surface of the body, the nacelle was moved up to a 36” spacing. A high speed Overflow solution for this final wing-body-nacelle unpowered configuration is shown in Figure 21. A top view of the same solution with the addition of local Mach numbers interpolated on a horizontal plane that bisects the center engine is shown in Figure 22. There is a separate legend in Figure 22 for the pressure coefficients on the nacelles and the local Mach number on the horizontal plane. Mach numbers greater than 1.0 are evident between the nacelles. The high Mach number forward of the nacelles is due to the lifting wing-body. A side view with a similar vertical plane is shown in Figure 23. Once again the local Mach number plane bisects the center nacelle. High Mach numbers and a well defined shock are evident between the nacelle and the surface of the body.

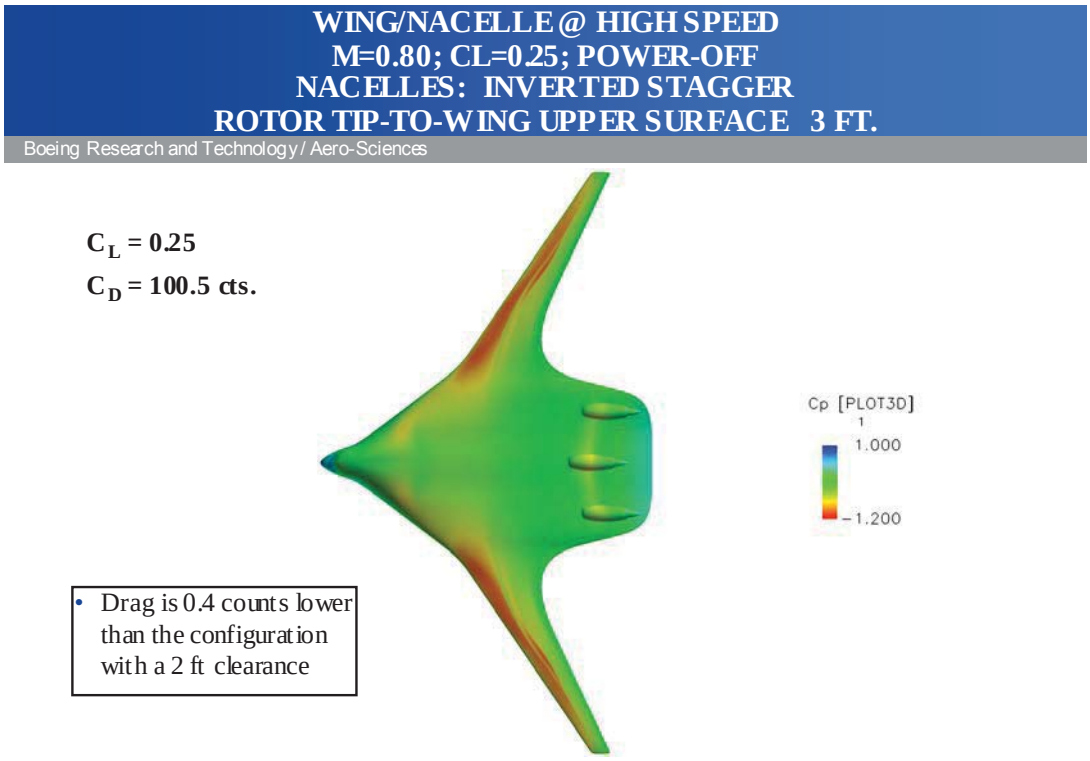

Figure 21. Wing-Body-Nacelle, 3ft rotor tip to body spacing, unpowered

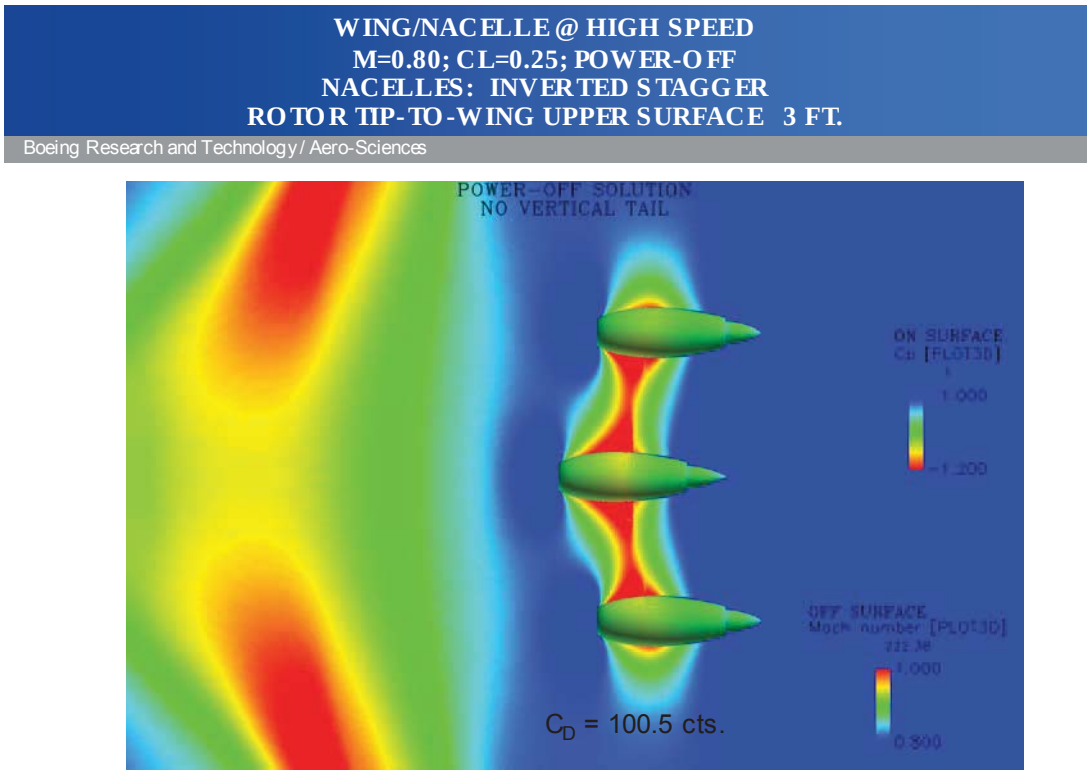

Figure 22. Wing-Body-Nacelle, 3ft Spacing, Mach number in horizontal off body plane

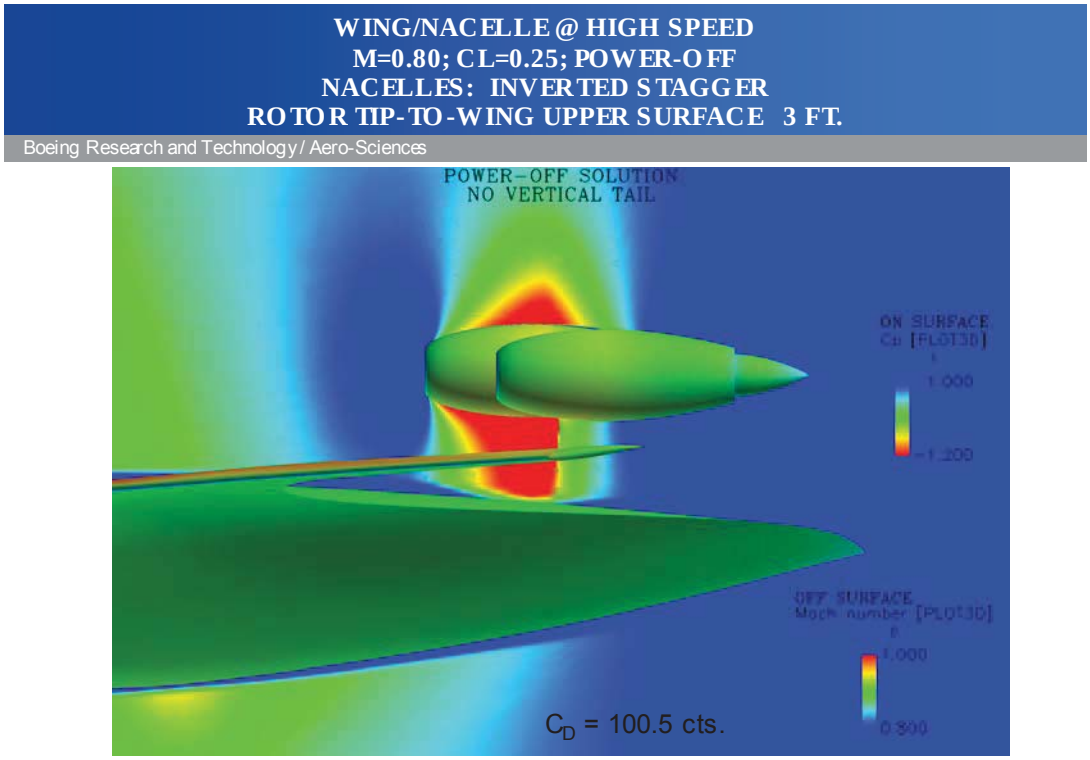

Figure 23. Wing-Body-Nacelle, 3 ft Spacing, Mach number in vertical off body plane

6 Propulsion Airframe Integration at Cruise, Powered

6.1 Method for Power

Power was simulated in the OREIO study by two methods: an actuator disk, and a rotor model. The actuator disk is a standard method of applying a pressure jump through the disk where the thrust is equal to the pressure jump multiplied by the disk area. In the case of this dual rotor geometry, both discs were assumed to produce the same amount of power per square foot. Since the forward rotor has more area, it produces more thrust. An example of an isolated nacelle with the actuator disk used for power is shown in the following Figures. The pressure jump across the disk is shown in Figure 24. The increase in velocity though the disk in shown in Figure 25. The velocity increase is smooth even though the pressure is discontinuous. The Mach number though the disk is shown in Figure 26. The Mach number jumps because the pressure jump causes a temperature jump which affects Mach number.

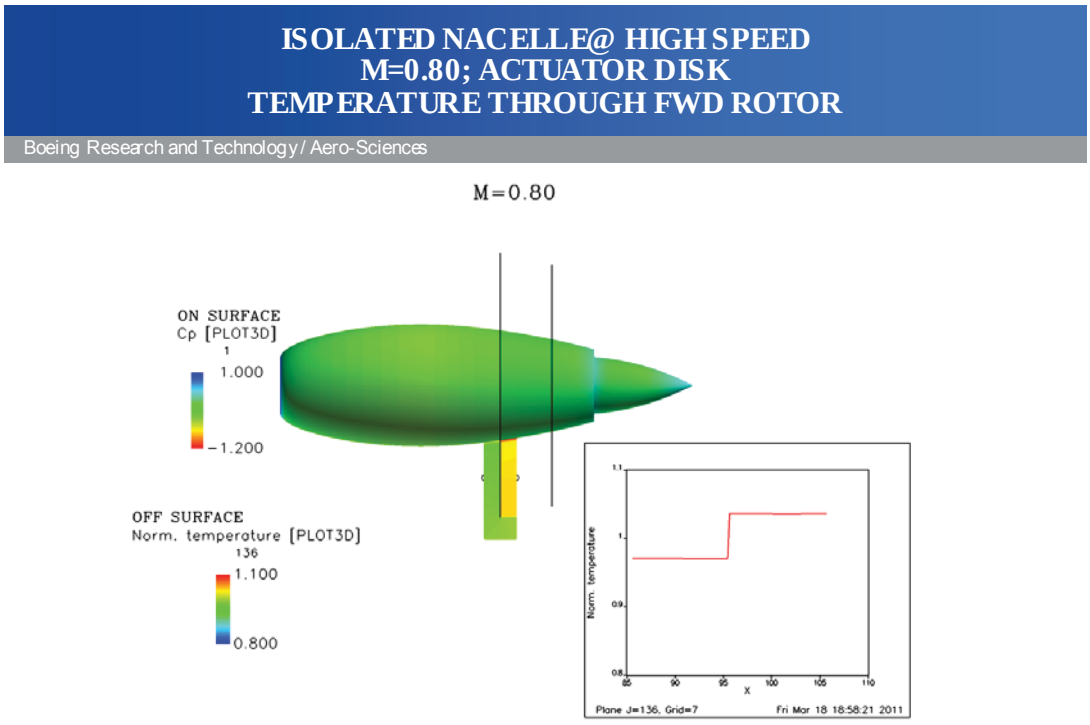

Figure 24. Pressure Jump through an Actuator Disk on the Isolated Baseline Nacelle

The rotor model is a relatively simple method that captures general rotor effects without the need to model moving blades. The rotor model adds momentum sources in the direction normal to the rotor plane to simulate thrust and tangentially to simulate blade drag. The result of the rotor model is temporally averaged thrust and swirl imparted to the flow field as momentum. The rotor model was attempted in some cases; however the rotor model needs more development for high speed (high

Mach number) cases. The actuator disk was the primary method for simulating power for the OREIO project.

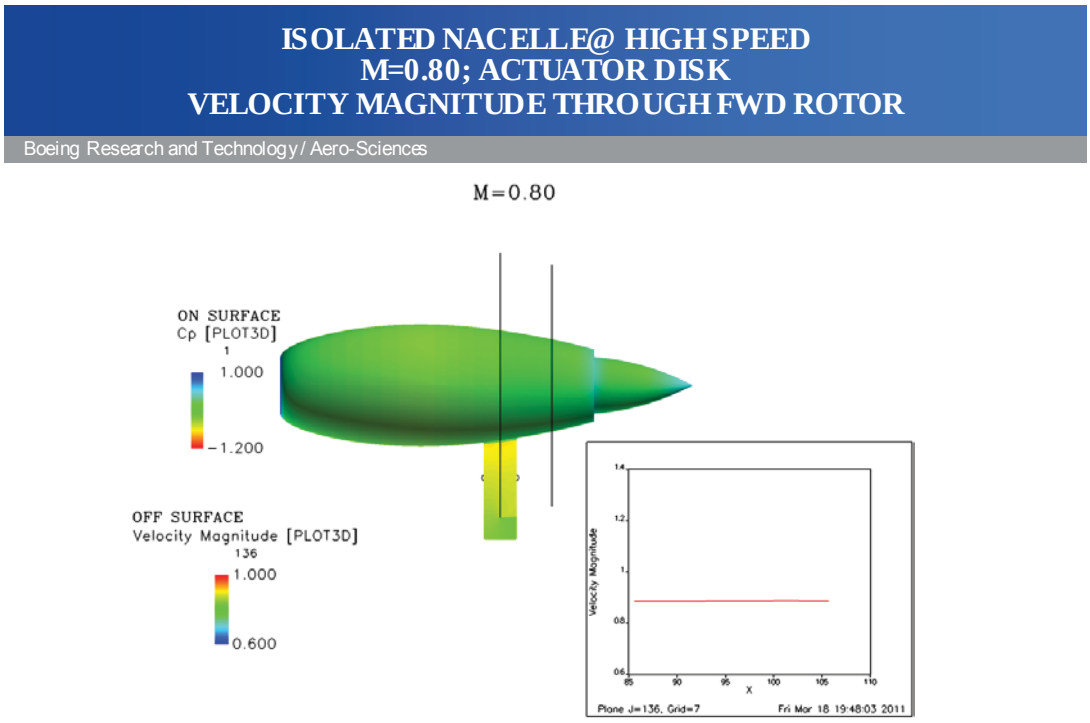

Figure 25. Velocity through an Actuator Disk on the Isolated Baseline Nacelle

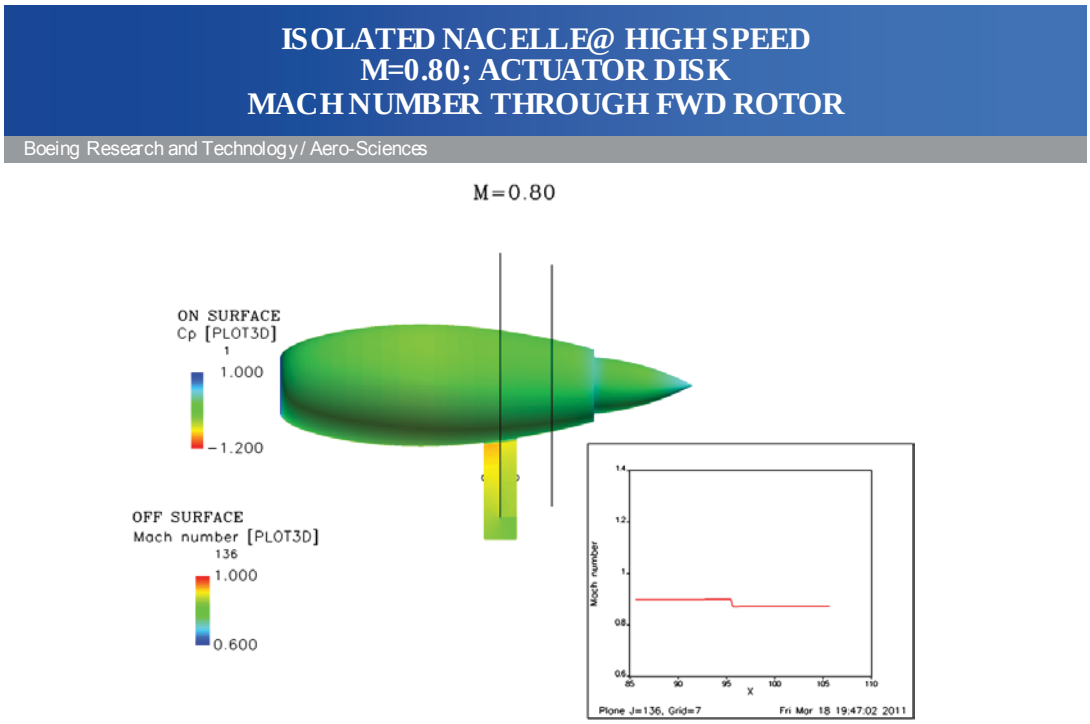

Figure 26. Mach Number through an Actuator Disk on the Isolated Baseline Nacelle

6.2 Wing-Body-Nacelle Configuration

The powered Overflow solution for the wing-body-nacelle configuration has a minor increase in drag due to power. The solution is shown in Figure 27. The drag is 0.8 counts higher than the unpowered solution shown in Figure 22. By comparing the amount of red shown in Figure 22 and Figure 27, it is apparent that the shock strength between the nacelles has increased.

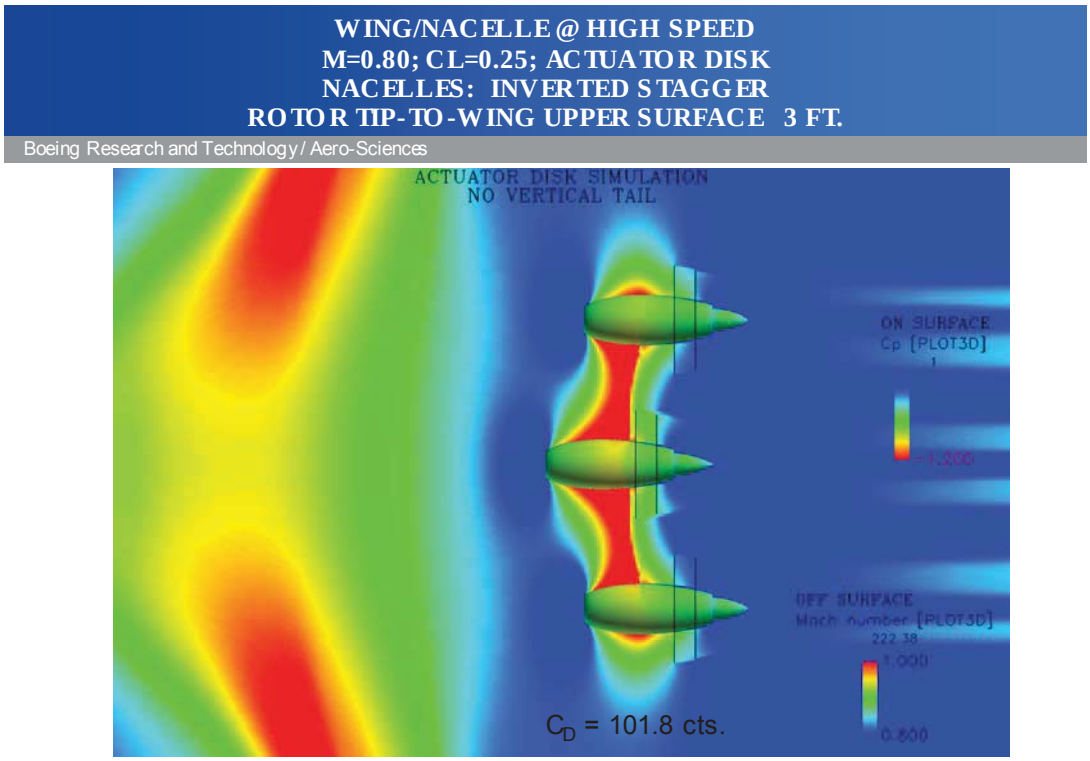

Figure 27. Wing-Body-Nacelle with power and Mach number in off body plane

6.3 Adding Vertical Tails

The revised vertical tail described in Section 5.2 was added to the configuration and twisted so that it would not lift at cruise. The new tail was placed in the same location as the old tail by matching the location of the quarter chord of the MAC for both tails. A twist distribution was developed by evaluating the flow-field of the powered wing-body-nacelle configuration. The twist angles were then checked by placing a floating vertical tail above the wing body, and finally by attaching the vertical tail and checking the lift at cruise. The intent was to have zero lift on the vertical tail at cruise. The floating vertical tails were used as a quick way to check for alignment without developing a complex grid that would be required by the intersection of the vertical tail and the body. A minor adjustment was made to the mid span airfoil twist after installation. The final rigging angles of the vertical tail are 10 degrees nose out at the root and 4 degrees nose out at the tip.

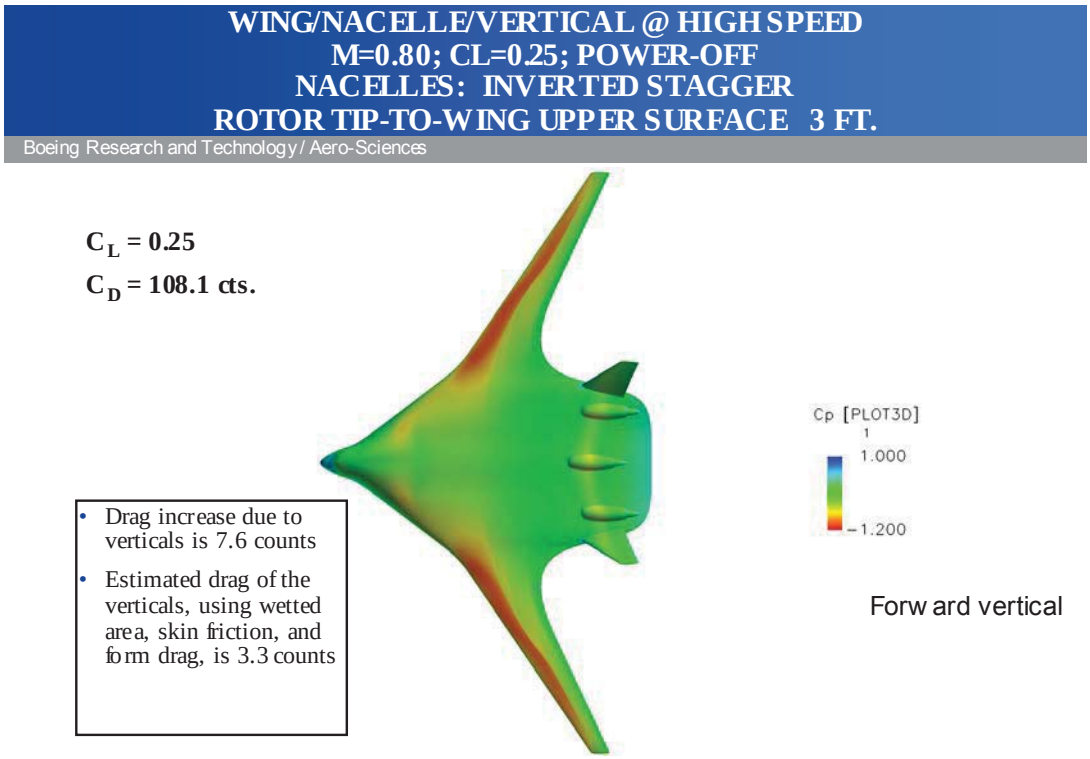

Figure 28. Unpowered Overflow Solution with Baseline Nacelles Unaligned

The initial Overflow solutions with the vertical tail had large amounts of interference drag. An unpowered solution is shown in Figure 28. The configuration drag was later reduced by aligning the nacelles as explained in Section 41.

The vertical tail was moved aft 40” to improve noise shielding for the outboard engines. NASA suggested to move the nacelles aft but did not recommend how far. A distance of 40” was used. The relative positions of the vertical tail and the engine rotors are shown in Figure 29. In the planform view before the 40” movement, the rotors were very close to the trailing edge of the vertical tail. The planform view is improved with the vertical tails 40” farther aft. However, the side view is opposite; more of the rotors are hidden with the vertical tails in the forward position than in the aft position. These pictures would look different if real swept blade geometry was used. Another thing to consider is the direction of noise propagation from the rotors; the aft position may be better.

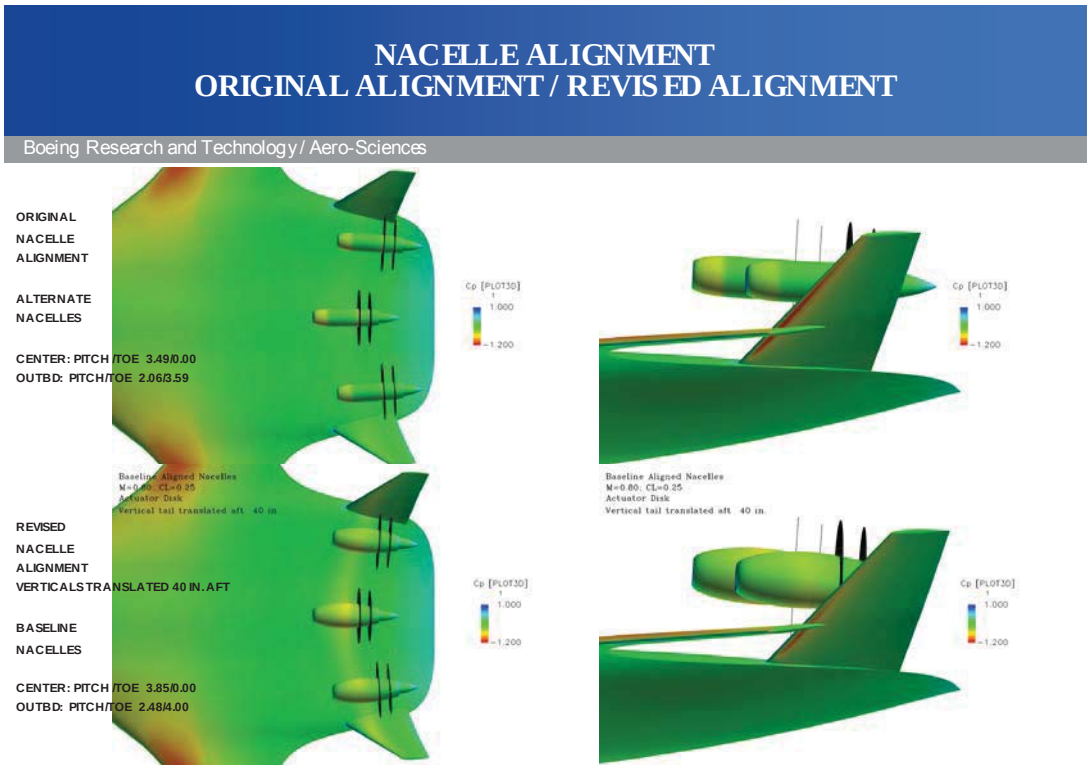

Figure 29. Relative Position of the Engine Rotors and the Vertical Tails

6.4 Aligning the Nacelles

The nacelles were aligned normal to the cruise onset flow to reduce the amount of flow distortion into the rotors. It was assumed alignment was necessary to provide high propulsive efficiency, long rotor life, and low cabin noise. All three goals would be impacted if the rotors were misaligned and experiencing a loading cycle with each revolution. Pointing the thrust vector away from the direction of flight will also reduce cruise efficiency but it was assumed that subjecting the rotors to cyclic loading would be worse. These assumptions need to be confirmed by an engine manufacturer.

The pitch and toe angles required for alignment were larger than expected. The rigging angles for the final configuration are listed in Table 7.

Table 7. Nacelle Rigging

Nacelle Rigging

	Toe Angle	Incidence Angle
Center Engine	0.00	3.85
Outboard Engine	2.48	4.00

Drag of the wing-body-nacelle-vertical tail configuration was reduced by aligning the nacelles. Aligning the nacelle is a powerful method to reduce drag. A significant drag reduction occurred for aligning the nacelles for both the baseline and alternate nacelles, for powered and unpowered cases, and for cases using the rotor model or the actuator disk to simulate power.

6.5 Wing-Body-Nacelle Configuration

The final configuration uses the baseline nacelles aligned as described in Section 7.4 with the aft location for the vertical tails as described in Section 7.3. Overflow solutions for this configuration are shown in Figure 30. The interference drag due to power is only 0.5 counts. The drag rise predicted from Overflow is shown in Figure 31. The drag rise is similar for both the powered and unpowered solutions. Drag divergence occurs at about a Mach number of 0.80. The largest difference in drag between the powered and unpowered cases is about 1.5 counts at low Mach numbers.

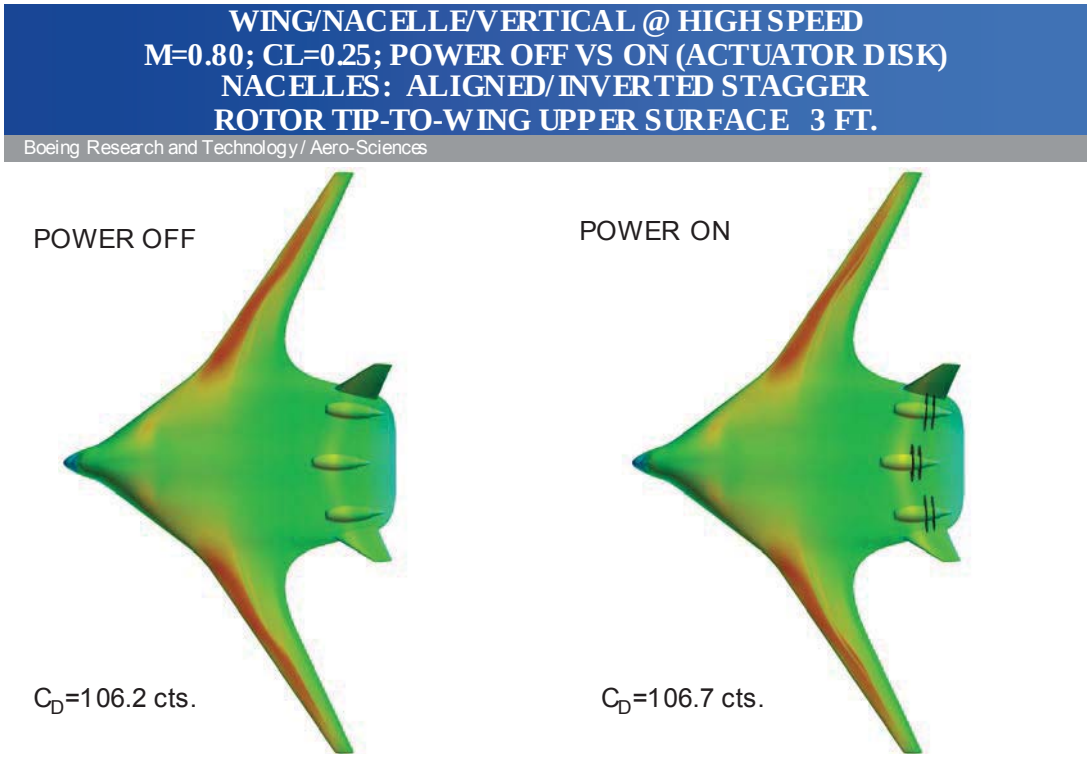

Figure 30. Overflow Solution, Concept Design Data Config, Unpowered & Powered

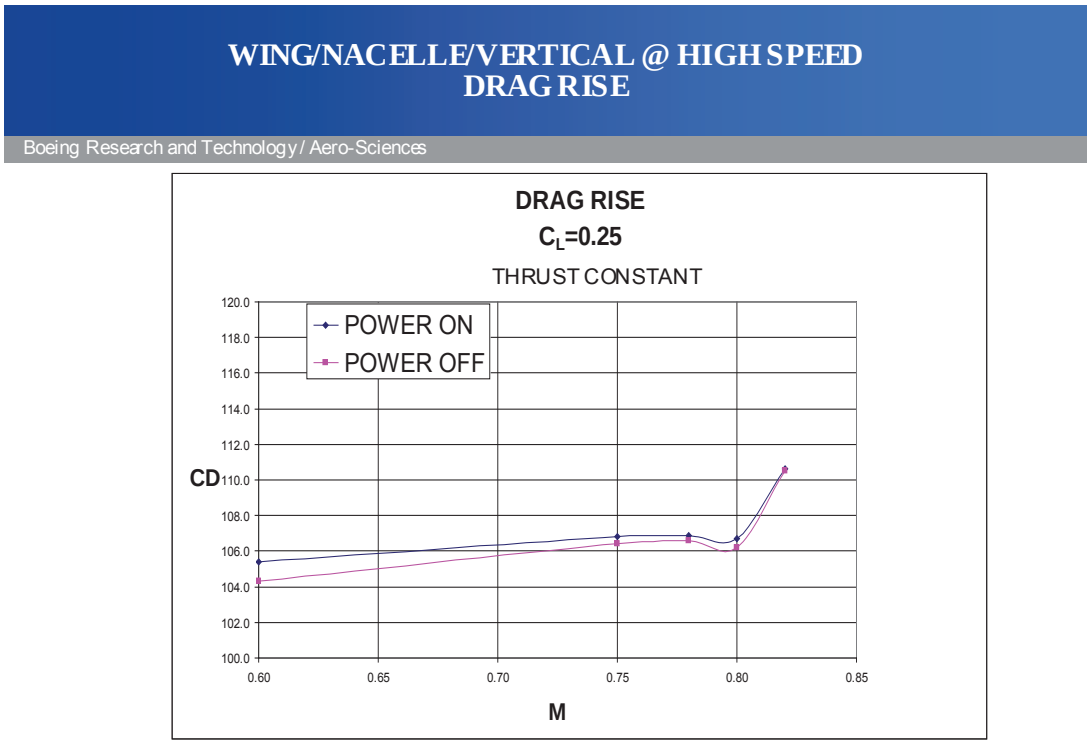

Figure 31. Drag Rise with Mach number from Overflow, Powered and Unpowered

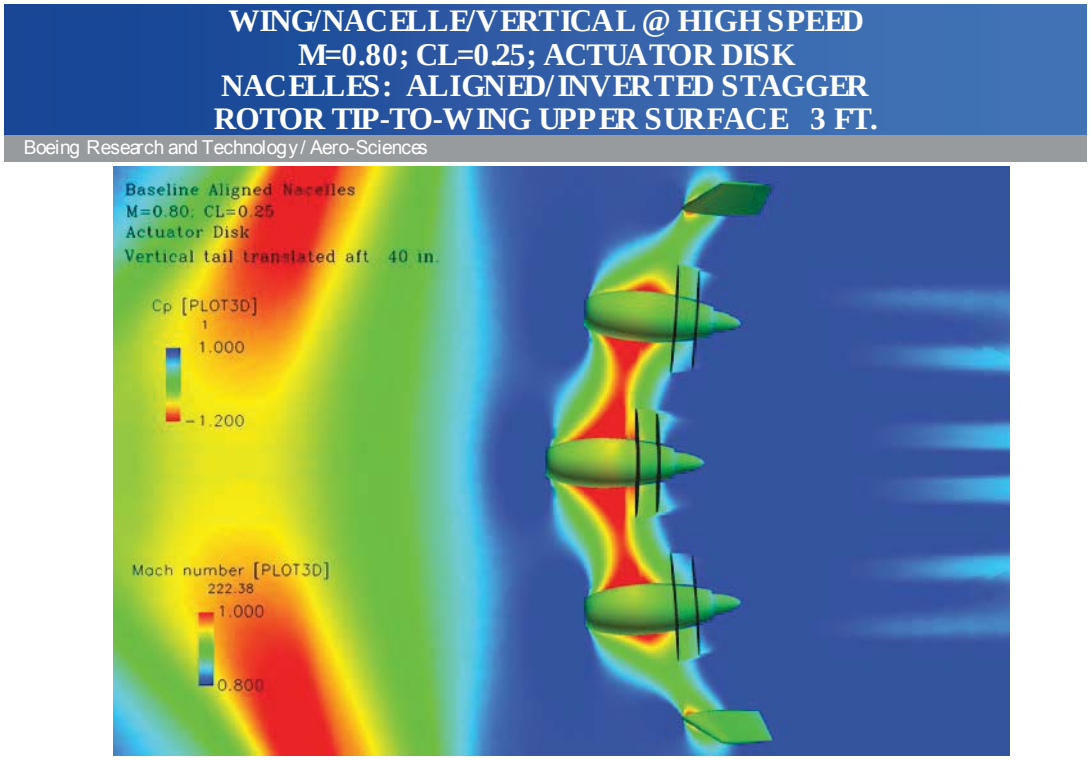

Figure 32. Final Configuration off body flow field in a horizontal plane

The flow field between the nacelles and the vertical tail has regions of high Mach number but the magnitude is less than before the nacelles were aligned. The off body flow field in a horizontal plane is shown in Figure 32. There is less air flow over Mach 1.0 in Figure 32 than in Figure 27.

The alternate nacelle has less drag than the baseline nacelle. An Overflow solution for the alternate nacelle is shown in Figure 33. The drag is 3 counts lower with the alternate nacelle than with the baseline nacelle. In this case 3 counts of drag is very close to 3% of cruise drag making the alternate nacelle a clear winner. The problem is that the large diameter of the baseline nacelle is not designed for the high Mach numbers that exist above the wing-body. The baseline nacelle is designed to condition the flow for the rotors when flying isolated at Mach 0.72. It is not clear which nacelle has the best flow field for the rotors when installed.

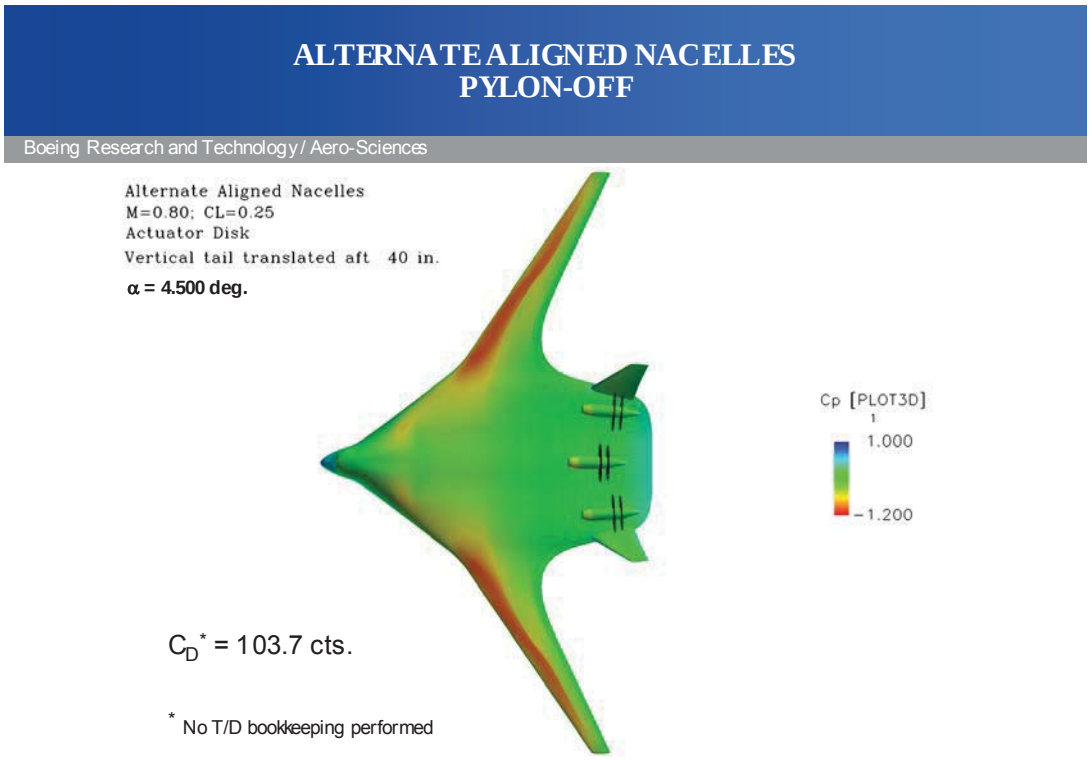

Figure 33. Overflow Solution for the Alternate Nacelle aligned with local flow

6.6 Adding Pylons

Pylons have been avoided so far in this study. The previous section reviewed the final configuration for the study; it did not have pylons. Several attempts were made to add pylons to the configuration near the end of the study. There was no effort to develop a final pylon that could be considered acceptable for this configuration. The quick looks were just to see how bad the problem was.

Two simple pylons were created. The pylons were created from a simple symmetric airfoil with a 12% thickness to chord ratio. One pylon has a 15 degree sweep and

the other has a 30 deg sweep. The 15 degree swept pylon was used because it would be closer to what was drawn on the 3-view where the pylons are nearly vertical so that they can provide better support for the engine. The 30 degree swept pylon was used because it is closer to the sweep that would be required for a 12% thick wing at Mach 0.80. The outboard pylons were toed out 4 degrees to align them with the local onset flow.

The depth of the spars assumed for the original OREIO configuration in Figure 7 is 20". The pylons that were used for the CFD evaluation will only support spars that are about 12" deep.

The Overflow solutions with pylons have significant amounts of interference drag. The solutions are shown in Figure 34. The configuration with the 15 degree swept pylon has a total drag of 126.2 counts. The configuration with the 30 degree swept pylon has a total drag of 117.1 counts. This is compared to 106.7 counts without the pylons. There is a significant amount of separation for both configurations but it is certainly worse for the 15 degree swept pylon. The 30 degree pylon has a classic aerodynamic advantage with higher sweep which is more appropriate for the cruise Mach number, but it may also have had a smoother progression of cross sectional area through the aft body region.

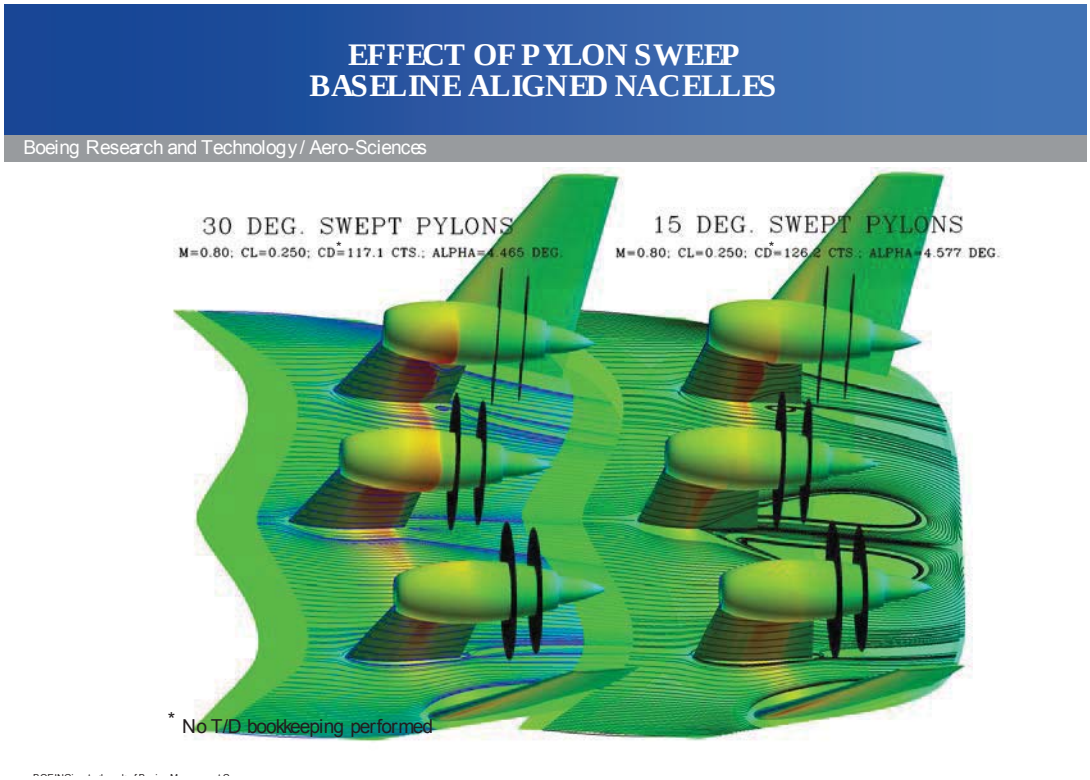

Figure 34. Overflow Solutions with Pylons for the Baseline Nacelle

The alternate nacelle had less drag when coupled to the 30 degree swept pylon. The Overflow solution for the baseline and alternate nacelles with the 30 degree

swept pylon is compared in Figure 35. The solution with the alternate nacelle has 4.9 counts less drag.

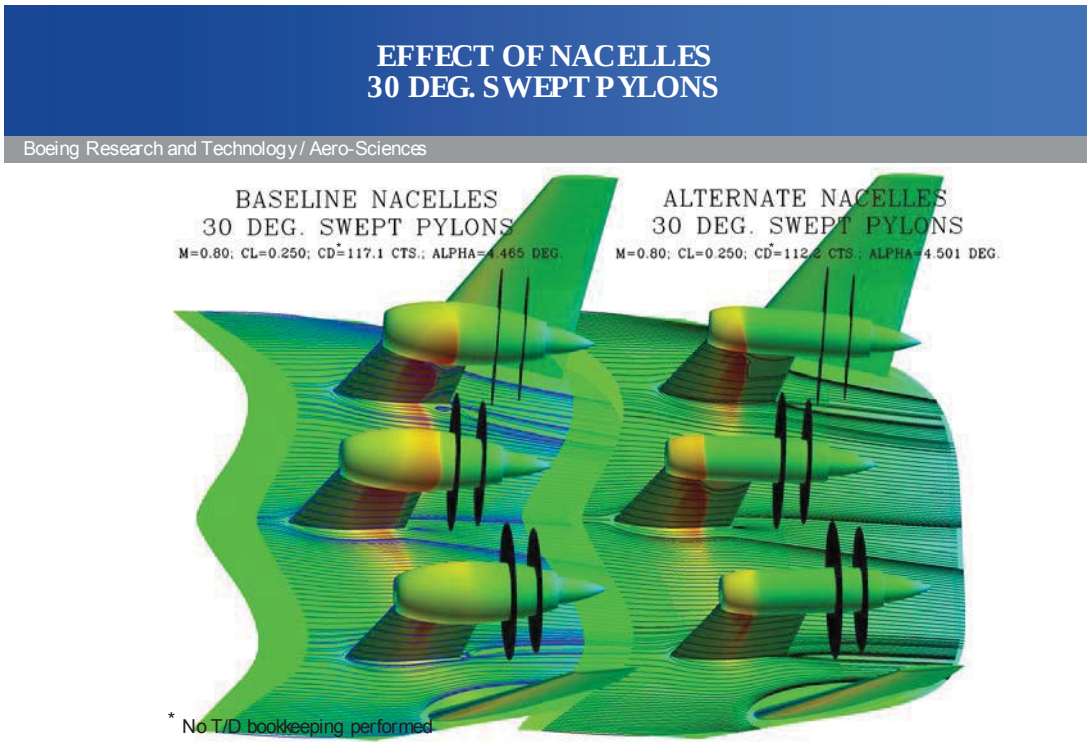

Figure 35. Overflow solutions with pylons for the baseline and alternate nacelles

6.7 High Speed Drag

An estimate of the high speed interference drag was developed. The total drag from Overflow for the wing-body-nacelle configuration was 106.7 counts. The interference drag of the wing-body-nacelle configuration is about 5 counts, based on an estimate of the vertical tail drag and the isolated wing-body and isolated nacelle drag from Overflow. The interference for the installations with the pylon are much higher. A decision was made to include an interference drag level of 4.5 counts for the nacelle and pylon installation. This includes 3 counts of interference for the nacelles and 1.5 counts of interference for the pylons. The 4.5 count increment was included in the total drag build up (Figure 65).

7 Propulsion Airframe Integration, Low Speed, Powered

7.1 Low Speed Flight Conditions

One of the goals established early in the OREIO study was that there should be no separation near stall. It was assumed that at the beginning of a takeoff run, the high power though the rotors combined with the low speed would lead to upper surface separation; this would be acceptable as long as there was no separation when the aircraft was flying. Separated airflow near the rotors could cause a non-linear response from the center elevon. It would also increase drag; the engine would have to produce more thrust to compensate for the drag which would increase noise. To ensure that there was no separation present when flying, the slowest flying speed possible was evaluated, this is the stall speed. Since the stall speed has not been established for the OREIO configuration an assumption was made that the stall speed would be at about Mach 0.15. A leading edge device such as a slat or Krueger has not been defined either so a solution for the cruise wing at an angle-of-attack of 10 degrees was used. A second condition was also evaluated. The second condition represented the takeoff climb out speed. This was a faster condition that was just used for comparison with the stall speed case because it was difficult to eliminate all the separation from the stall speed case. The speed used for the takeoff climb out condition was Mach 0.20.

The thrust used for the Overflow evaluations came from the data provide by NASA. The thrust levels from NASA for Sea Level static and Mach 0.25 were 37,000 lbs and 29,000 lbs. The thrust levels for CFD were interpolated from this data. The thrust level for Mach 0.15 and 0.20 were 32,200 lbs and 30,600 lbs.

7.2 Wing Body

Powered Overflow solutions for the wing body had significant upper surface separation. Power off and power on Overflow solutions at stall are shown in Figure 36. For this comparison the angle-of-attack for the power on solution was reduced so that both solutions were at the same lift coefficient. The amount of separation is considered unacceptable. The effectiveness of the elevon behind the engines will be reduced and may be non linear.

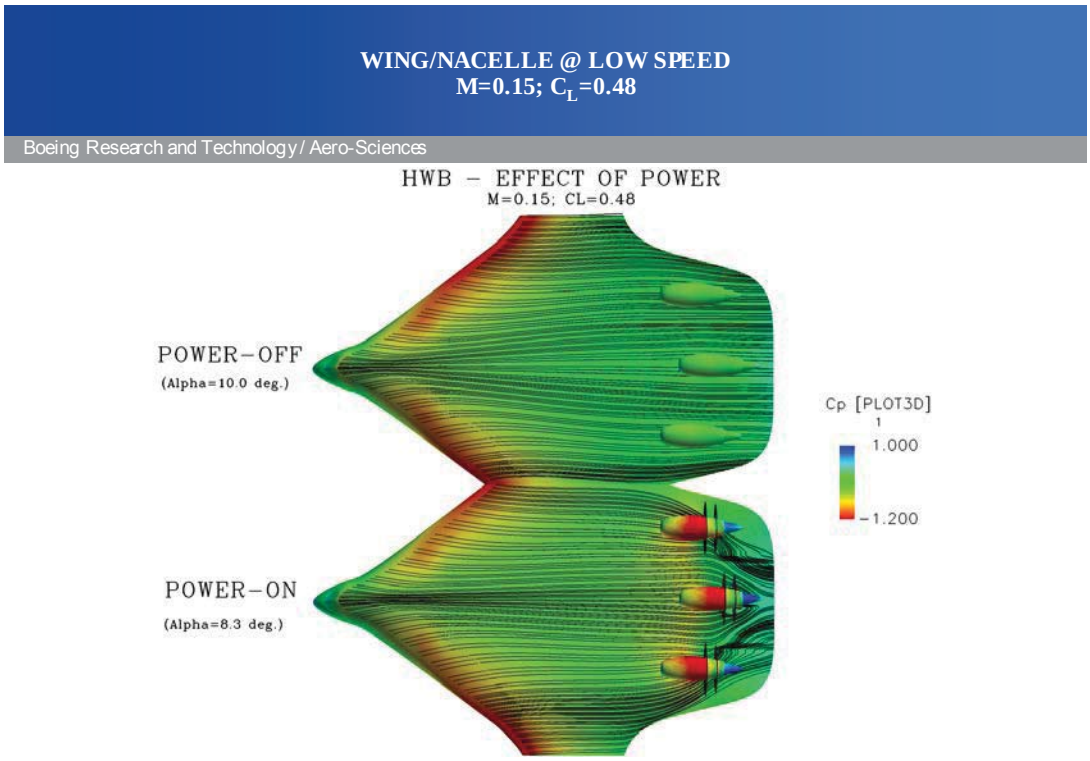

Figure 36. Power off and Power on Overflow Solutions at Stall

The Overflow solution was evaluated to see if other characteristics of the flow field could help to understand the reason for the separation on the upper surface of the body. Streamlines were traced up and down stream of the rotor tips to develop stream tubes of airflow that go though the rotors. The stream tubes are shown in Figure 37. The area of the stream tubes decreases rapidly as the airflow is accelerated through the rotors. On the surface of the body the high power accelerates the airflow forward of the rotors, but then when the cross sectional area of the stream tubes decrease at the rotors, there is a large adverse pressure gradient. The pressure gradient on the upper surface of the body is shown in Figure 38. The adverse pressure gradient is causing the separation on the body.

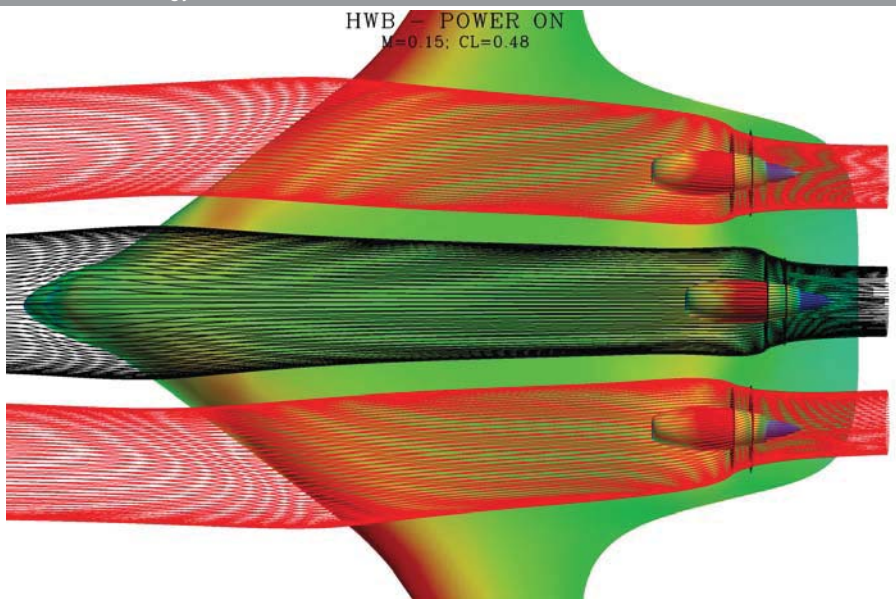

Figure 37. Contracting Streamtubes Caused by High Power

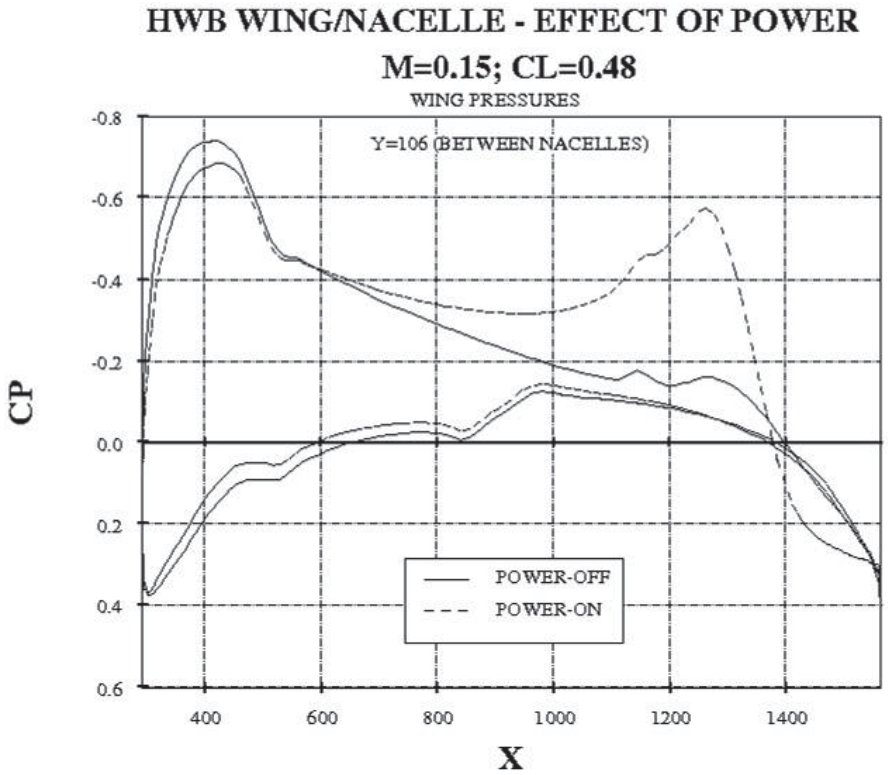

Figure 38. Severe Adverse Pressure Gradient Caused by High Power

The upper surface separation was similar for two different methods of simulating power. The separation pattern from an Overflow solution using the rotor model was compared to the pattern from a solution using an actuator disk and is shown in Figure 39. There are some differences but the area that is separated is generally the same in both solutions.

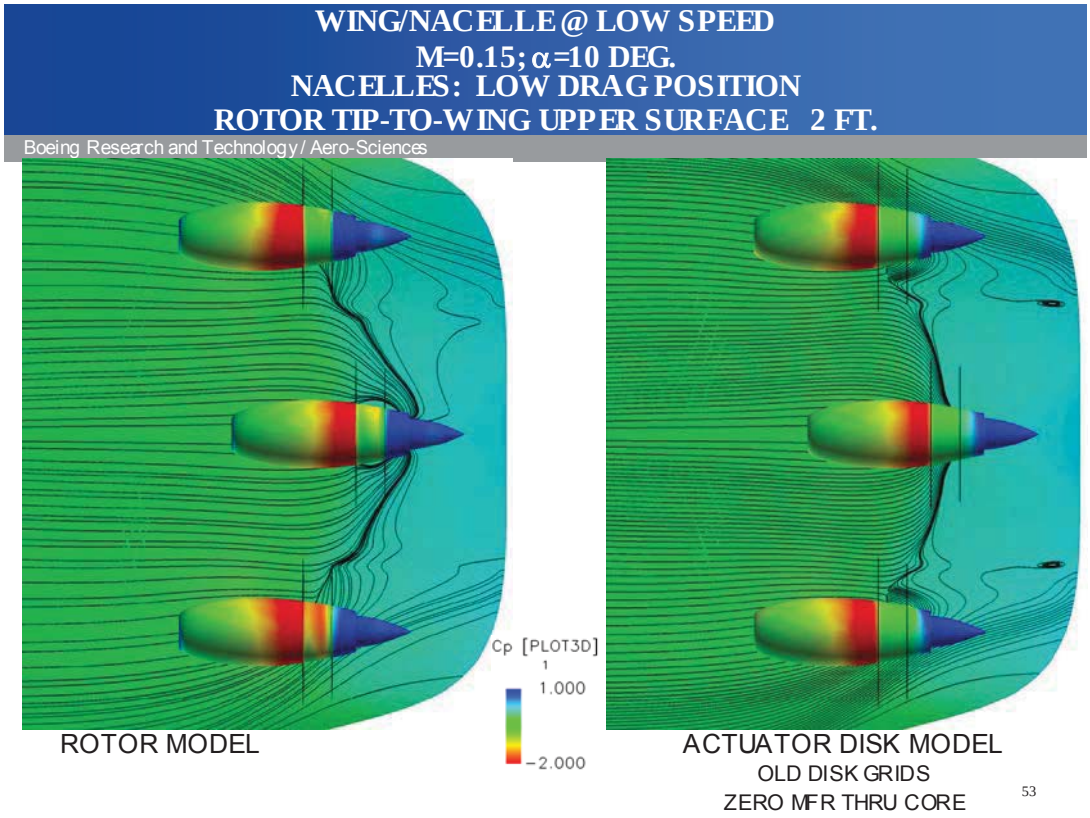

Figure 39. Similar Separation Patterns from Different Methods for Simulating Power

The Overflow solutions that were discussed so far were completed early in the study before the engine stagger was changed by moving the center engine forward. The separation pattern with the center engine staggered forward is different than what was shown so far; this pattern is shown in Figure 40. There is still severe separation but it might be slightly better than what is shown in Figure 39.

In order to relieve the separation problem the engine was moved up so that there was a distance of 3 ft between the rotor tip and the body upper surface. The upper surface separation pattern with a 3 ft clearance is shown in Figure 41. The separation pattern has improved but was not completely eliminated.

The decision to increase the distance between the rotor tip and the body was made after consulting with others on the project to determine if the stall condition was too severe and maybe an unrealistic case to evaluate. The conclusion was that it was not unrealistic. If this airplane is built and stall tested, it will be flown to stall at high power and all the control surfaces must have good effectiveness and a linear

response. In order to have the proper response there cannot be a large amount of separation on the upper surface of the body. Flow control on the upper surface of the body is another option to reduce separation that was discussed. Flow control may be effective but is beyond the scope of this study.

A second faster condition was evaluated to see how quickly the separation would decrease with speed. The condition selected is the takeoff climb out speed. It was selected because it is within the typical operation envelope of the aircraft. The stall speed is not within the operational envelope of the aircraft, only the flight test aircraft will be evaluated at stall. The takeoff climb out condition is at a speed of about Mach 0.20. The angle-of-attack would also be slightly lower, but the angle-of-attack of 10 degrees was maintained for consistency; the only change would be speed and thrust. The flow solution reflected the same engine and power setting. The thrust was only changed because of the typical lapse rate that would be experienced. The upper body airflow patterns from the Overflow solutions from Mach 0.15 and Mach 0.20 are shown in Figure 42. There is certainly less separation at the faster speed. It is difficult to say that there is no separation, there is no reversed flow, but there are streamlines that converge in a manner that may indicate that off body vortices are present. Further configuration changes due to low speed separation were stopped after seeing these results. Some additional work was done to help understand the problem, but there were no configuration changes. The configuration with a distance of 3 ft between the rotor tip and the body upper surface became the baseline for the remainder of the study. The configuration being evaluated at cruise conditions was also changed to the 3 ft clearance.

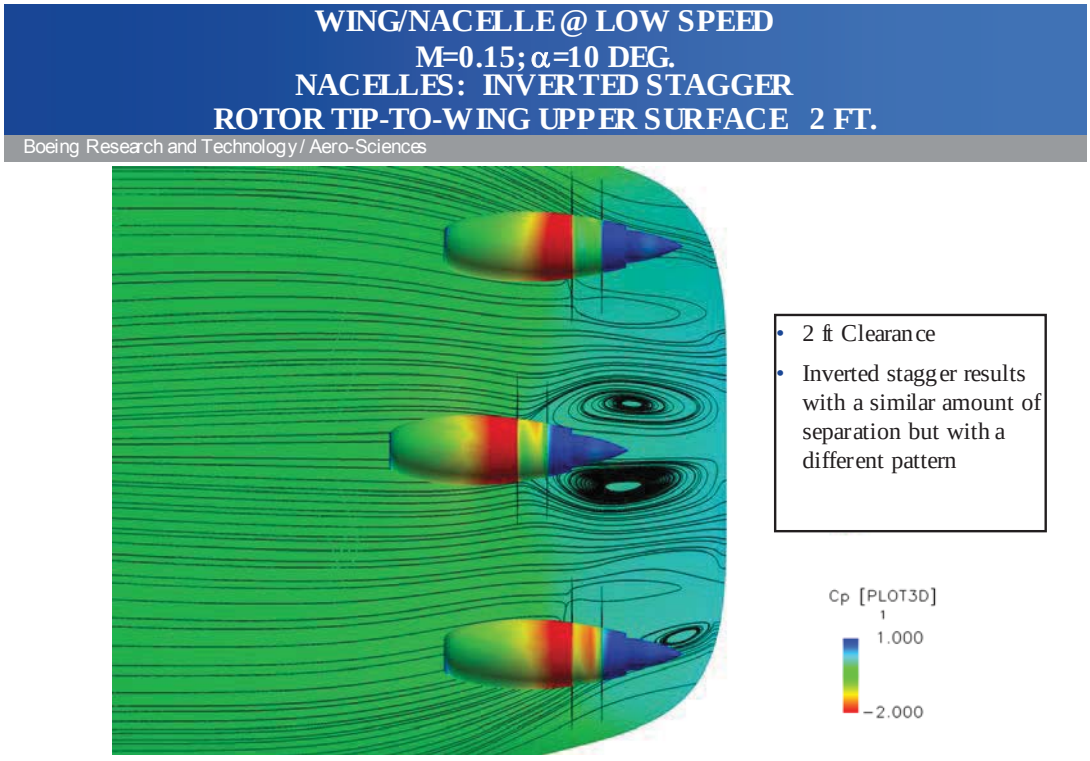

Figure 40. Separation Pattern with the Center Engine Forward

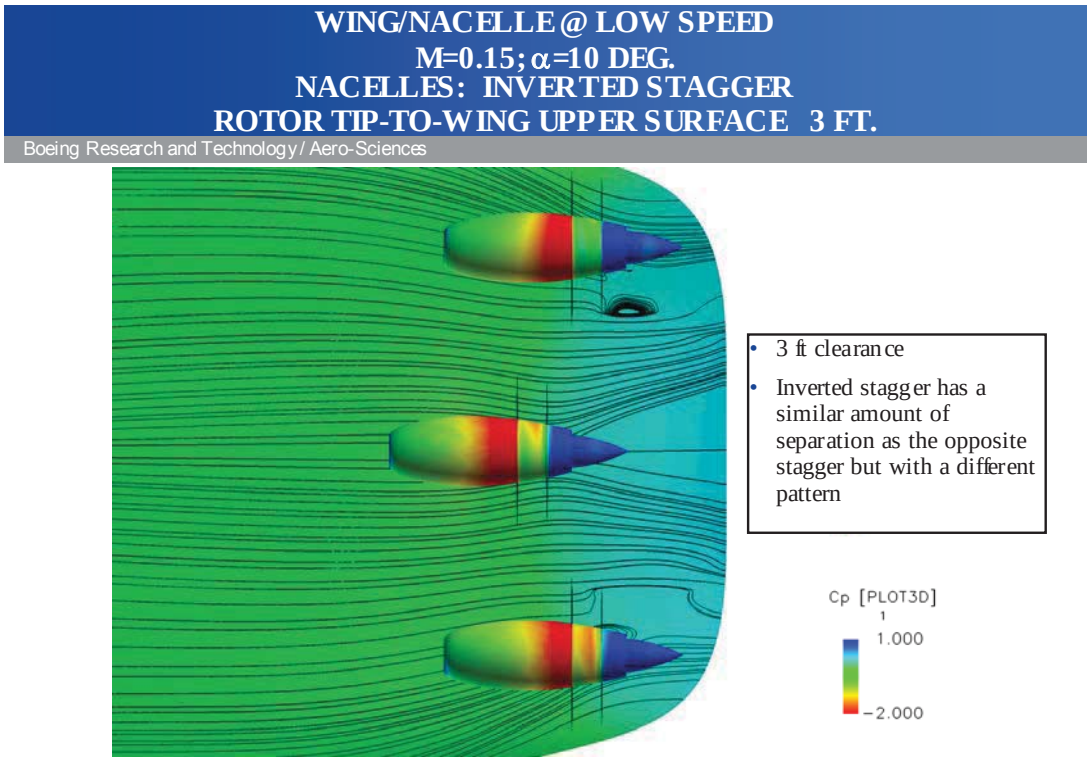

Figure 41. Separation Pattern with a 3 ft Clearance between Rotor Tip and Body

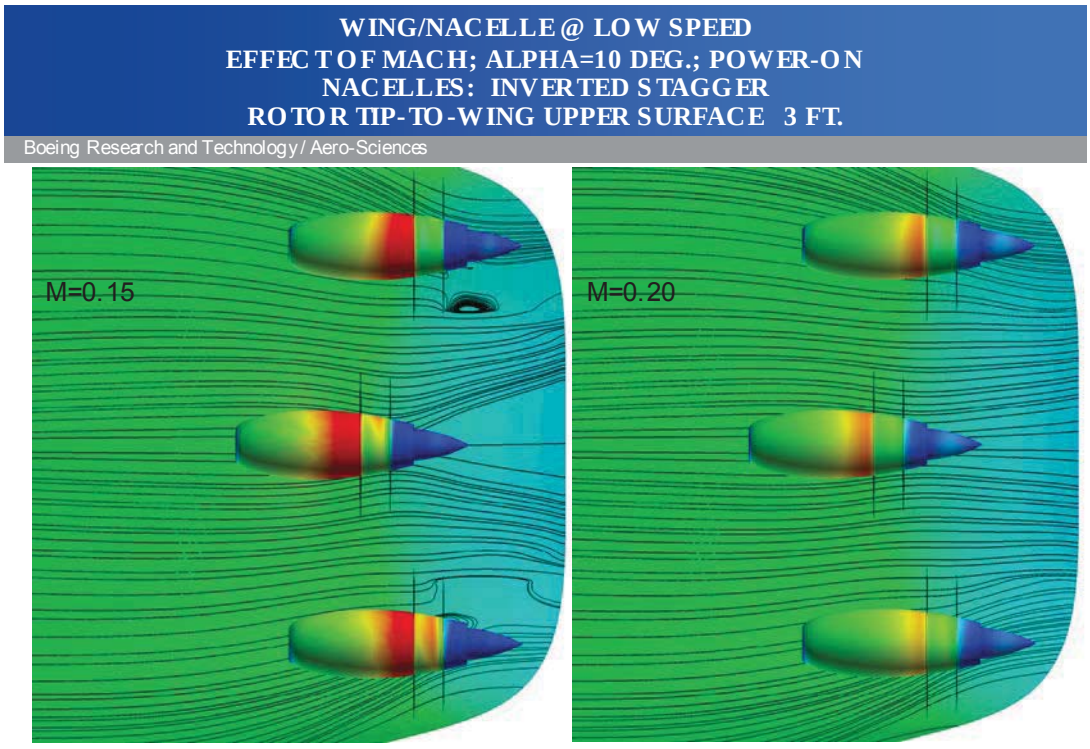

Figure 42. Reduced Separation at Higher Speed

7.3 De-rated Thrust

A brief study was done to see how quickly the upper surface separation problem improved with reduced thrust. The nacelles used for this study had capped off inlets and exits as explained in Section 8.5. Four Overflow solutions were completed at an angle-of-attack that was approximately 8 degrees but varied slightly so that a constant lift coefficient was maintained. The stall condition was used for this evaluation. The stall condition is at a Mach number of 0.15 and has a significant amount of separation on the upper surface of the body. The results are shown in Figure 43 through Figure 46. The first solution is unpowered and shows that the upper surface of the body has attached airflow at this condition. The first solution with power show significant separation. As power is reduced to 90% and then 80% of full takeoff power the separation improves but is not eliminated. Something else will have to be changed on the configuration, if the separation must be eliminated to provide the proper control effectiveness from the center elevon. Flow control through suction or blowing is one possibility.

The aircraft performance resulting from de-rating the engine thrust was checked. The configuration can meet the takeoff field length requirement of 10,500 ft with a SLST of 33,870 lbs or a de-rate of about 90%.

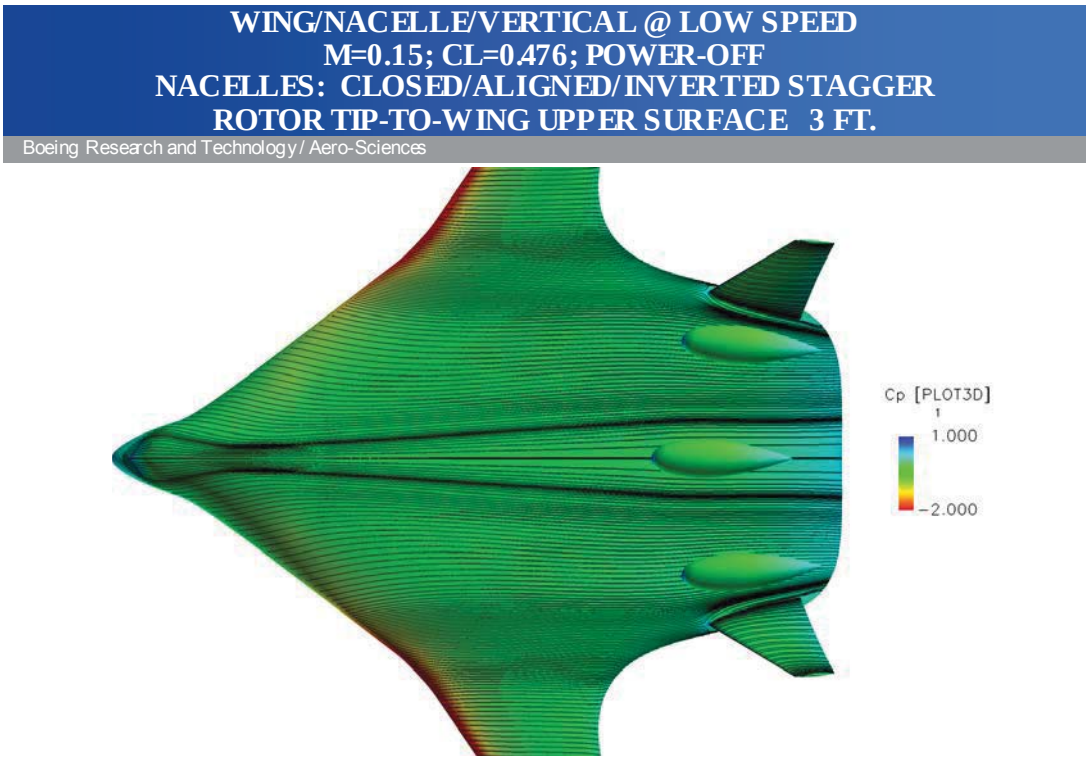

Figure 43. Final Configuration, Power off with Closed Nacelles

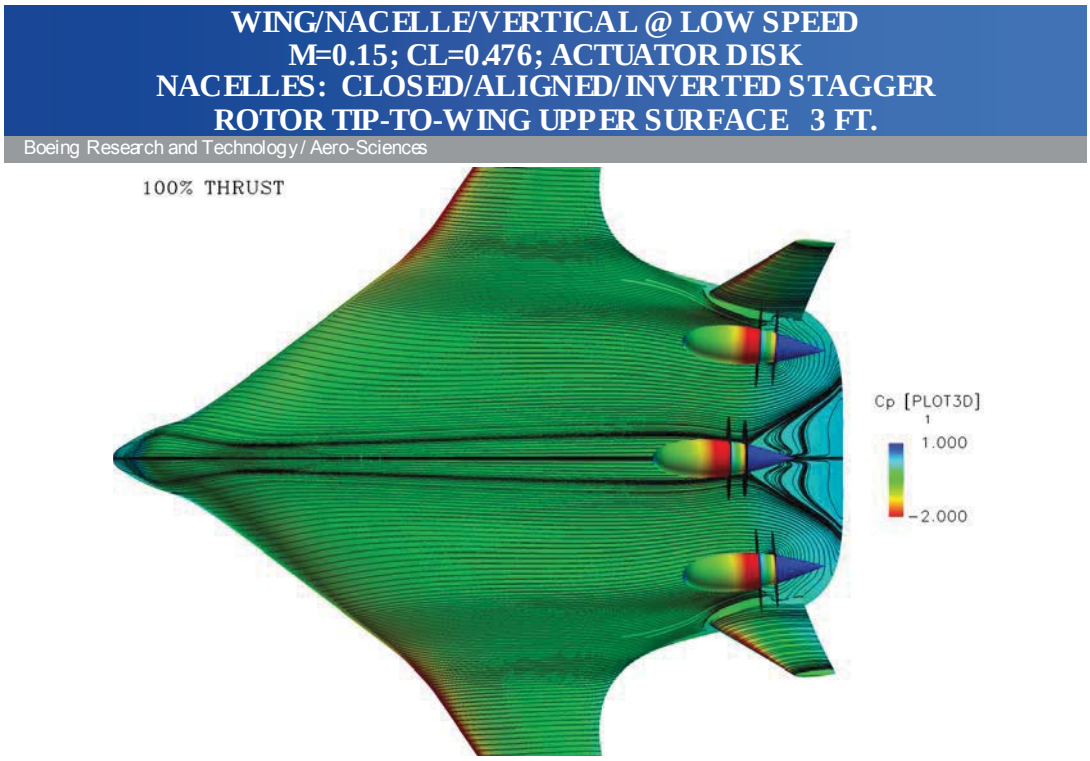

Figure 44. Final Configuration, 100% Thrust with Capped Nacelles

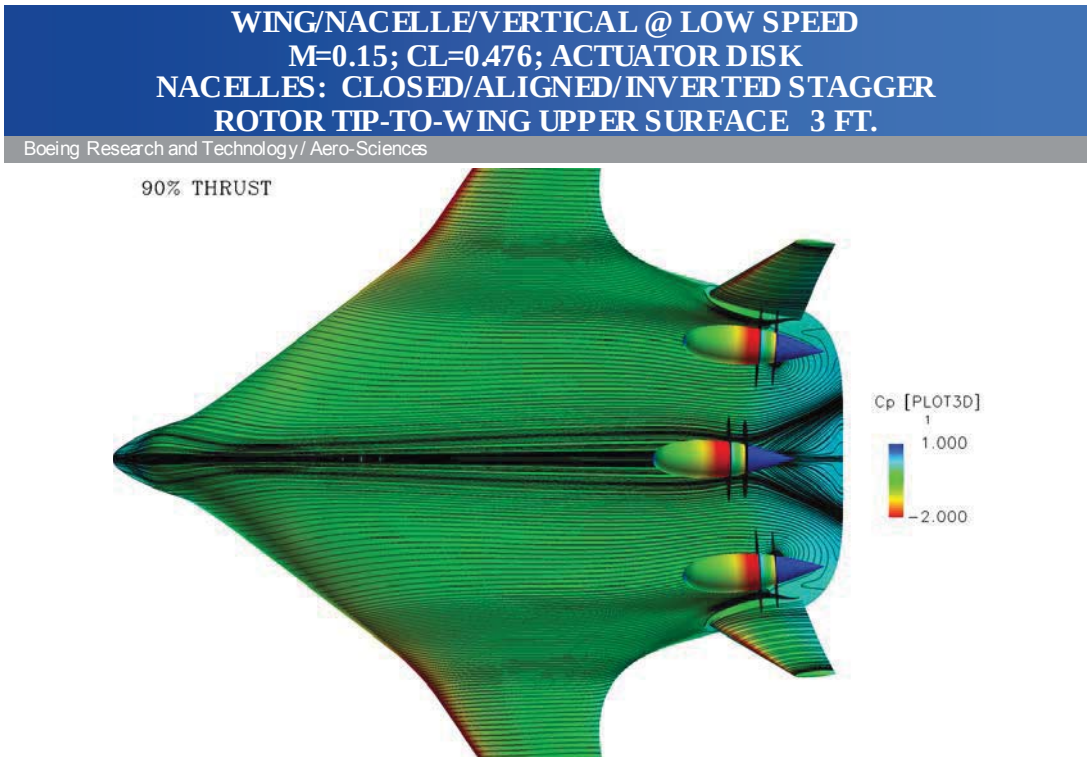

Figure 45. Final Configuration, 90% Thrust with Capped Nacelles

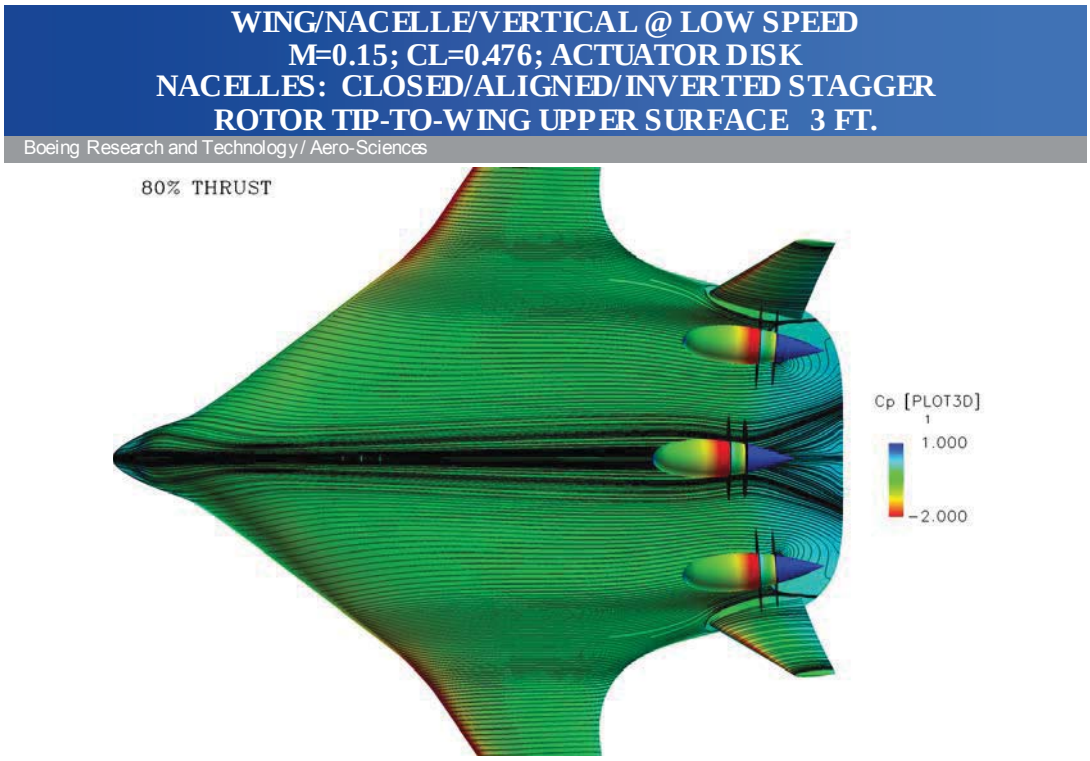

Figure 46. Final Configuration, 80% Thrust with Capped Nacelles

7.4 Deflected Elevon

The control effectiveness of the center elevon was evaluated using the Overflow CFD code. The center elevon was deflected both trailing edge up and trailing edge down, at a Mach number of 0.15 and 0.20. The upper surface separation and the pitching moment change for each solution were evaluated. This work was completed before the nacelles were aligned. The alternate nacelle was used because at that time in the study it was felt that the alternate nacelle would become the primary nacelle. The nacelle alignment and shape will not have much of an effect on the results; the key flow feature is the large pressure jump through the rotors required to produce the thrust required for takeoff. Results are shown in Figure 47 through Figure 50. Flow separation is present at a Mach number of 0.20 for the center elevon at deflection angles of 0.0, 10.0, and 20.0 degrees trailing edge up. At 0.0 degrees of deflection the amount of separation is small, similar to Figure 42, but the amount of separation increases as the trailing edge is moved up. The pitching moment provided by deflecting the center elevon is plotted in Figure 50. The pitching moment is surprisingly linear for all three elevon deflection angles. The elevon also produces similar levels of pitching moment and at both Mach numbers and it has already been shown that there is more separation at the lower Mach number. The question of the effectiveness of the center elevon with power requires more investigation.

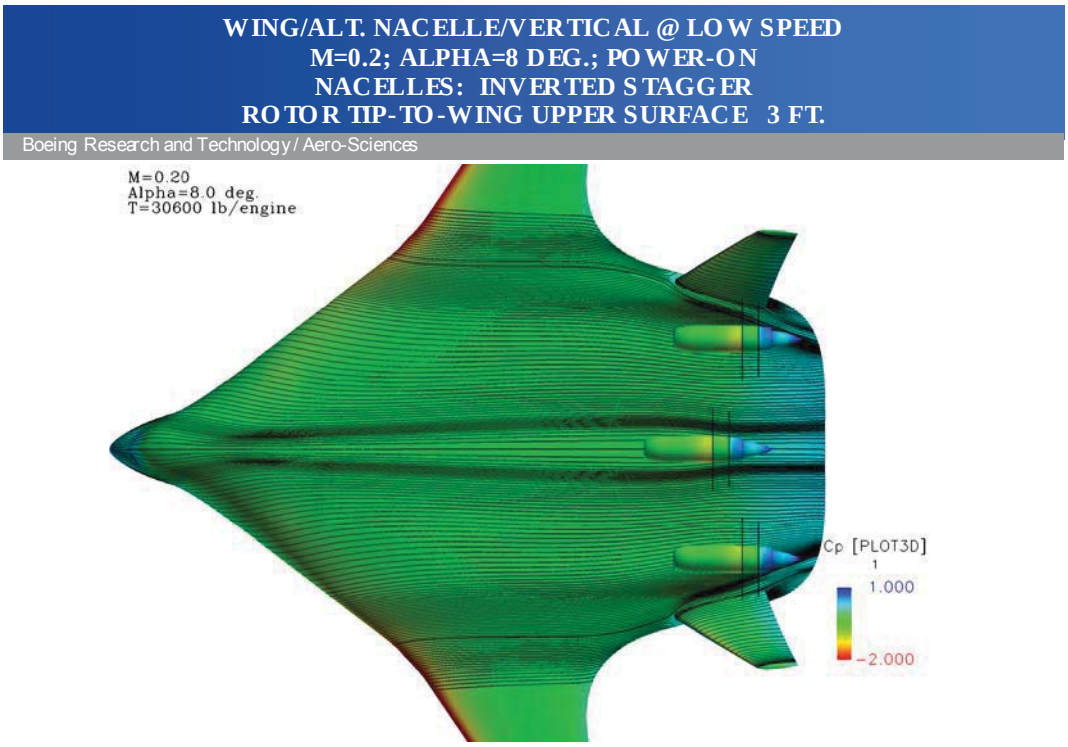

Figure 47. Powered Low Speed Configuration, Elevon at 0.0 Degrees

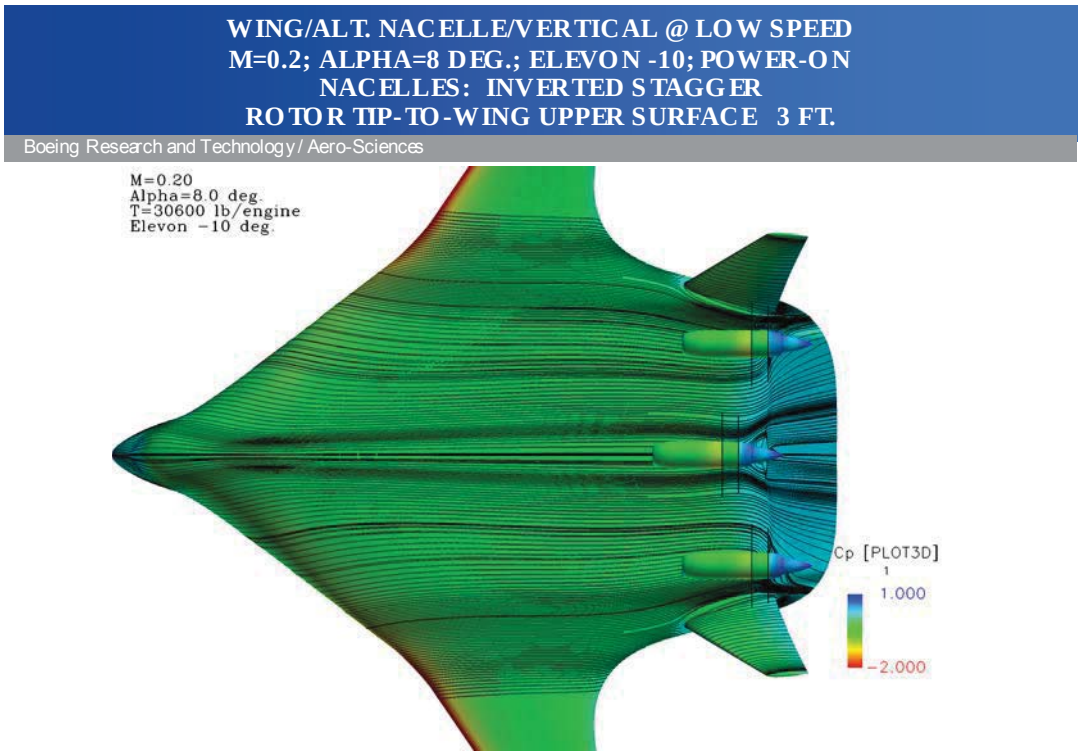

Figure 48. Powered Low Speed Configuration, Elevon at 10 Degrees TEU

WING/ALT. NACELLE/VERTICAL @ LOW SPEED
M=0.2; ALPHA=8 DEG.; ELEVON -20; POWER-ON
NACELLES: INVERTED STAGGER
ROTOR TIP-TO-WING UPPER SURFACE 3 FT.

Boeing Research and Technology / Aero-Sciences

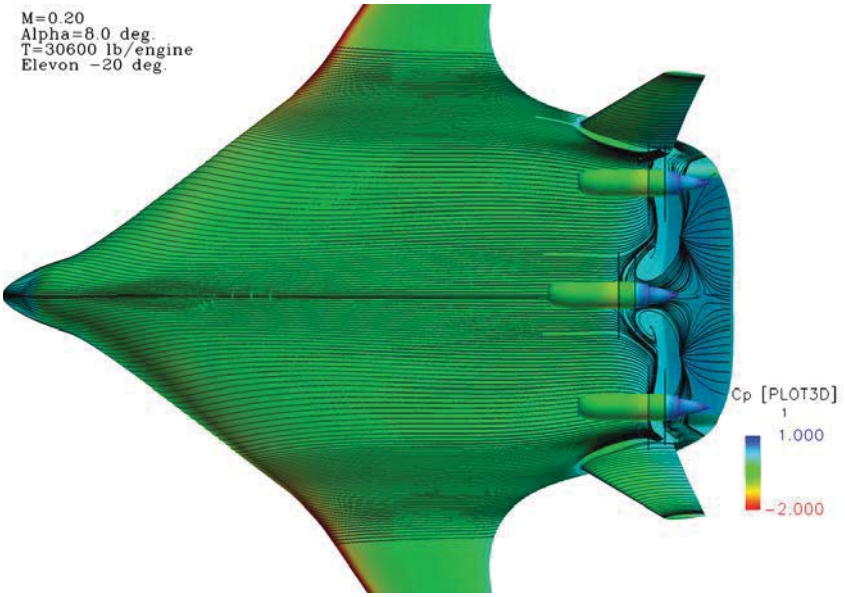

Figure 49. Powered Low Speed Configuration, Elevon at 20 Degrees TEU

CONTROL SURFACE EFFECTIVENESS

Boeing Research and Technology / Aero-Sciences

- LOOK AT ELEVON DEFLECTIONS OF 0, 10, -20 AT M=0.15 AND M=0.20
- DETERMINE ELEVON EFFECTIVENESS ($\Delta C_M/\Delta \delta e$)

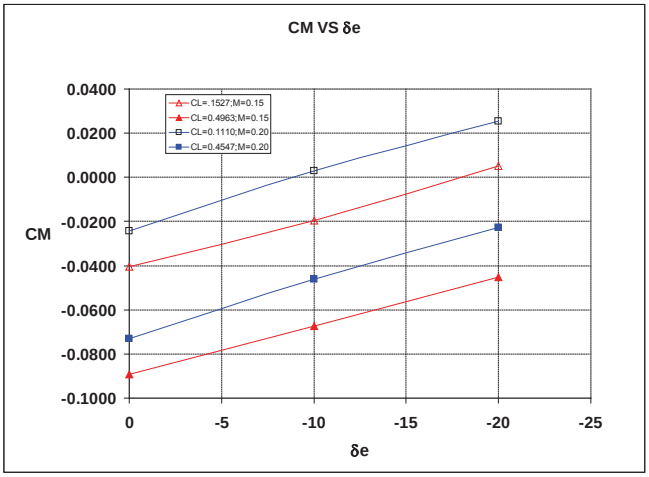

Figure 50. Powered Low Speed Configuration, Elevon Effectiveness

7.5 Thrust Drag Bookkeeping

In order to predict the drag from a powered solution the thrust had to be removed, this led to an exercise in thrust-drag bookkeeping.

The first step was to evaluate the isolated nacelle. A closed body nacelle was created to eliminate bookkeeping problems that would result from tracking the mass flow through the nacelle. Powered and unpowered Overflow solutions were obtained using this isolated nacelle. The solutions are shown in Figure 51 and Figure 52. The powered nacelle has negative drag; it produces thrust. To obtain the proper drag for the configuration at low speed the nacelle drag change due to power had to be removed. The nacelle drag change due to power was considered part of the thrust. The following equations were used to develop the configuration drag when powered.

$$C_D = C_D^* - \Delta C_{D)NAC}$$

Where

$$\Delta C_{D)NAC} = \{C_{D)CENTER} + C_{D)OUTBOARD}\}_{POWER\text{-}ON} - \{C_{D)CENTER} + C_{D)OUTBOARD}\}_{POWER\text{-}OFF}$$

C_D^* Is the drag of the complete configuration from Overflow

Thirty Overflow solutions were evaluated to develop powered and unpowered drag polars for the OREIO configuration at low speed. Solutions were obtained for 5 angles-of-attack with 3 elevator angles both powered and unpowered. The results are shown in Figure 53. There is a drag penalty that is close to 50 counts at low lift coefficients, decreasing to about 25 counts at high lift coefficients. The takeoff climb out condition is at the higher lift coefficients where the penalty is near 25 counts.

ISOLATED NACELLE @ LOW SPEED
M=0.20; POWER-OFF

Boeing Research and Technology / Aero-Sciences

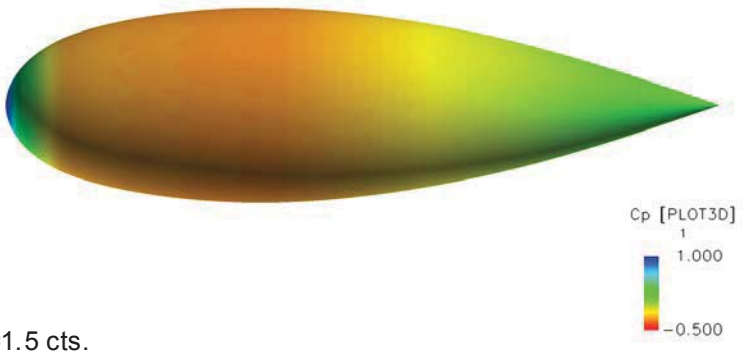

C_D=1.5 cts.

Figure 51, Isolated Nacelle Solution, Unpowered

ISOLATED NACELLE @ LOW SPEED
M=0.20; POWER-ON (ACTUATOR DISK)

Boeing Research and Technology / Aero-Sciences

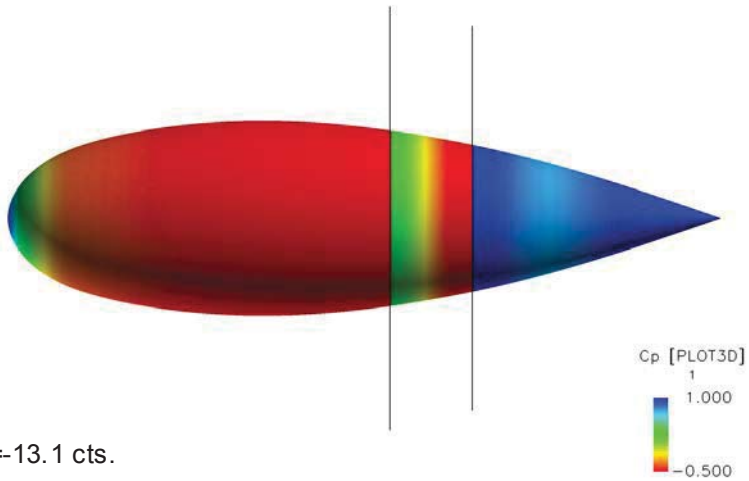

C_D=-13.1 cts.

Figure 52. Isolated Nacelle Solution, Powered

LOW SPEED TRIMMED DRAG POLAR

Boeing Research and Technology / Aero-Sciences

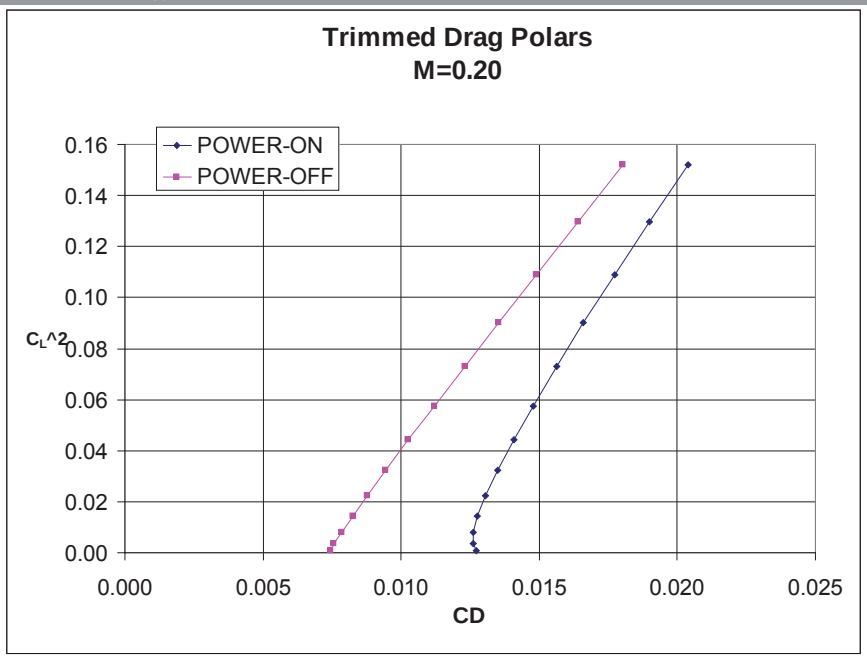

70

Figure 53. Powered and Unpowered Trimmed Drag Polars

The same Overflow solutions that were used to create the low speed trimmed drag polars were also used to determine the elevator angle required for trim. The Overflow runs were completed with deflections of the center elevon only. The results are shown in Figure 54. For takeoff with high power the elevon would have to be at a negative angle of about 14 degrees. The exact angle varies somewhat with lift coefficient. Note that a negative angle is trailing edge up. The power-off solutions require a positive or trailing edge down elevon angle of about 3 degrees for trimming. Landing cases have so little thrust that they are very close to the power-off cases. An estimate of the pitching moment due to thrust was included in the analysis to get the elevator angle required for trim.

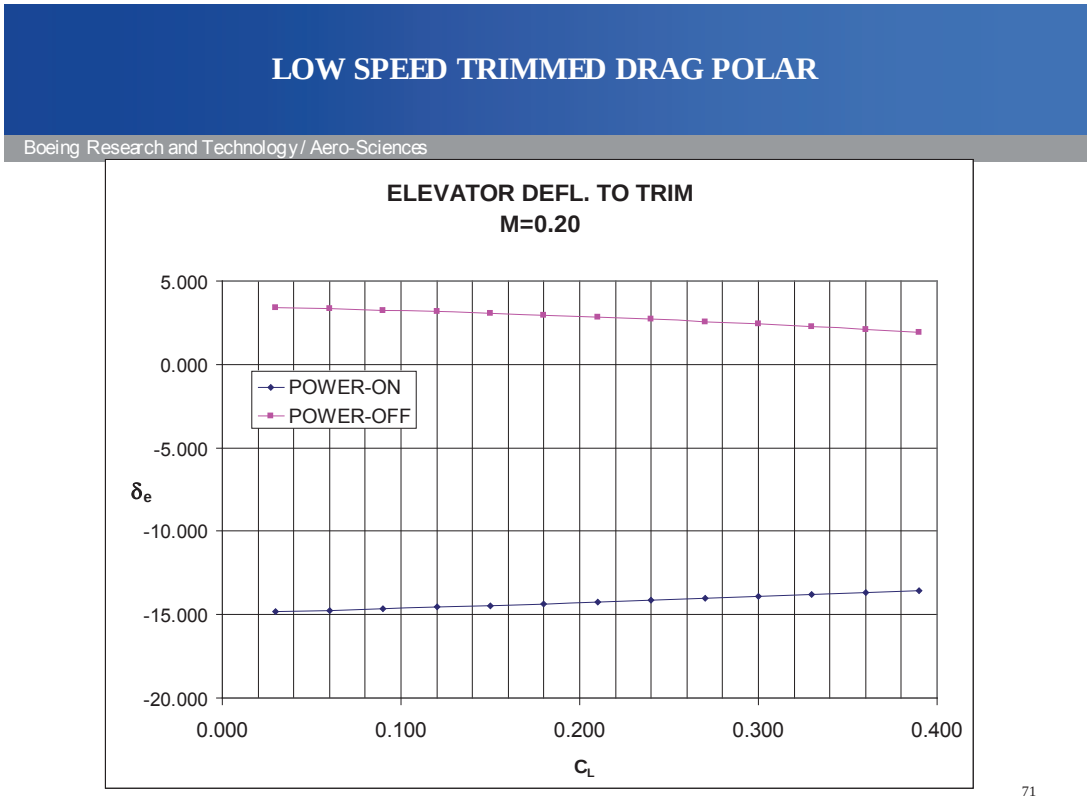

Figure 54. Elevator Required for Trim

8 Rotor Flow Field

The rotor flow field was evaluated for the cruise and low speed conditions. The rotor flow field is very important to the rotor and rotor manufacturer. The rotor flow field can have an effect on the performance of the rotor, the blade stresses, and the noise produced by the rotors. The goal would be to have a uniform flow field that is at or below the free stream velocity of the aircraft. The flow field for the OREIO configuration is not perfect.

The configuration used for the flow field evaluation includes the wing, body, nacelles, and vertical tails. The vertical tails have been twisted for near zero lift at cruise. The nacelles are positioned so the spacing between the rotor tips and the body upper surface is 3 ft and are oriented so that the rotors are normal to the cruise onset flow. The flow fields are shown in Figure 55 through Figure 58, for the cruise case, and Figure 59 through Figure 62, for the low speed takeoff condition. Four figures are shown for each condition. The components of velocity were converted to polar coordinates so that they would be more relevant to the rotor. The components are axial, radial, and circumferential velocity. The axial velocity is aligned with the nacelle axis. The radial velocity is inward or outward from the center of the rotor disk. The circumferential velocity is also referred to as V-theta.

The results show that the flow field is not ideal for the rotors. The circumferential velocity is sometimes positive and sometimes negative. This indicates that the flow field is sometimes clockwise and sometimes counterclockwise around the nacelle. The axial velocity was converted to Mach number for easier comparison to the free stream condition. Much of the axial Mach number ranges from about 0.83 to 0.89 and the peak speeds are higher. The radial velocity is not shown. The axial and circumferential velocity and were combined to evaluate the flow angle in the front rotor plane. The “alpha” plotted is not the angle-of-attack that a blade would see, that would depend on the rpm of the rotor and the blade twist. The alpha shown is the flow angle that the front rotor will be immersed in. The front rotor will experience the alpha variation in Figure 57. Alpha varies from -2.8 degrees to +2.2 degrees. The last flow field figure shows the total pressure in the forward rotor plane. The pressure is all near free stream. There is no total pressure loss from strong shocks, vortices, or boundary layer ingestion.

The flow field was improved by orienting the rotor disks normal to the onset flow. The alpha variation in the front rotor disk when the nacelles were aligned parallel to the body axis was from about -9 to +9 degrees.

The flow field of the front rotor was also checked at the takeoff climb out condition. An Overflow solution at Mach 0.20 and 8.0 degrees angle-of-attack was evaluated. The results are shown in Figure 59 through Figure 62. The alpha variation in the front rotor disk is greater because the nacelles were aligned for the cruise onset flow. There is a misalignment at this condition. The alpha varies from about -5 degrees to +4 degrees. Mach number is much higher than free stream because of the large power setting and the large pressure jump through the rotors.

The flow field in the front rotor plane can be improved. The evaluation of the flow field was done late in the study and nothing was done to improve what was found. The nacelles were aligned normal to the power-off flow field. The power-on flow field can be checked to see if there is any misalignment. It is possible that slight misalignment in the right direction may even help. The peak velocity in the rotor disks can be reduced by reducing the diameter of the nacelles at the rotor hub. Depressions in the body surface may also help. Changes in the camber of the aft

body or position of the vertical tails may also help to reduce the velocity in the rotor disks. The development of design techniques to improve the flow field in the front rotor plane will have to wait for a future project.

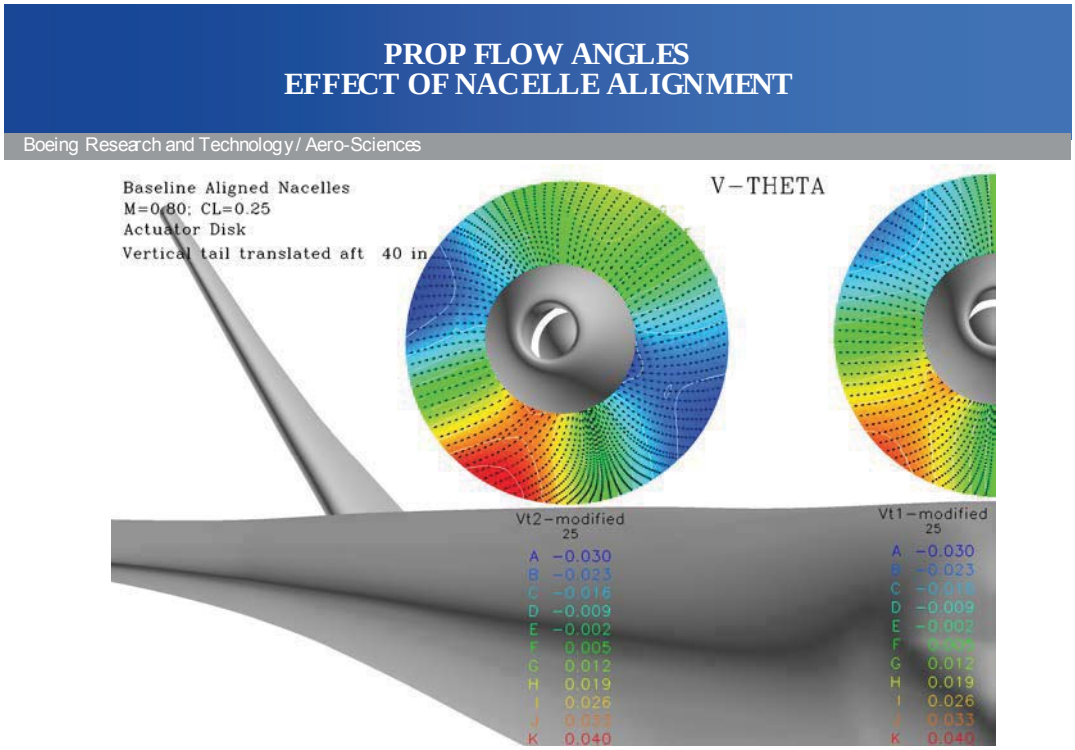

Figure 55. Circumferential Flow in the Forward Rotor Disk at Cruise

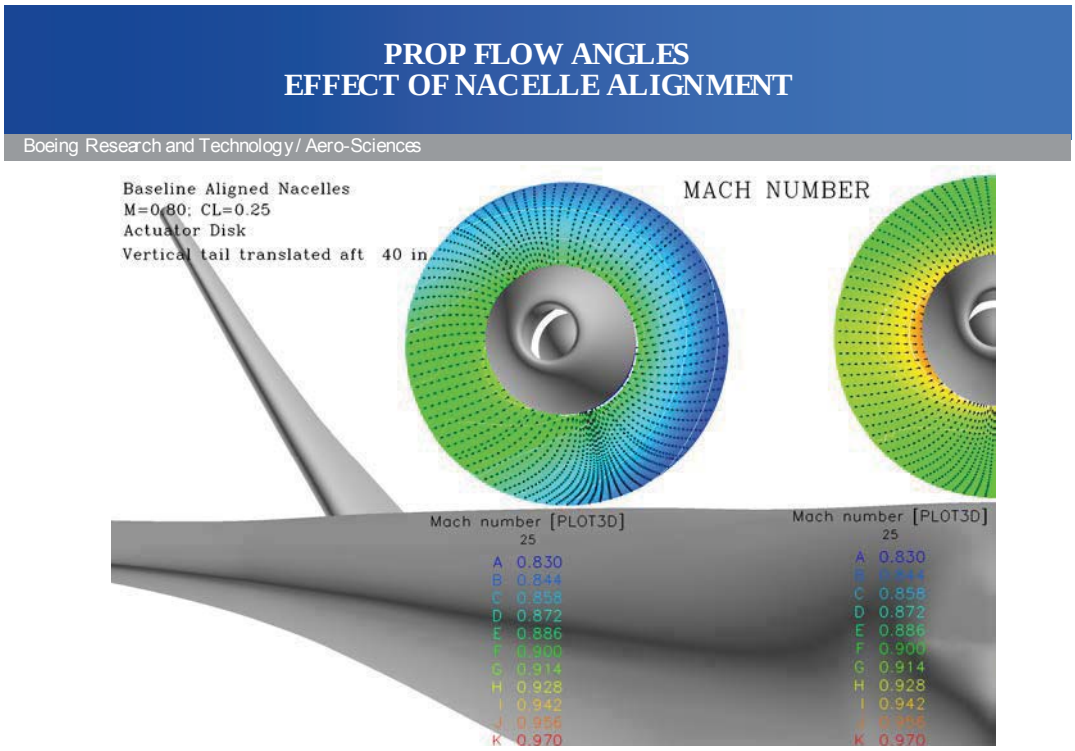

Figure 56. Mach Number in the Forward Rotor Disk at Cruise

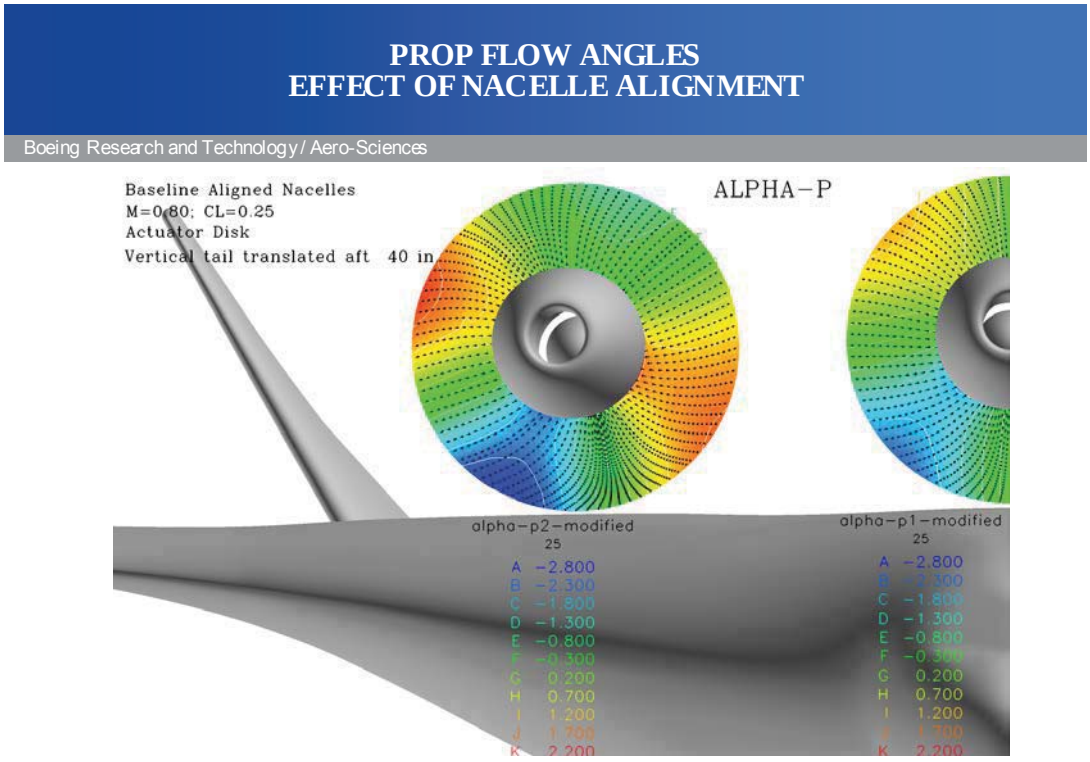

Figure 57. Flow Angle in the Forward Rotor Disk at Cruise

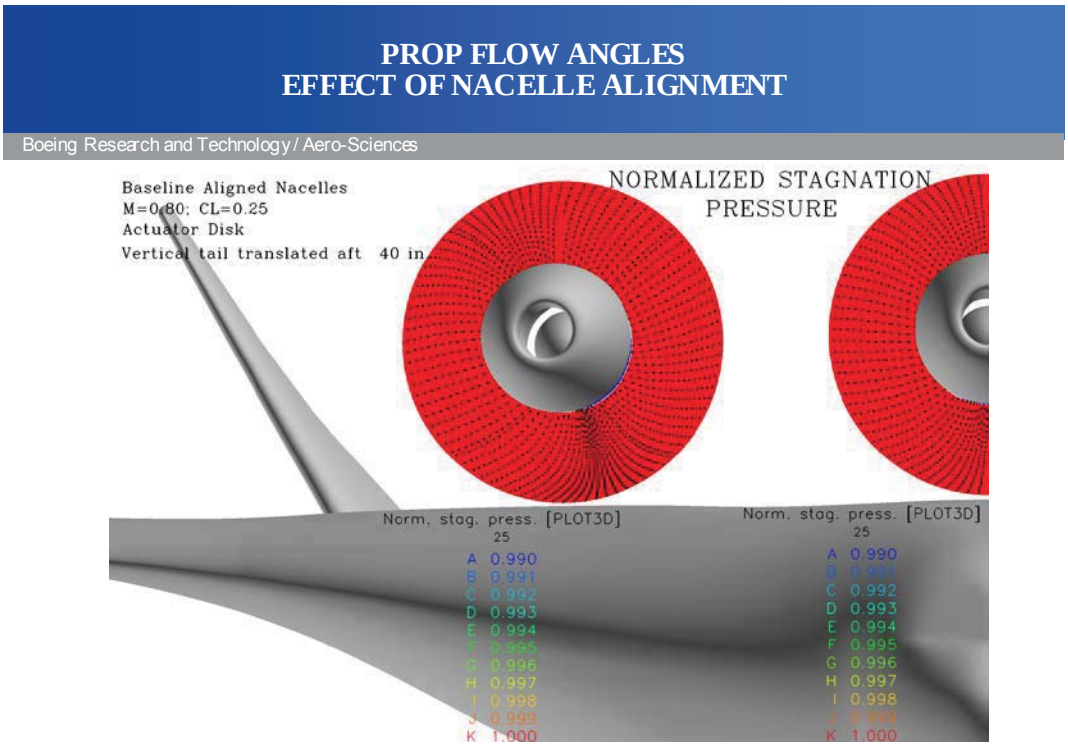

Figure 58. Total Pressure in the Forward Rotor Disk at Cruise

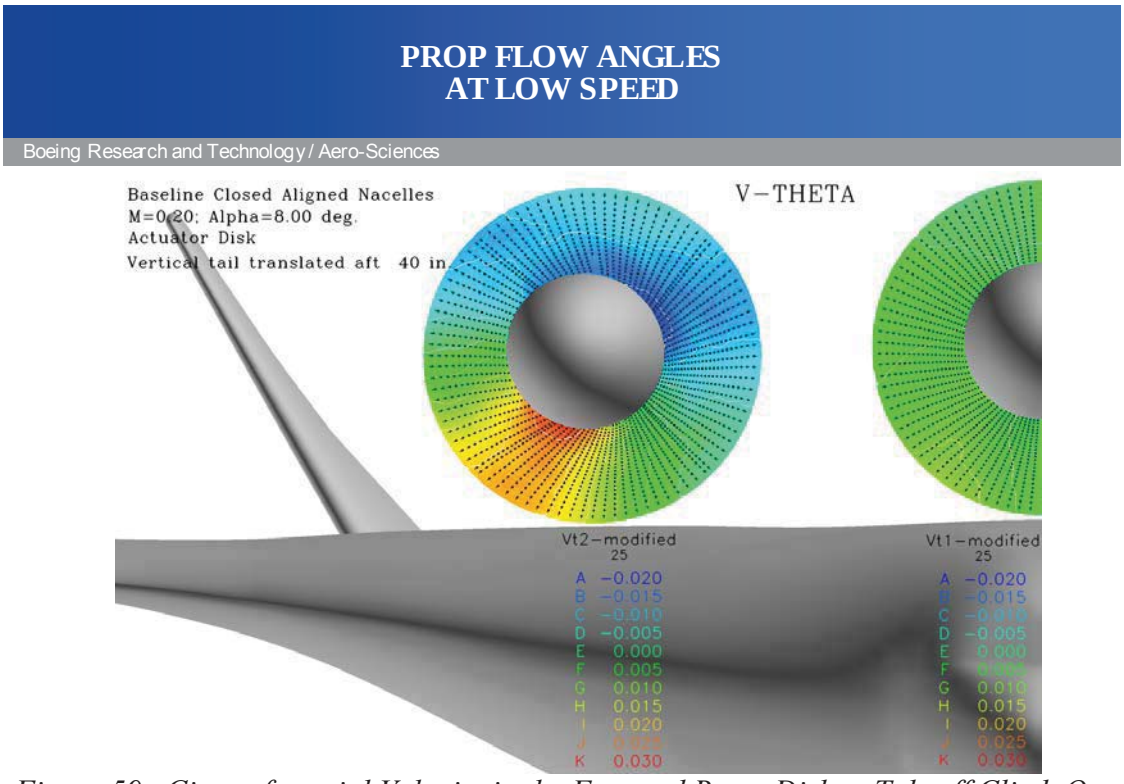

Figure 59. Circumferential Velocity in the Forward Rotor Disk at Takeoff Climb Out

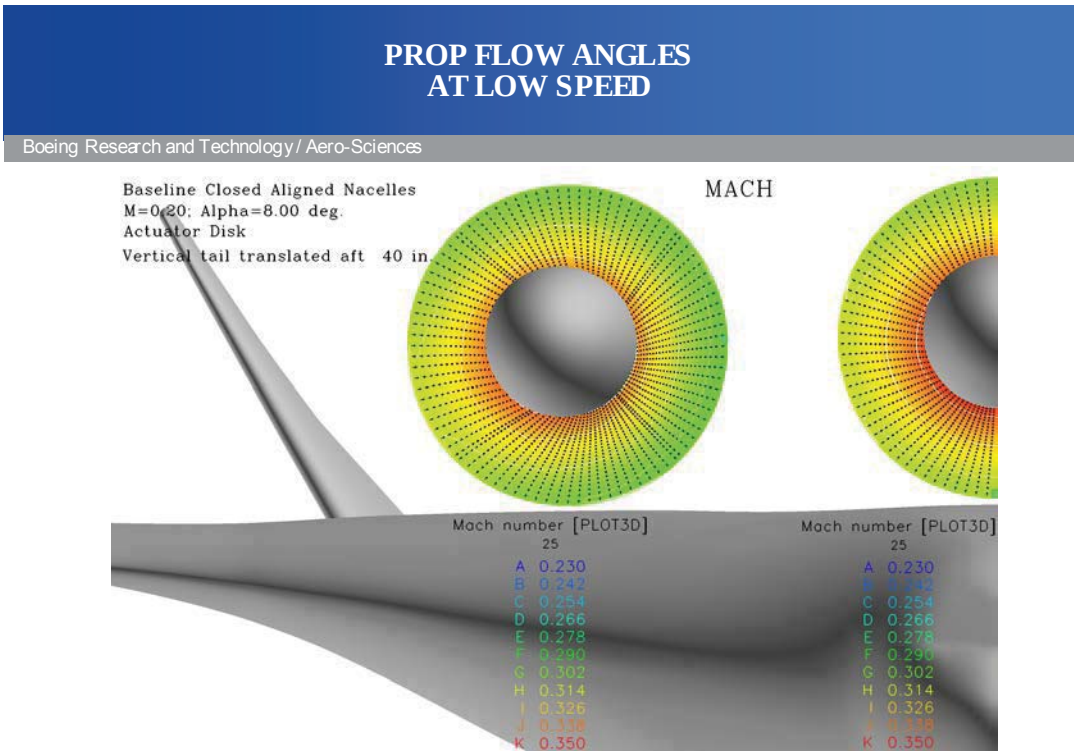

Figure 60. Mach Number in the Front Rotor Disk at Takeoff Climb Out

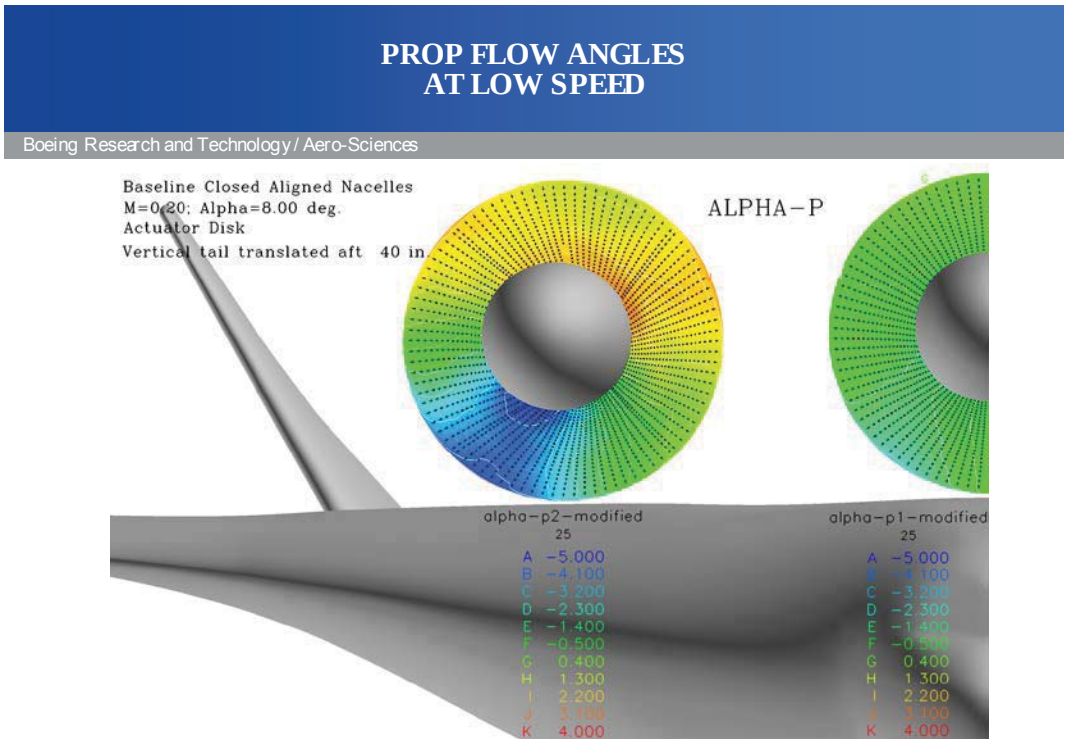

Figure 61. Flow Angle in the Front Rotor Disk at Takeoff Climb Out

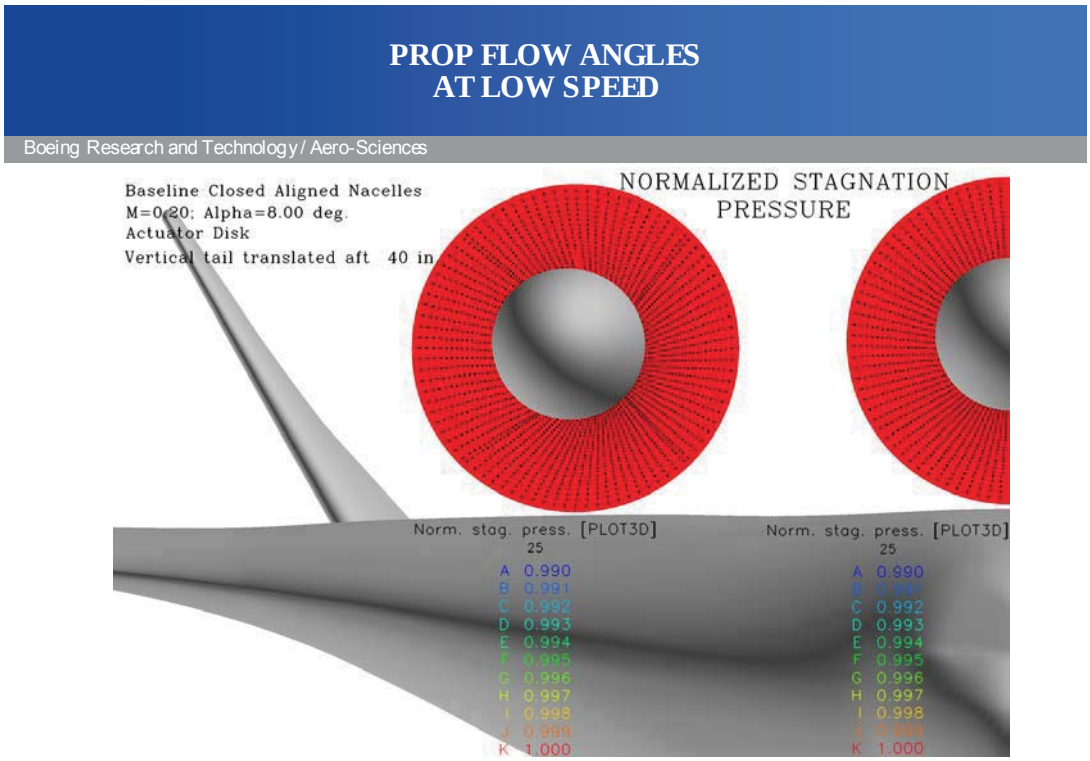

Figure 62. Total Pressure in the Front Rotor Disk at Takeoff Climb Out

9 Concept Design Data Summary

9.1 Final Configuration

During the initial performance evaluation of the geometry shown in Figure 7, a quick balance analysis showed the configuration was not viable. A chord extension was added to allow room for a possible aft body depression to reduce the drag of the nacelle installation (Section 5.1). Then when the PAI was started it was found that the engines needed to be located as close to the trailing edge as possible because the local velocity above the body continues to decrease up to the trailing edge (Figure 17). After the vertical tails were evaluated they were also moved aft to provide better acoustic shielding (Figure 29). The aft engine and tail also required an increased amount of aft body structure for attachment. The impact of this was to move the center of gravity of the configuration too far aft. To improve balance and loadability the aft most portion of the configuration was shortened by 80". A new geometry was created that effectively removed an 80" plug forward of the engines but aft of the wing, and allowed workable vehicle balance and loadability. This new geometry is shown in the final 3-View in Figure 63.

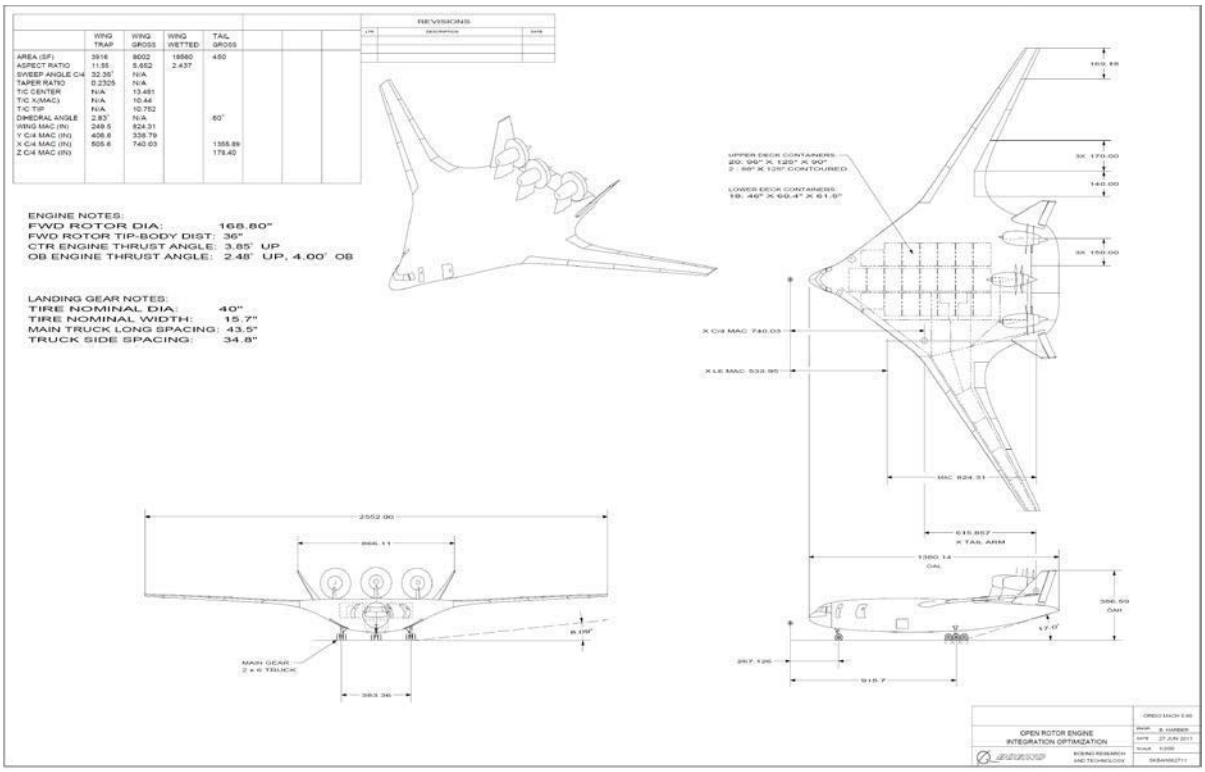

Figure 63. Final 3-View Drawing

9.2 Drag Build-up

The cruise drag was built up using a standard bookkeeping system within the CASES program. The CASES program is a standard program used at Boeing for estimating aero, weight, and propulsion characteristics. It can also size a configuration and run mission performance. The bookkeeping system is shown in Figure 64. The high speed drag consists of parasite, induced, compressibility and trim drag. The high speed drag build up for the final configuration of the OREIO project is shown in Figure 65. The drag build up includes an estimated drag reduction for HLFC (Hybrid Laminar Flow Control) and riblets. The assumptions that were used for estimating the drag reduction for the application of HLFC and riblets are shown in Figure 66 and Figure 67. The drag build-up also includes a penalty of 4.5 counts for the open rotor nacelle and pylon as discussed in Section 7.

Cruise Drag Bookkeeping System

Boeing Research and Technology / Aero-Sciences

CASES Standard Buildup : $C_D = C_{Dp} + C_{Di} + C_{Dc} + C_{Dtrim}$

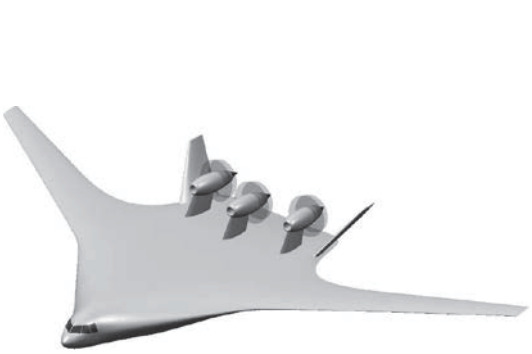

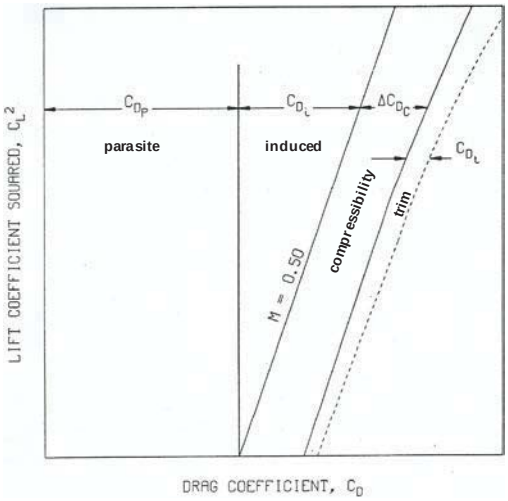

Figure 64. Cruise Drag Bookkeeping

High Speed Drag Build-Up

Boeing Research and Technology / Aero-Sciences

PROJECT NAME	rnasaera0x18 Shortened OREIO	
SREF (FT**2)	8010.000	
FN (LBS)	37000.0	
AR	5.646	
SWEEP (DEG)	32.119	
T/C-AVE	0.1178	
S-VERT (FT**2)	442.513	
F BUILD-UP (FT**2)		
WING	44.5750	
VERTICAL	2.5460	
N&P	4.6120	
HLFC & RIBLETS	-5.7300	
EXCRESCENCE	2.9810	(0.0648)
WING TWIST	1.1215	
NACELLE INTERFERENCE	3.6050	
F-TOTAL (FT**2)	53.7105	
E-VISC	0.8823	
CRUISE CD BUILD-UP		
M-CRUISE	0.8000	
CL-CRUISE	0.2650	
CD0	0.00671	(0.595)
CDI	0.00449	(0.398)
CDC	0.00007	(0.006)
CDTRIM	0.00000	(0.000)
CDTOT	0.01126	
L/D	23.5287	
ML/D	18.8230	

BOEING

13

Figure 65. Detailed High Speed Drag Build-Up

HLFC Assumptions

Boeing Research and Technology / Aero-Sciences

WING

- Applies only to outboard wing upper surface.
- Suction to front spar[1], then Rn=17 million[2] from the front spar unless there is a shock before Rn=17 million. (front spar to Rn=6 million at inboard extent of laminar run)
- Use leading edge break plus an 8 deg. turbulent wedge as the start of span for LFC.
- Assumes that there will be a Krueger rather than a slat.
- Apply the scale factor from EET-100 HLFC study.

TWIN VERTICAL

- 40% chord for vertical tails.

NLF NACELLE

- 25% of nacelle cowl length.
- Only use 80% of laminar area due to pylon interference effects.

NLF PYLON

- 40% of pylon chord.
- 8 deg. Turbulent wedge from pylon/body intersection.
- Only use 80% of laminar area due to nacelle interference effects.

70% factor applied to laminar improvements only

BOEING

[1] Passive system
[2] Rn=17 million is a goal

17

Figure 66. Hybrid Laminar Flow Control Assumptions

Riblet Assumptions

Boeing Research and Technology / Aero-Sciences

APPLICATION

- Apply riblets aft of transition on the wing surfaces.
- Apply riblets aft of the transition of the vertical tails.
- Apply riblets aft of the transition of the nacelles.
- Apply riblets aft of the transition of the pylons.
- Use riblets on entire centerbody

6% component skin friction improvement for riblets[1]

10% improvement on excrescence trend

[1] BTWT riblet measurements

Figure 67. Riblet Assumptions

9.3 Weight and Balance

The Group Weight Statement for the final OREIO configuration is shown as Table 8. The weights include the assumption that primary structure consists of PRSEUS (Pultruded Rod Stitched Efficient Unitized Structure) type construction.

Table 8. Group Weight Statement

OREIO	
FUNCTIONAL GROUP	**WEIGHT (LB)**
WING-BODY	118,387
OUTERWING	61,143
CENTERBODY	51,600
AFTERBODY	5,645
WINGLET/VERTICAL TAILS	2,394
LANDING GEAR	19,500
ENGINE & NACELLE	42,923
ENGINE SYSTEMS	399
ENGINE PYLON	6,932
FUEL SYSTEM	9,209
APU	1,000
FLIGHT CONTROLS & HYDRAULICS	11,798
ELECTRICAL	3,953
PNEUMATICS & AIR CONDITIONING	7,775
ANTI-ICING	526
FURNISHINGS AND EQUIPMENT	5,498
INSTRUMENTS	1,155
AVIONICS	3,434
LOAD & HANDLING	11,664
WEIGHT EMPTY	**246,548**
STANDARD & OPERATIONAL ITEMS	2,242
OPERATING WEIGHT	**248,790**
MISSION FUEL	127,010
PAYLOAD	100,000
MAXIMUM TAKEOFF WEIGHT	**475,800**

A quick analysis shows that the vehicle's center of gravity, building up from Weight Empty through Operating Weight and Max Takeoff Weight, match reasonably well with the centers of pressure ranges discussed in the Wing-Body development section and will enable workable balance and loadability.

9.4 Propulsion Characteristics

The purpose for this project is to provide the hybrid wing body air vehicle for flyover acoustic analyses, particularly for use in making flyover and community noise assessments using the noise data taken in the Boeing LSAF with an open rotor model on a hybrid wing body configuration. To have a one-to-one assessment basis, since the LSAF tests used the GE 36 F7/A7 model rotors, the propulsion performance and weights used this same rotor configuration. An OREIO propulsion

system data requirement is also for the data base and results to be non-proprietary. NASA GRC therefore created the engine performance, dimensions, and weight using NPSS and rotor characteristics for the F7/A7. These data are based on the convention where propulsion performance is based on freestream to freestream flow such that the forebody and afterbody surfaces scrubbed by the inflow and outflow from the propulsor are included in net thrust.

9.5 Performance

The aerodynamic, weight, and propulsion data were combined to produce the aircraft performance. The constraints used to size the aircraft are listed in Table 9. The constraints are consistent with the final requirements discussed in Section 10 with the exception of initial cruise altitude. In order to achieve the required initial cruise altitude the engine would have to be increased above the reference thrust of the engine supplied by NASA. NASA requested for the final performance to be completed without scaling the engine to make it easier to perform the acoustic analysis. Therefore two sets of data were generated, one with the engine scaled up to 41,500 lbs SLST and a second with an unscaled engine with 37,250 lbs of SLST. A summary of the OREIO performance with the two sizes of engines is shown in Table 10. The larger engine resulted with lower block fuel burn because of a better lift to drag ratio and lower SFC as shown in Figure 68 and Figure 69.

Table 9. OREIO Performance Sizing Constraints

OREIO Performance Sizing Constraints
Payload: 100,000 lbs Range: 6500 nm
Critical Field Length: 10,500 ft at SL, standard day Engine out climb gradient: 2.7% (3-engine aircraft)
Approach Speed: 155 KCAS Landing field length: 5200 ft at SL, standard day
Cruise Mach: 0.80 Initial cruise altitude: 35,000 ft (achieved 32,945 ft)
Measure of Merit: maximize ton-nm/lb fuel At fixed range and payload this is minimize block fuel

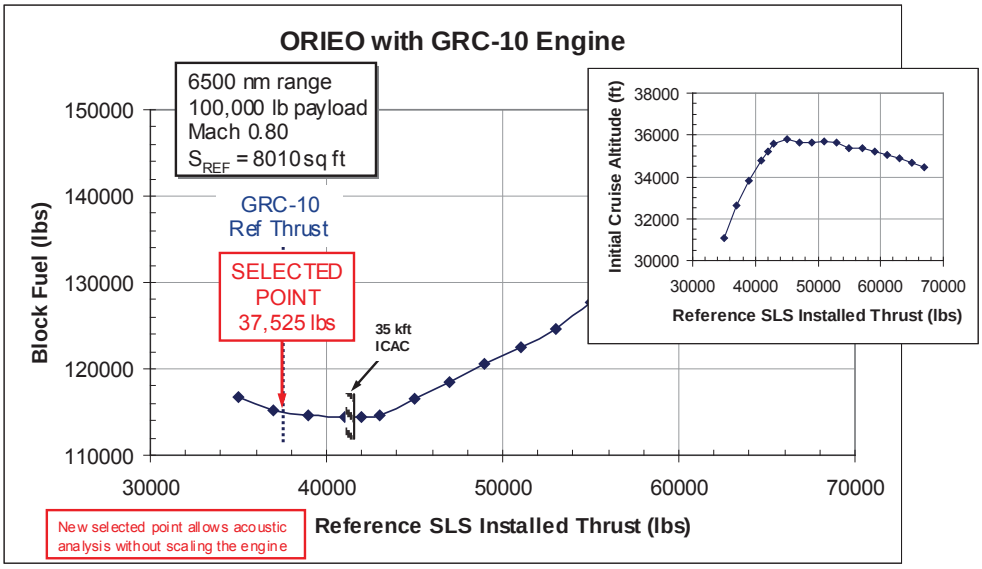

Figure 68. Thrust Trade for Minimum Fuel

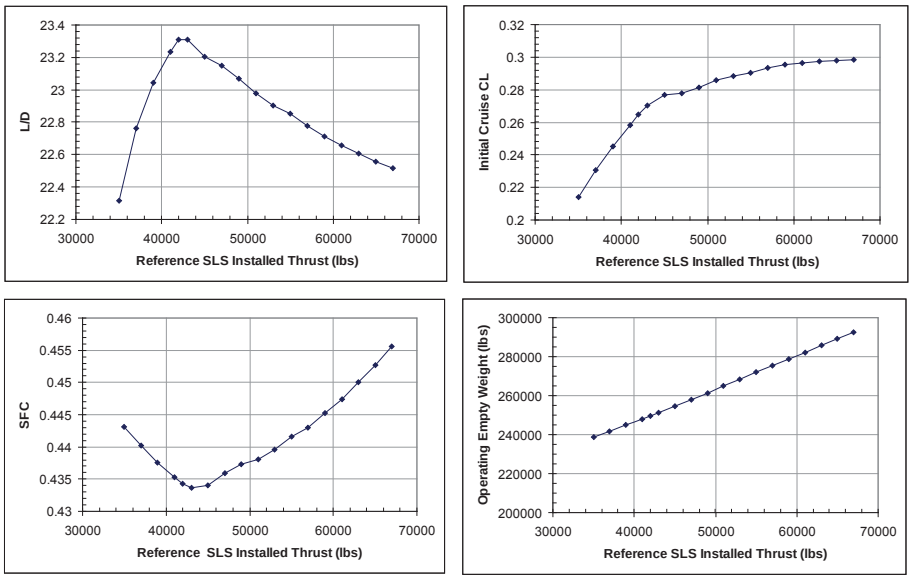

Figure 69. Results of Thrust Trade

Table 10. Performance Summary

Reference	Required Perf.	OREIO BWB-short Mcr=0.80 GRC-10 BL	OREIO BWB-short Mcr=0.80 GRC-10 Scaled
MTOGW		470138	475800
OEW		242517	248795
Payload	**100,000**	100000	100000
Fuel at Max PL		127621	127005
Range (nm)	**6500**	6500	6500
Block Fuel Burned		115187	114385
Ton-nm/lbf		2.82	2.84
Reference Wing Area (sqft)		8010	8010
Aspect Ratio		5.646	5.646
Span (ft)		212.7	212.7
TO Ref FN @ SL, 0.0, +27F (lbf/eng)		**37524.7**	**41500**
Number of Engines		3	3
T/W		0.24	0.26
W/S		59	59
Optimum Altitude (ft)		36257	36085
Initial Cruise Thrust Ceiling (ft)		32945	35012
Initial Cruise Buffet Ceiling (ft)		40470	40233
Initial Cruise Altitude Capability (ft)		32945	35012
Cruise type		Climb-Cruise	Climb-Cruise
Initial cruise altitude (ft)	**35000**	32945	35012
Initial cruise thrust (all engines)		21184	21058
Initial cruise mach		0.8	0.8
Initial cruise L/D		22.849	23.274
Initial cruise SFC		0.4395	0.4347
Initial cruise tau		0.956	0.955
Initial cruise CL		0.2344	0.2614
Balanced field length @ SL, 59F (ft)	**10500**	8118	7407
2nd Segment Gradient (%)	**2.7**	2.7	3.8
Landing field length (ft)	**5200**	6120	6212
Approach speed (KCAS)	**155**	141	142

10 Conclusions and Recommendations

A BWB configuration with an open rotor installation was developed for NASA to study the noise shielding features of this configuration. It is thought that noise shielding features of a BWB are uniquely suited to the use of an open rotor engine. The configuration meets the requirements established early in the project. The wing-body configuration was developed for a cruise Mach number of 0.80, which is lower than many other BWB configurations because of the open rotor engine. PAI was studied; some of the configuration changes were based on the PAI work. The PAI work also highlighted the need for future studies to determine the viability of open rotors on the BWB platform.

The engine positioning was all based on the PAI work. The engine was moved aft because the local Mach numbers were lower near the trailing edge. The engines were moved up because the upper surface of the body separated when the large thrust levels required for takeoff were used. The engines are aligned to orient the rotor disk normal to the cruise onset flow. The vertical tails were moved aft to provide better noise shield for sideline noise from the open rotors.

Mission performance was estimated for the final configuration. Engine performance was supplied by NASA GRC. The estimated weight and aero characteristics were supplied by Boeing. Some aerodynamic interference penalties were included for the installation of the open rotor engine. The flight conditions for potential noise measurements at takeoff and landing were included.

This study highlighted some of the problems that will be encountered with an open rotor engine installation. Several solutions were tried but there is a considerable amount of work remaining. The following is a list of areas that need more investigation.

A puller or tractor engine concept may be better for the configuration. It has advantages over the pusher concept. The pylon wake would not cause distortion through the rotors. Filling in the wake with a blowing system for a pusher engine would just add complexity. The engine airflow would also be simpler; there is added complexity for a push engine to get the airflow past the rotors, either externally or internally. A future study should include a revised rotor configuration with the right diameter, blade count and thrust loading.

The rotor flow is higher than free stream and not uniform. Many aspects of the configuration may have to be changed to improve the flow field. The camber of the entire aft fuselage, the local shape of the fuselage under the nacelle and rotors, and the vertical tail position and camber may all have to be changed

The engine support or pylon needs more investigation. Based on the work of this study, it will be difficult to develop a low drag pylon installation and if the engine is a pusher there is the problem of wake ingestion that needs to be addressed.

The low speed upper surface separation resulted with adverse configuration changes. If the separation can be controlled better the engine height can be reduced which will improve the weight and controllability of the configuration.

The nacelle shape should be investigated. The shape used for this study was not designed for the cruise speed of this configuration. The nacelle shape was designed to provide the proper rotor flow field at Mach 0.72 for an isolated nacelle. Some investigation is required to determine the best shape for an installed nacelle at the higher cruise speed of this configuration.

11 References

1. http://lemanusa.com/wp-content/uploads/2010/01/Air-Cargo-ULD2.pdf

REPORT DOCUMENTATION PAGE

Form Approved
OMB No. 0704-0188

1. REPORT DATE *(DD-MM-YYYY)*	2. REPORT TYPE	3. DATES COVERED *(From - To)*
01- 11 - 2011	Contractor Report	September 2010 to August 2011

4. TITLE AND SUBTITLE

Blended Wing Body Concept Development with Open Rotor Engine Integration

5a. CONTRACT NUMBER

NNL10AA05B

5b. GRANT NUMBER

5c. PROGRAM ELEMENT NUMBER

6. AUTHOR(S)

Pitera, David M.; DeHaan, Mark; Brown, Derrell; Kawai, Ronald T.; Hollowell, Steve; Camacho, Peter; Bruns, David; Rawden, Blaine K.

5d. PROJECT NUMBER

5e. TASK NUMBER

NNL10AC78T

5f. WORK UNIT NUMBER

699959.02.10.07.01

7. PERFORMING ORGANIZATION NAME(S) AND ADDRESS(ES)

NASA Langley Research Center
Hampton, Virginia 23681-2199

The Boeing Company
Boeing Research and Technology
5301 Bolsa Avenue
Huntington Beach, CA 92647

8. PERFORMING ORGANIZATION REPORT NUMBER

9. SPONSORING/MONITORING AGENCY NAME(S) AND ADDRESS(ES)

National Aeronautics and Space Administration
Washington, DC 20546-0001

10. SPONSOR/MONITOR'S ACRONYM(S)

NASA

11. SPONSOR/MONITOR'S REPORT NUMBER(S)

NASA/CR-2011-217303

12. DISTRIBUTION/AVAILABILITY STATEMENT

Unclassified - Unlimited
Subject Category 05
Availability: NASA CASI (443) 757-5802

13. SUPPLEMENTARY NOTES

Langley Technical Monitor: Craig L. Nickol

14. ABSTRACT

The purpose of this study is to perform a systems analysis of a Blended Wing Body (BWB) open rotor concept at the conceptual design level. This concept will be utilized to estimate overall noise and fuel burn performance, leveraging recent test data. This study will also investigate the challenge of propulsion airframe installation of an open rotor engine on a BWB configuration. Open rotor engines have unique problems relative to turbofans. The rotors are open, exposed to flow conditions outside of the engine. The flow field that the rotors are immersed in may be higher than the free stream flow and it may not be uniform, both of these characteristics could increase noise and decrease performance. The rotors sometimes cause changes in the flow conditions imposed on aircraft surfaces. At high power conditions such as takeoff and climb out, the stream tube of air that goes through the rotors contracts rapidly causing the boundary layer on the body upper surface to go through an adverse pressure gradient which could result with separated airflow. The BWB / Open Rotor configuration must be designed to mitigate these problems.

15. SUBJECT TERMS

Advanced concept; Blended wing body; Emissions; Fuel burn; Noise; Open rotor

16. SECURITY CLASSIFICATION OF:			17. LIMITATION OF ABSTRACT	18. NUMBER OF PAGES	19a. NAME OF RESPONSIBLE PERSON
a. REPORT	b. ABSTRACT	c. THIS PAGE			STI Help Desk (email: help@sti.nasa.gov)
					19b. TELEPHONE NUMBER *(Include area code)*
U	U	U	UU	76	(443) 757-5802